





This is to certify that the

thesis entitled

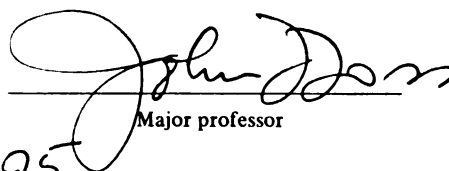
THE DESIGN OF A FIBER GLASS CHOPPER FOR  
USE IN VARIABLE LENGTH AND DIRECTION  
CONTROLLED PREFORMING PROCESSES

presented by

Edward J. Eshelman

has been accepted towards fulfillment  
of the requirements for

Master of Science degree in Mechanical Engineering

  
Major professor

Date 27 March 1995



**PLACE IN RETURN BOX** to remove this checkout from your record.  
**TO AVOID FINES** return on or before date due.

DATE DUE	DATE DUE	DATE DUE
_____	_____	_____
_____	_____	_____
_____	_____	_____
_____	_____	_____
_____	_____	_____
_____	_____	_____
_____	_____	_____

**THE DESIGN OF A FIBER GLASS CHOPPER FOR USE IN VARIABLE LENGTH  
AND DIRECTION CONTROLLED PREFORMING PROCESSES**

**By**

**Edward J. Eshelman**

**A THESIS**

**Submitted to  
Michigan State University  
in partial fulfillment of the requirements  
for the degree of**

**MASTER OF SCIENCE**

**Department of Mechanical Engineering**

**1995**



## **ABSTRACT**

### **THE DESIGN OF A FIBER GLASS CHOPPER FOR USE IN VARIABLE LENGTH AND DIRECTION CONTROLLED PREFORMING PROCESSES**

**By**

**Edward J. Eshelman**

**A conceptual design has been developed for a device which will draw fiber glass  
tows into it, cut them to variable lengths, and spray them, in a manner suitable for  
direction controlled preforming. The device is intended to be used as part of a high speed  
resin transfer molding process. By controlling the length and orientation of the fibers  
within composite parts, the parts can be made stronger while saving material. The device  
is designed to utilize an intermittent motion, driven by a Geneva mechanism, with an  
entraining airflow to pull the fibers into the device. Any combination of six blades would  
then be selected for each cutting cycle. This blade selection process would be performed  
via pneumatically controlled selecting pins. Finally, the cut fibers would be sprayed out of  
a narrow channel, propelled by a high speed air flow.**

## **ACKNOWLEDGMENTS**

**The author would like to thank The State of Michigan Research Excellence Fund for supporting this work financially. He would also like to thank the following faculty at Michigan State University:**

**John F. Foss, Ph.D. (major professor & thesis committee member)**

**Martin Ostojka, Ph.D. (thesis committee member)**

**Robert Wm. Soutas-Little, Ph.D. (thesis committee member)**

**In addition, the author would like to thank his parents, Cliff & Mary Eshelman.**

## TABLE OF CONTENTS

LIST OF TABLES .....	v
LIST OF FIGURES .....	vi
NOMENCLATURE .....	viii
CHAPTER 1 -- INTRODUCTION.....	1
CHAPTER 2 -- SYNTHESIS OF DESIGN II.....	8
CHAPTER 3 -- ANALYSIS OF DESIGN II INTAKE MECHANISM.....	14
CHAPTER 4 -- ANALYSIS OF DESIGN II CUTTING MECHANISM.....	26
CHAPTER 5 -- ANALYSIS OF DESIGN II DELIVERY CHANNEL.....	41
CHAPTER 6 -- CONCLUSIONS AND RECOMMENDATIONS.....	46
APPENDIX A -- FINITE ELEMENT ANALYSIS OF COMPOSITE BEAM.....	48
APPENDIX B -- SYNTHESIS OF INITIAL DESIGN.....	54
APPENDIX C -- ANALYSIS OF INITIAL DESIGN BLADE MECHANISM.....	64
APPENDIX D -- EVALUATION OF INITIAL DESIGN .....	85
APPENDIX E -- MATLAB PROGRAMS .....	87
BIBLIOGRAPHY .....	110

## **LIST OF TABLES**

- 1      Cycle timing chart (design II)**
- 2      Maximum pressure angles for various base circle radii**
- 3      Convergence of results for isotropic beam**
- 4      Extreme displacements for various fiber orientations**
- 5      Typical values to be differentiated numerically**

## LIST OF FIGURES

- 1 Illustration of fiber glass packaging
- 2 Illustration of commonly used delivery process
- 3 Illustration of proposed delivery process
- 4 The design algorithm (Thompson)
- 5 Schematic of 4-slot external Geneva mechanism
- 6 Schematic of fiber intake mechanism
- 7 Schematic of fiber cutting process
- 8 Multiple blade arrangement
- 9 Blade selection process
- 10 Schematic of Geneva mechanism for analysis
- 11 Schematic of tows at pinch rollers
- 12 Position of tows at roller contact point vs.  $\theta$
- 13 Velocity of tows at roller contact point vs.  $\theta$
- 14 Acceleration of tows at roller contact point vs.  $\theta$
- 15 Schematic of tow intake process
- 16 Schematic of experimental setup to determine drag properties
- 17 Position of tows as a function of time, for various air velocities
- 18 Velocity of tows as a function of time, for various air velocities
- 19 Schematic of cutting mechanism
- 20 Position curve of follower during rise and return
- 21 Velocity curve of follower during rise and return
- 22 Acceleration curve of follower during rise and return
- 23 Illustration of cam profile relation to pitch curve
- 24 Illustration of cam profile determination, given a pitch curve
- 25 Pitch curve (outside) and cam profile (inside)
- 26 Free body diagram of blade
- 27  $F_1$  vs.  $\theta$
- 28 Free body diagram of blade actuation link
- 29  $F_2$  vs.  $\theta$
- 30 Free body diagram of follower
- 31  $F_3$  vs.  $\theta$
- 32 Three short noodles moving in 3/8" tall channel
- 33 One 3 inch noodle, discharged to screen (channel height 1/16")
- 34 One 3 inch tow segment (channel height 3/8")
- 35 One 3 inch tow segment, screen impact (channel height 3/8")
- 36 One 3 inch tow segment, screen impact (channel height 1/16")
- 37 Schematic of beam with oriented fibers

38	Schematic of model problem
39	Displacement of isotropic beam, calculated with various models
40	Displacement of beams with various fiber orientations
41	Schematic of fiber intake mechanism, design I
42	Multiple blade arrangement, design I
43	Blade selection process
44	Mechanism used to obtain an RDR motion (Soni, p.361)
45	Schematic of four bar linkage used to obtain a “straight” coupler curve
46	Schematic of design I -- front view
47	Schematic of design I -- right side view
48	Coupler curve generated when $CA = 1.00$
49	“Straight” portions of coupler curves for various values of $CA$
50	Coupler curve with best fit line ( $CA = 1.20$ units)
51	Distance of coupler curve from best fit line ( $CA = 1.20$ units)
52	Properly scaled and oriented mechanism
53	Trajectories of points A, B, C
54	Parametric velocity curves of points A, B, C
55	Parametric acceleration curves of points A, B, C
56	Free body diagram of the coupler (link 2)
57	$F_{42,I}$ vs. $\theta_1$
58	$F_{42,J}$ vs. $\theta_1$
59	$ F_{42} $ vs. $\theta_1$
60	$F_{32,T}$ vs. $\theta_1$
61	$F_{32,R}$ vs. $\theta_1$
62	$ F_{32} $ vs. $\theta_1$
63	$F_{12,T}$ vs. $\theta_1$
64	$F_{12,R}$ vs. $\theta_1$
65	$ F_{12} $ vs. $\theta_1$

## NOMENCLATURE

### Greek Symbols

$\alpha$	angle of the blade
$\phi$	angle of driven wheel in Geneva mechanism
$\theta$	device phase angle
$\rho$	density
$\rho_1$	linear strand density of fiber tow
$\zeta$	effective circumference of tow (as related to drag properties)
$\bar{\theta}$	non-dimensionalized phase angle

### Arabic Symbols

$a$	acceleration
$i$	electric current
$\hat{i}$	unit vector in the x-direction
$\hat{j}$	unit vector in the y-direction
$k$	spring constant
$h$	height
$m$	mass
$x$	position
$v$	velocity
$A_s$	surface area
$B$	magnetic field vector
$C$	arbitrary constant
$C_D$	drag coefficient
$F$	force
$I_o$	mass moment of inertia, about point O
$L$	length
$M$	rate of fiber deposition
$N$	number of tows, number of blades
$P$	pressure
$R$	position vector
$W$	weight
$Y$	non-dimensionalized displacement
$Z$	mathematical quantity used to simplify calculations

## CHAPTER 1 -- INTRODUCTION

Currently there is considerable interest in the optimization of molded glass mat reinforced thermoplastic (GMT) components; i.e., fiber glass composite parts as expressed in common usage. Composite parts are lighter than steel parts of similar strength. However, fabrication of composite parts is slower and more expensive. In the February 1993 issue of "Automotive Engineering", the feasibility of using a composite floorpan was described. The following two quotes are from the article entitled "Composite Floorpan":

"The composite floorpan did improve upon most of the technical properties of the steel design. However, the application of composite structures will mostly depend on the production costs and large-scale manufacturing capabilities."

"Also, the manufacturing issues for high-volume production of the foam cores, glass preforms, molding, and automation need to be solved."

Several processes are used to manufacture fiber glass composite materials. Typically, a perforated steel sheet (similar to a screen) is coated with fibers as a suction flow through the screen is used to hold the fibers in place. This process is termed "preforming". The preform is subsequently coated with a resin and hardened. The steel sheet is then removed, cleaned, and used again. There are different ways to coat the preform with resin, and there are several types of resin in current use. Two such methods are called resin transfer molding (RTM) and structural reaction injection molding (SRIM).

The fiberglass comes in spools of tow. This tow is on the order of 3 mm (1/8 inch) in diameter when held in tension. The tow consists of 28 strands, each of which is composed of dozens of thin fibers (see figure 1). Tow segments are delivered to the



perforated sheet in several ways during the preforming process. The segments may be either chopped or continuous. In addition, they may be oriented or have random direction. The present work focuses on preforming involving chopped, oriented tow segments.

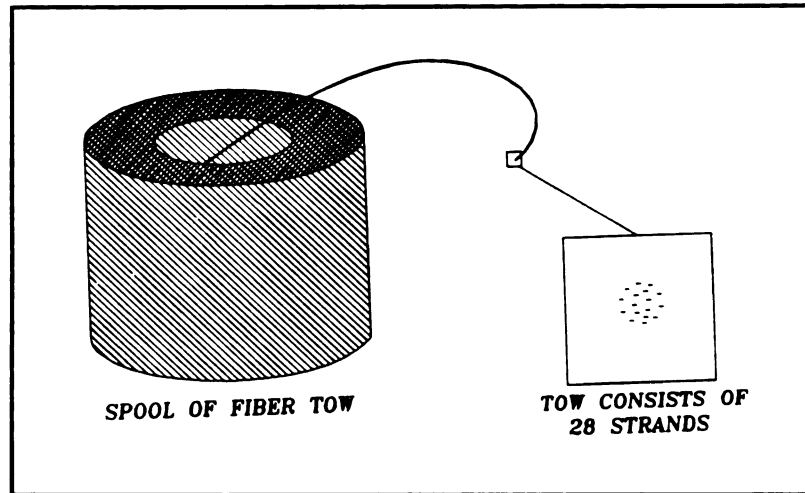


Figure 1: Illustration of fiber glass packaging

Current processes deliver the cut segments, via a nozzle, in a direction along the axis of the tow. This type of delivery process is illustrated in figure 2. A common method, used to help orient the tow segments, is to attach two plates at oblique angles to the end of the delivery nozzle. The tow is usually drawn into the device and cut by a pair of pinch rollers, one of which is fitted with embedded blades. After a given length of tow is cut, it proceeds down the cylindrical flow tube and out the nozzle. One limitation of the pinch roller cutting method is that the length of the tow segments cannot be changed without changing the cutting wheel.

Studies have shown that significant increases, in both tensile and flexural strengths of composite parts, may be achieved by using an appropriate fiber mesh (i.e., correctly oriented tow segments of the proper length). Methods for estimating the tensile, transverse and flexural strengths of composite parts, as functions of strand length, have been developed (Ericson & Berglund). Factors which would determine the desired length

of fiber stands, at a given location of a part, include the radius of curvature and the expected loading conditions as well as the strand orientation with respect to the load. The tensile and transverse strengths of a fiber glass reinforced composite material, with oriented fibers, are quite different. Hence, by orienting the fiber strands in the direction of the expected loading, a substantial savings in materials cost may be realized. This is illustrated by a finite element method (FEM) analysis of a composite beam, in appendix A.

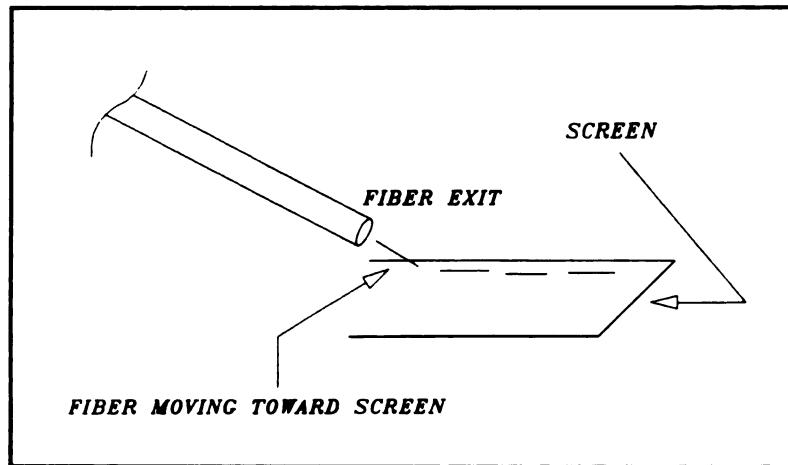


Figure 2: Illustration of commonly used delivery process

As with any production line, the “line speed” is restricted by the speed of the slowest station. Since preforming takes much longer than all subsequent steps, the overall time required to manufacture a composite part is constrained by the preforming process. For this reason, a more efficient preforming process can drastically reduce the time to produce composite parts. Hence, a well designed fiber delivery device will save money in two ways. A materials savings, because of better oriented strands of the proper length, will be realized and a savings in production time will reduce the capital cost per part.

There is a need for a new device which is able to deliver chopped strands at a desired rate, of a desired length, and in a controlled direction in the preforming process.

Current designs provide various approximations to achieving these objectives (Jander, 1991); however, in all of these known processes, the length of the tow segments is predetermined and can not be changed during the deposition process. For parts with complex shapes, it would be beneficial to change the length of the fiber stands within each part. This is not currently possible without lengthy time delays or multiple delivery devices. The evolved process should be capable of delivering at least one pound (198m or 217 yards) of tow per minute, and this rate of delivery should be controllable. In addition, the length of the cut segments should be varied from 1.27 cm to 7.62 cm (0.5 inches to 3 inches), and the orientation of the strands relative to the preform should be controllable. These specifications were provided by Barron (1993).

In contrast to current delivery systems, in which a pair of pinch rollers shear the tow and propel it in the direction of its axis, in the proposed -- variable length -- delivery system the tow must be delivered and cut by two independently adjustable processes. The need for three phases of the process has emerged. The current report presents the design of a device which involves a multi-stage, cyclic process. Specifically, the fiber tow is drawn into the new device in three inch lengths, cut to incremental lengths of 0.5, 1.0, 1.5, ..., 3 inches, and blown onto the preform. Note that this selection of the incremental lengths can be made independently for each cycle of the device's operation.

Furthermore, the new process will better control the orientation of the strands relative to the preform. The strands shall be delivered, via a narrow channel, with the channel outlet perpendicular to the strands' direction of motion. The strands will be propelled through the channel with a high speed air flow. In order to vary the orientation of the

strands on the preform, a mechanism to permit relative motion between the exit of the channel and the preform will be used. Any combination of motions between the delivery device and the preform itself will suffice; however, because of the complexity of the fiber cutting and delivering device, the first generation design will involve a stationary fiber chopper. Hence, provision to move the preform with respect to the fixed delivery channel is an implicit attribute of this first generation design. The proposed delivery process is illustrated in figure 3.

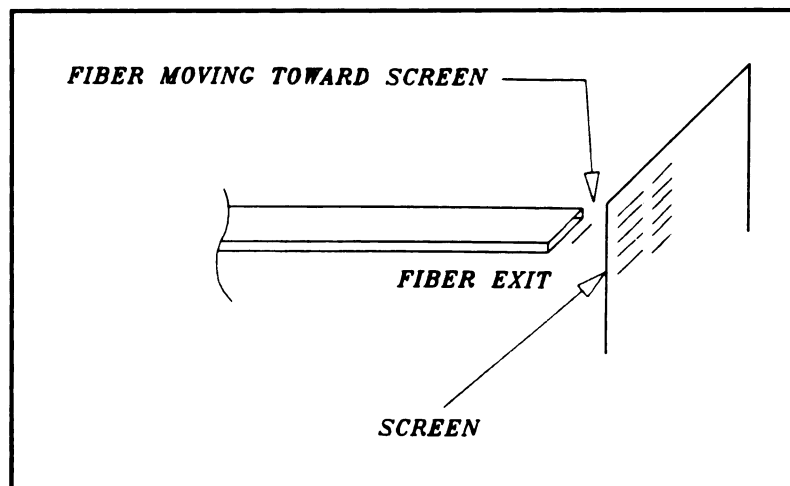


Figure 3: Illustration of proposed delivery process

The need for a new delivery device for use in the preforming process has been established. The task of conceiving a new device and/or process is a large one. It is useful to think of the overall design as a sequence of smaller design phases. A design algorithm is given in Design Creativity, by B. S. Thompson, and is shown below in figure 4. This procedure is useful for the description of the design of the fiber chopper.

As shown in figure 4, the first step of the design process is the recognition of the need. The need was described in the first several paragraphs of this chapter. The second

phase of the design process involves the problem definition. This was crucial to the present work. Before the present design work began, a group of seniors at Michigan State University had designed a chopper for the same purpose. However, the problem was defined somewhat differently from that in the present work. In their work, the problem definition stated that the chopper should be suitable for mounting on a robot arm.

The problem definition for the present work can be stated as follows:

**"Design a device which will cut fibers to a variable length, and deliver the tow segments in a manner suitable for direction controlled preforming. Furthermore, the device should be capable of delivering at least 1 lb<sub>m</sub> of fiber per minute, and the length of chopped strands should be changeable without delaying the process."**

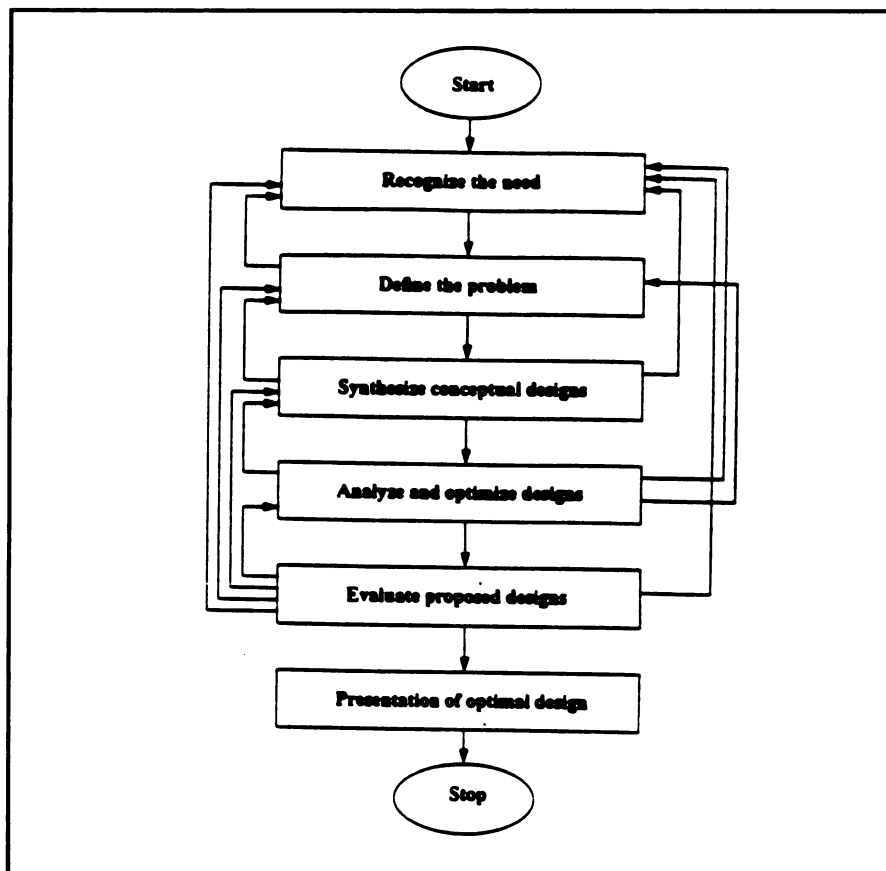


Figure 4: The design algorithm (Thompson).

Delivering the tow segments "in a manner suitable for direction controlled preforming" is a fairly broad statement. Although current designs use a robot arm to spray the chopped strands on to the preform, this is not the required course of action. It is possible to move the preform relative to the fiber delivery device (Barron). The stands' orientation would then be controlled by delivering them via a narrow channel, rather than a tube, as was described previously. Recall that the length of the cut tow segments did not need to be continuously variable (i.e., 1/2" intervals is adequate).

After defining the problem, designs were synthesized, and one was chosen. This design was analyzed in detail, and a portion of it was manufactured for evaluation. The evaluation provided valuable insights, but ultimately proved that design to be inadequate. Therefore, the second iteration of the design algorithm started with the synthesis of design II. This paper will focus on the synthesis and analysis of design II. For those readers interested in the evolution of the design, or the design process, the synthesis, analysis, and evaluation of the initial design are located in appendices B, C, and D respectively. Hence, if the reader wished to follow the design chronologically he/she should read chapter 1, then appendices B, C, and D, before moving on to chapter 2.

## CHAPTER 2 -- SYNTHESIS OF DESIGN II

The synthesis of design II is presented in this chapter. Portions of the design are presented schematically; detailed drawings are not shown. Chapters 3, 4, and 5 examine the intake process, the cutting mechanism, and the delivery channel in considerable detail. As described in chapter 1, the process will be a cyclic one, consisting of three phases (intake, cut, and delivery). The delivery process was described in the Introduction; recall that the fibers' orientations are controlled by using a high speed airflow to propel the strands through a narrow channel. The syntheses of the fiber intake and cutting processes are the focus of this chapter.

In the existing fiber choppers, the fibers are drawn into the device and cut by the same mechanism (i.e., a pair of pinch rollers, one of which is embedded with blades). In contrast, the fibers must be pulled into the device and cut by two distinct mechanisms in order to independently control the rate of fiber intake and the length of cut fibers. Two pairs of pinch rollers and an entraining air flow will be used to pull the fibers into the device and position them for the cutting process. The first pair of pinch rollers will be driven continuously to pull the tows from the spools, at a constant rate, and feed them to the device. The second pair of pinch rollers will be driven intermittently, via a four slot external Geneva mechanism. The Geneva mechanism provides an intermittent rotation of 90 degrees for every 180 degrees of input rotation. Manufacturers of the Geneva mechanism indicate a maximum input rotational speed of 300 rpm. Schematics of a

Geneva mechanism and the intake mechanism as a whole are shown in figures 5 and 6, respectively.

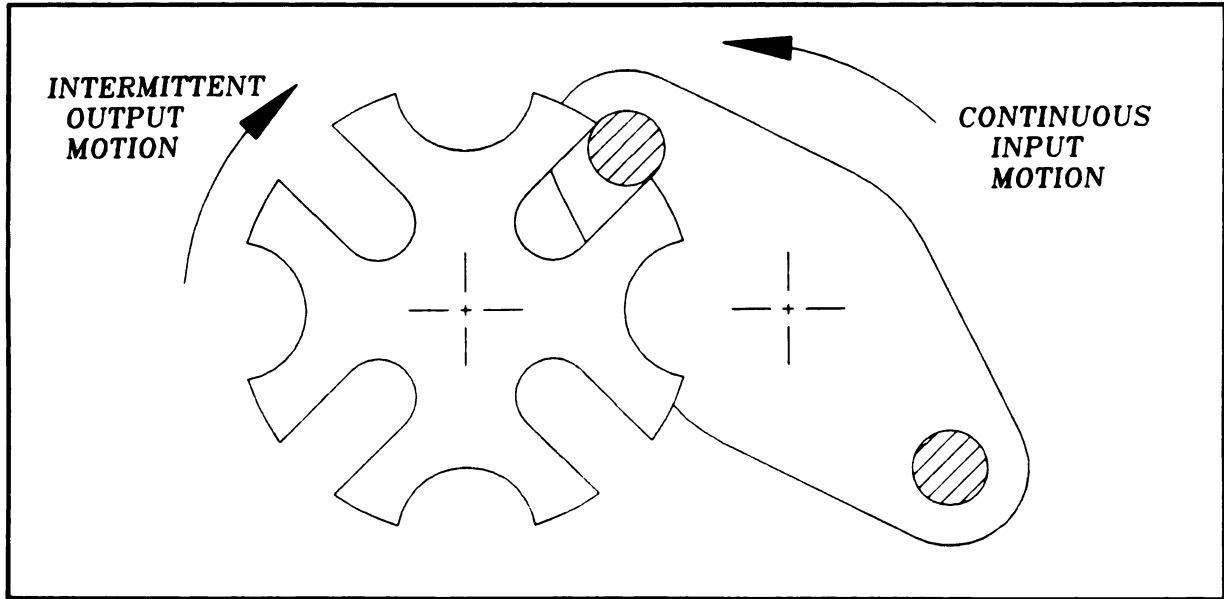


Figure 5: Schematic of 4-slot external Geneva mechanism

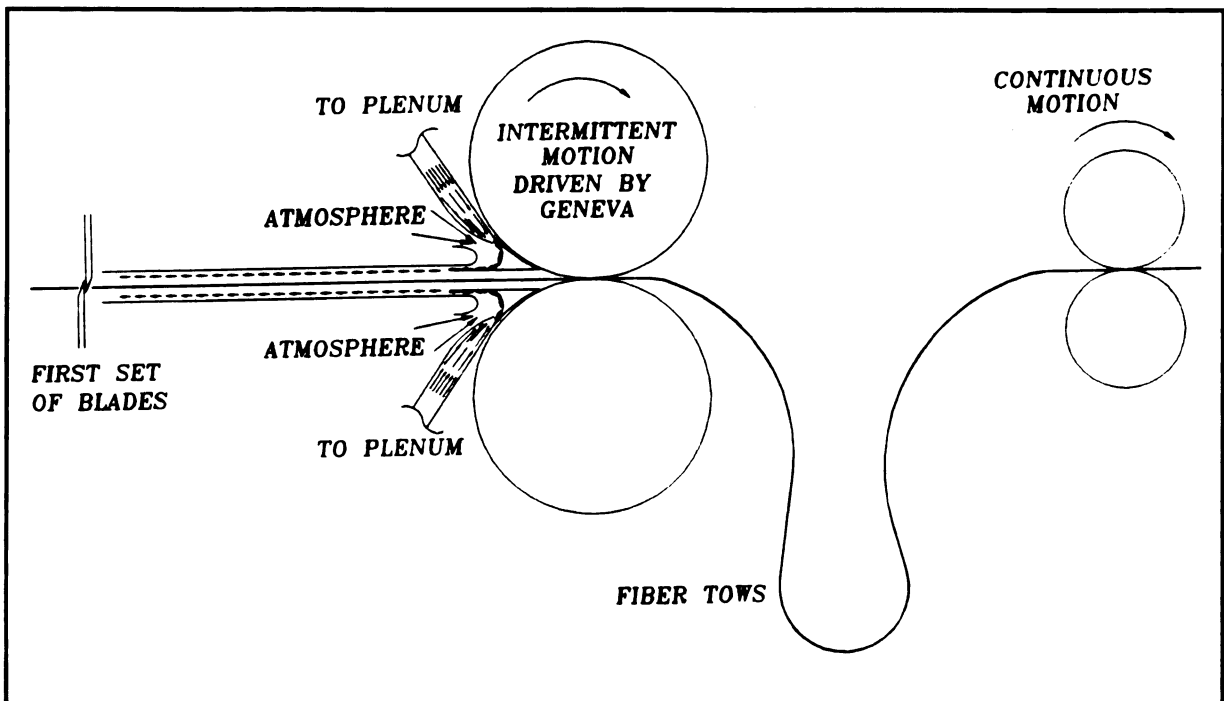


Figure 6: Schematic of fiber intake mechanism

Multiple tows must be fed to the device simultaneously to achieve the goal of



depositing 0.454 kg (1.0 lb<sub>m</sub>) of fiber per minute. Recall that each tow is pulled a distance of 7.62 cm into the device, for each cycle. The Geneva mechanism has a maximum operating speed of 300 rpm, but completes two tow delivery cycles per input revolution. Hence, if there are “n” tows being fed to the device, and “M” is the rate of fiber deposition, having units of lb<sub>m</sub> per minute, then:

$$\frac{M \cdot \text{lb}_m}{\text{min}} = \left( \frac{600 \cdot \text{cycles}}{\text{min}} \right) \left( \frac{7.62 \cdot \text{cm}}{\text{tow} \cdot \text{cycle}} \right) \left( \frac{\text{m}}{100 \cdot \text{cm}} \right) \left( \frac{\text{lb}_m}{198 \cdot \text{m}} \right) n \cdot \text{tows}$$

Simplifying yields  $M=0.23n$ . Therefore, the minimum number of tows (to achieve the goal of depositing one pound of fiber per minute) is 5.

Each of the five tows will travel through one of five (1/2 inch diameter) cylinders. An entraining airflow will be used to propel the fiber strands through each cylinder, and into position for the cutting process, as shown in figure 6. This entraining flow actually serves two purposes. First, it propels the strands through the inlet tube. Subsequently, it holds the strands in a horizontal position for the cutting process, which is described below.

The system of parts used to cut the fiber tows is termed the “cutting mechanism”. A shearing action will be used to sever the fiber tows once they have been drawn into the device. The tows are held in place by the aforementioned entraining airflow, and are constrained by the pinch rollers being driven by the Geneva mechanism.. The shearing force will be generated by a pair of sharp edged blades, hinged at one point (similar to a pair of scissors). This shearing action has the advantage of maintaining contact between the “leading edge” of the cutting surfaces (note the shearing action proposed for design I lacked this quality). This process is shown schematically in figure 7. The blades rotate about 6 degrees during each cycle of operation.

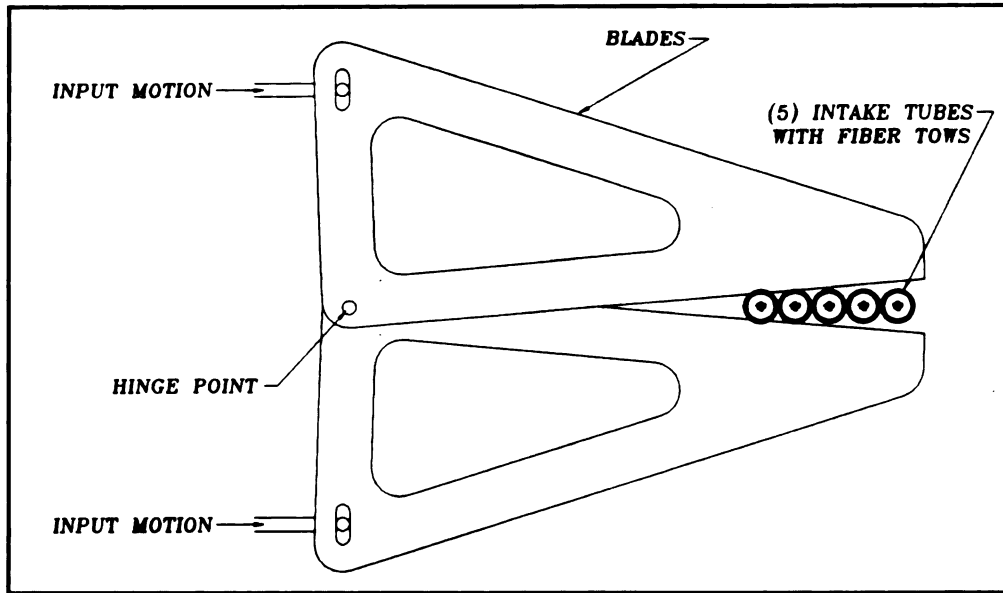


Figure 7: Schematic of fiber cutting process.

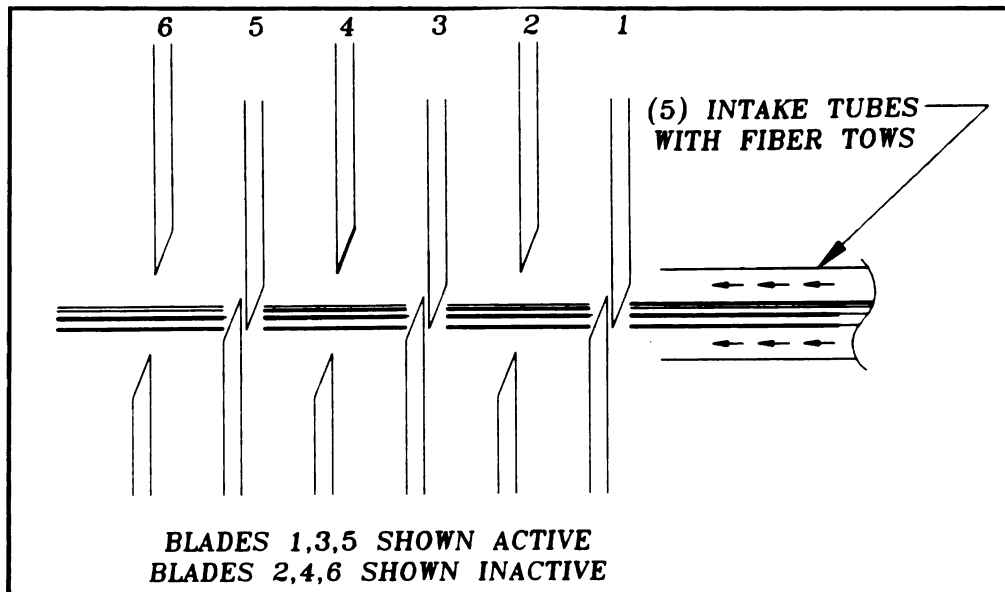


Figure 8: Multiple blade arrangement.

A row of six pairs of blades on 1/2 inch intervals will be used to modify the length of the cut tow segments (see figure 8). The first pair of blades will always be active. Any desired combination of the other five pairs of blades can be selected for use during each cycle of operation. Recall that three inches of each tow are pulled into the device for each

cycle. It follows that any combination of multiples of 1/2 inch that add up to 3 inches may be cut during each cycle of operation. For example, the device could cut (6) 1/2 inch pieces, (1) 3 inch piece, (3) 1 inch pieces, (1) 1 inch and (4) 1/2 inch pieces, etc.

There are two reasons to have the first set of blades be active for every cycle of operation. First, all combinations which add to three inches utilize the first set of blades. An additional benefit of always using the first set of blades, is that when they are closed, they isolate the cut segments from the entraining flow. Once the tows have been cut, the entraining flow is blocked by the first set of blades. The impulse flow then propels the cut fibers through the delivery channel, and out of the device.

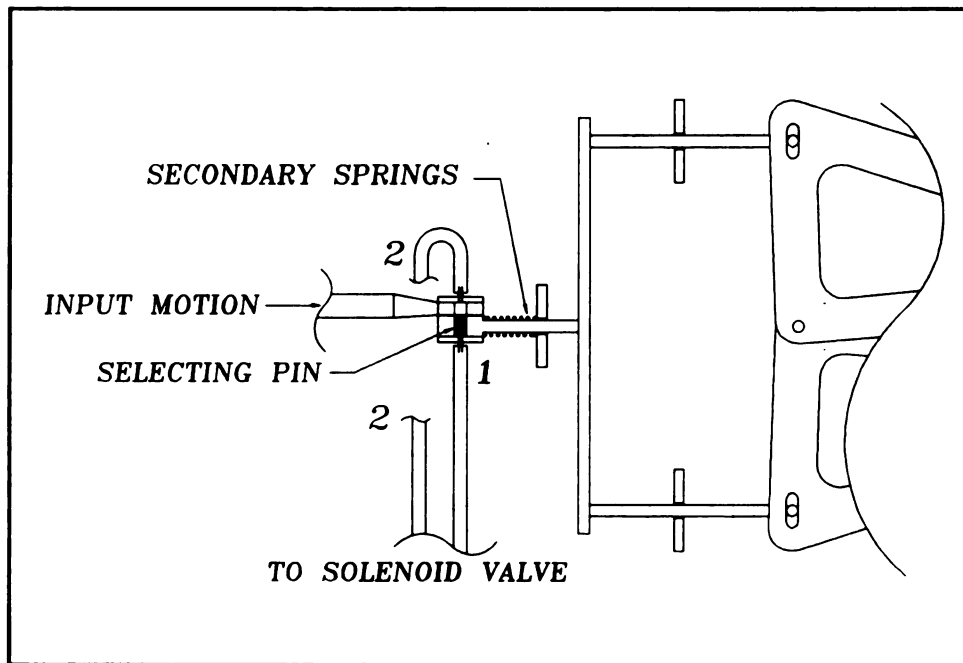


Figure 9: Blade selection process.

Several methods were synthesized to select the blade combination during each cycle of operation. The chosen method involves the use of a pneumatically controlled

selecting pin. Each of the five selecting pins is controlled by a solenoid valve (as shown in figure 9). The input motion is driven by a cam-follower system. The two-way valve can cause either line 1 or line 2 to be pressurized (with the other line open to the atmosphere). If line 1 is pressurized and line 2 is at atmospheric pressure, the selecting pin is forced to the “active” position. Conversely, if line 2 is pressurized and line 1 is at atmospheric pressure, the selecting pin is forced to the “inactive” position.

A feasible process has been synthesized. This process first pulls three inches of tow from each of five spools into the device. Then any combination of the six sets of blades (with the first set always active) is chosen. The fiber tows are then cut into segments of the appropriate lengths. Finally, an impulsive air flow is used to propel the fibers out of the device in the desired fashion. The analysis of the intake, cutting, and delivery processes are described in the next three chapters, respectively.

### CHAPTER 3 -- ANALYSIS OF DESIGN II INTAKE MECHANISM

The analysis of the intake mechanism for design II is presented in two sections in this chapter. First, the kinematics of the Geneva mechanism are discussed. Then, the entraining flow around the strands within each of the delivery tubes is examined. Properties of the tow (drag coefficient and effective surface area) are found experimentally, and the dynamics of the intake process are investigated. The results yield the position, velocity, and acceleration of the incoming tows as functions of the entraining flow velocity and phase angle of the Geneva mechanism (for an input rotational speed of 300 rpm).

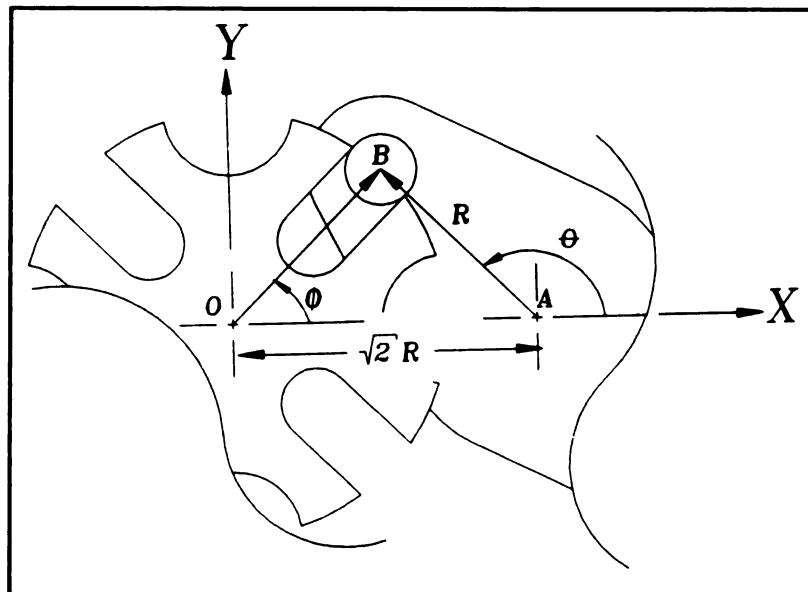


Figure 10: Schematic of Geneva mechanism for analysis

The vector position equation (sometimes termed the "loop closure equation") can be expressed as follows:

$$(1) \quad \vec{R}_{B/O} = \vec{R}_{A/O} + \vec{R}_{B/A}, \forall \theta \text{ s.t. } \theta \in [135^\circ, 225^\circ]$$

where,

$$\begin{aligned} \vec{R}_{B/O} &= R_{B/O} \hat{R}_{B/O} \\ \vec{R}_{A/O} &= \sqrt{2}R \hat{i} \\ \vec{R}_{B/A} &= R \hat{R}_{B/A} \\ \hat{R}_{B/O} &= \cos(\phi) \hat{i} + \sin(\phi) \hat{j} \\ \hat{R}_{A/O} &= \hat{i} \\ \hat{R}_{B/A} &= \cos(\theta) \hat{i} + \sin(\theta) \hat{j} \end{aligned}$$

Note that the " ^ " notation is used to denote a unit vector, and  $\hat{i}$  and  $\hat{j}$  are unit vectors in the X and Y directions, respectively.

Taking the dot product of equation (1) with  $\hat{i}$  yields:

$$(2) \quad R_{B/O} \cos(\phi) = R\sqrt{2} + R \cos(\theta), \forall \theta \text{ s.t. } \theta \in [135^\circ, 225^\circ]$$

Similarly, taking the dot product of equation (1) with  $\hat{j}$  yields:

$$(3) \quad R_{B/O} \sin(\phi) = R \sin(\theta), \forall \theta \text{ s.t. } \theta \in [135^\circ, 225^\circ]$$

Summing the squares of equations (2) and (3), and using the identity,  $\sin^2(\theta) + \cos^2(\theta) = 1$ , results in equation (4).

$$(4) \quad (R_{B/O})^2 = R^2 [3 + 2\sqrt{2} \cos(\theta)], \forall \theta \text{ s.t. } \theta \in [135^\circ, 225^\circ]$$

Hence,

$$(5) \quad R_{B/O} = R \sqrt{3 + 2\sqrt{2} \cos(\theta)}, \forall \theta \text{ s.t. } \theta \in [135^\circ, 225^\circ]$$

It is convenient to define a variable, "Z", as follows:

$$(6) \quad Z \equiv \sqrt{3 + 2\sqrt{2} \cos(\theta)}$$

therefore,

$$(7) \quad \dot{Z} = \frac{-\dot{\theta}\sqrt{2} \sin(\theta)}{\sqrt{3 + 2\sqrt{2} \cos(\theta)}} = -Z^{-1} \dot{\theta}\sqrt{2} \sin(\theta)$$

Substituting (5) and (6) into (3) and simplifying gives  $\sin(\phi)$  as a function of  $\theta$ , as shown in equation (8), below.

$$(8) \quad \sin(\phi) = \frac{\sin(\theta)}{Z}, \quad \forall \theta \text{ s.t. } \theta \in [135^\circ, 225^\circ]$$

Differentiating both sides of (8) with respect to time, yields equation (9).

$$(9) \quad \dot{\phi} \cos(\phi) = Z^{-1} (\dot{\theta}) \cos(\theta) - Z^{-2} \sin(\theta) \dot{Z}$$

Substituting (7) into (9) yields:

$$(10) \quad \dot{\phi} \cos(\phi) = (\dot{\theta}) [Z^{-1} \cos(\theta) + Z^{-3} \sqrt{2} \sin^2(\theta)]$$

Differentiating (10) yields:

$$(11) \quad \ddot{\phi} \cos(\phi) - (\dot{\phi})^2 \sin(\phi) = (\ddot{\theta}) [Z^{-1} \cos(\theta) + Z^{-3} \sqrt{2} \sin^2(\theta)] \\ + (\dot{\theta}) [-Z^{-2} \cos(\theta) \dot{Z} - Z^{-1} (\dot{\theta}) \sin(\theta) - 3 Z^{-4} \sqrt{2} \sin^2(\theta) \dot{Z} \\ + Z^{-3} (\dot{\theta}) 2\sqrt{2} \sin(\theta) \cos(\theta)]$$

If the mechanism is operating at a constant input speed, then  $(\ddot{\theta})$  is zero. Using  $(\ddot{\theta}) = 0$ , and using (7) to substitute for  $\dot{Z}$  in (11) yields:

$$(12) \quad \ddot{\phi} \cos(\phi) - (\dot{\phi})^2 \sin(\phi) = (\dot{\theta})^2 Z^{-1} \sin(\theta) [6 Z^4 \sin^2(\theta) + 3\sqrt{2} Z^2 \cos(\theta) - 1]$$

The Geneva Mechanism turns the pinch rollers through 90 degrees for each cycle, and the tows should be pulled 3 inches; hence, the circumference of the pinch rollers should be 12 inches, and the radius should be  $6/\pi$  inches, or  $1/(2\pi)$  feet. According to the manufacturers, the Geneva mechanism has a maximum input rotational speed of 300 rpm. Hence,  $(\dot{\theta}) = 10\pi$  rad/sec. The desired results are the position, velocity, and acceleration of the incoming tows at the point of contact with the pinch rollers. Assuming that there is no slip between the tows and the rollers, the distance traveled by each tow is equal to the arc length traveled by the driving pinch roller (see figure 11).

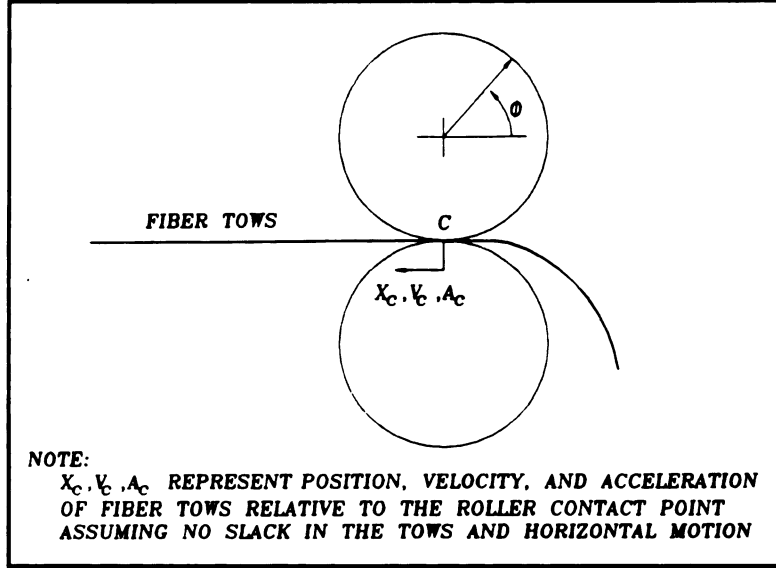


Figure 11: Schematic of tows at pinch rollers.

The kinematics of the incoming tows, pulled by the Geneva mechanism, are summarized in equations (13) through (15) below:

$$(13) \quad x_c = R (\phi - \pi/4) ; \text{ i.e., } x_c = 0 \text{ when } \phi = 45 \text{ degrees.}$$

$$(14) \quad v_c = R\dot{\phi} = \frac{R\dot{\theta}}{\cos(\phi)} \left[ Z^{-1} \cos(\theta) + \sqrt{2}Z^{-3} \sin^2(\theta) \right]$$

$$(15) \quad a_c = R\ddot{\phi} = \frac{R}{\cos(\phi)} \left\{ \dot{\phi}^2 \sin(\phi) + \dot{\theta}^2 Z^{-1} \sin(\theta) \left[ 6Z^{-4} \sin^2(\theta) + 3\sqrt{2}Z^{-2} \cos(\theta) - 1 \right] \right\}$$

where  $\phi$  and  $Z$  are known functions of  $\theta$ , as given by equations (6) and (8).

Equations (13), (14), and (15) are solved for each degree of  $\theta$ , for all  $\theta$  between 135 and 225 degrees (i.e., when the driven wheel is engaged), and results are plotted in the following three figures.



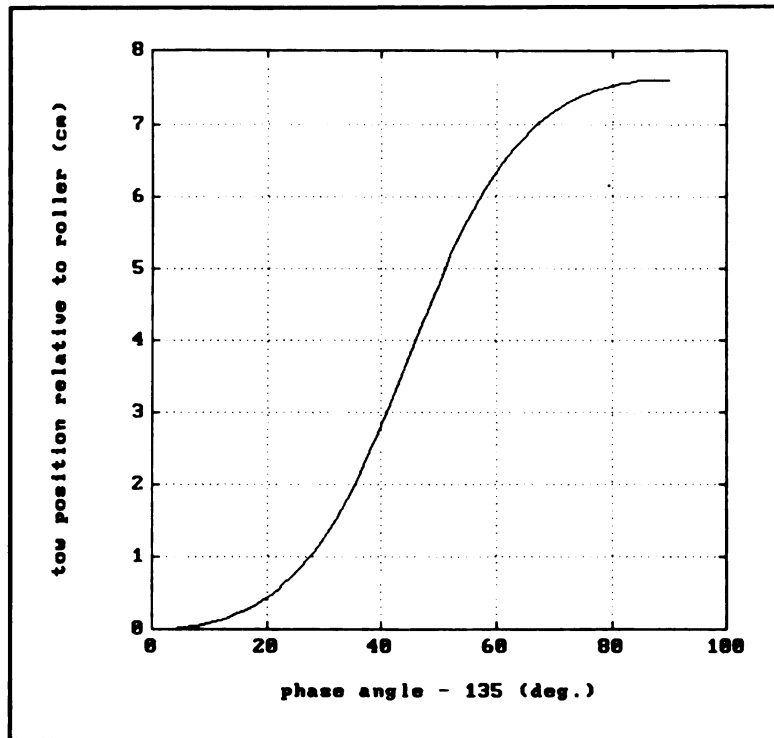


Figure 12: Position of tows at roller contact point vs.  $\theta$

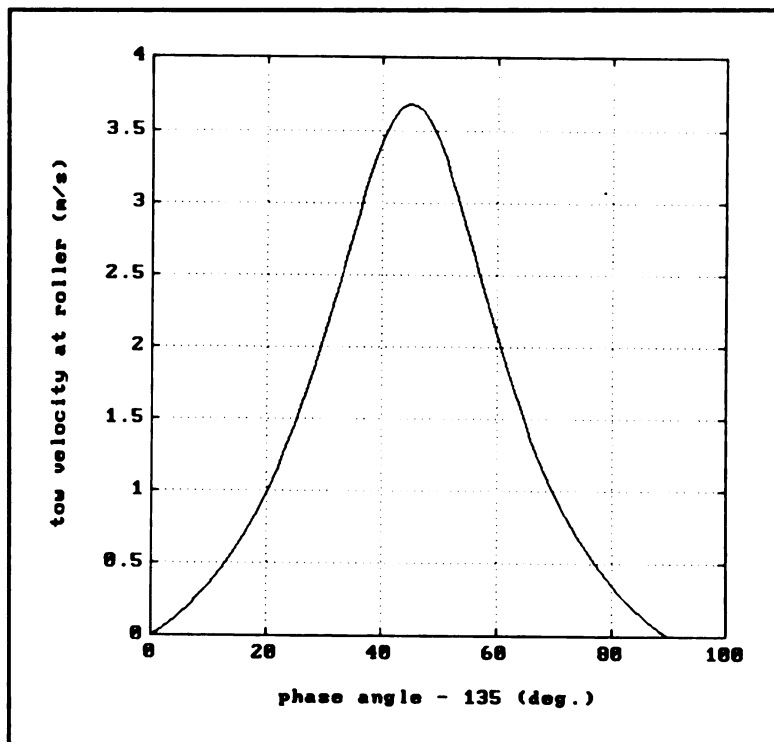


Figure 13: Velocity of tows at roller contact point vs.  $\theta$

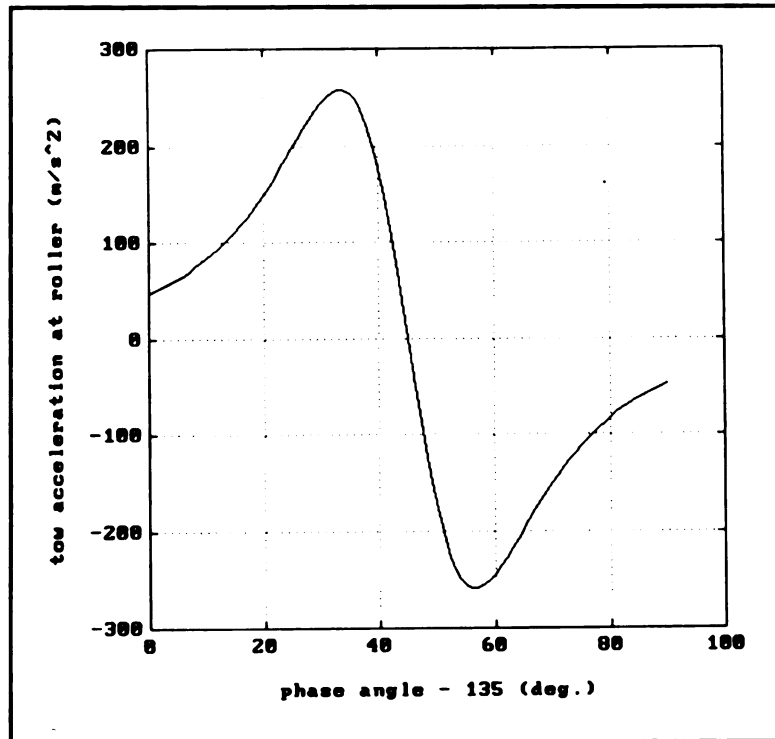


Figure 14: Acceleration of tows at roller contact point vs.  $\theta$

The kinematics of the tows at the roller contact point ( $x_c$ ,  $v_c$ , and  $a_c$ ) have been completely determined. The objective of the analysis is to determine the kinematics of the tows as they move between the blades. If there is no slack in the tows, then the motion between the blades is identical to that at the roller contact point. The following analysis presents a method to determine the kinematics of the tows, at the outlet of the entraining flow tubes ( $x_{tow}$ ,  $v_{tow}$ , and  $a_{tow}$ ) as functions of  $v_{air}$ ,  $x_c$ ,  $v_c$ , and  $a_c$ . The objective is to estimate the air velocity required to provide a sufficient drag force on the incoming tows. The tows must be pulled into position in a maximum of 90 degrees of phase, or 0.05 seconds if operating at 300 rpm. The analysis will examine the amount of slack in the tows between the outlet and the rollers. A schematic of the process is shown in figure 15.

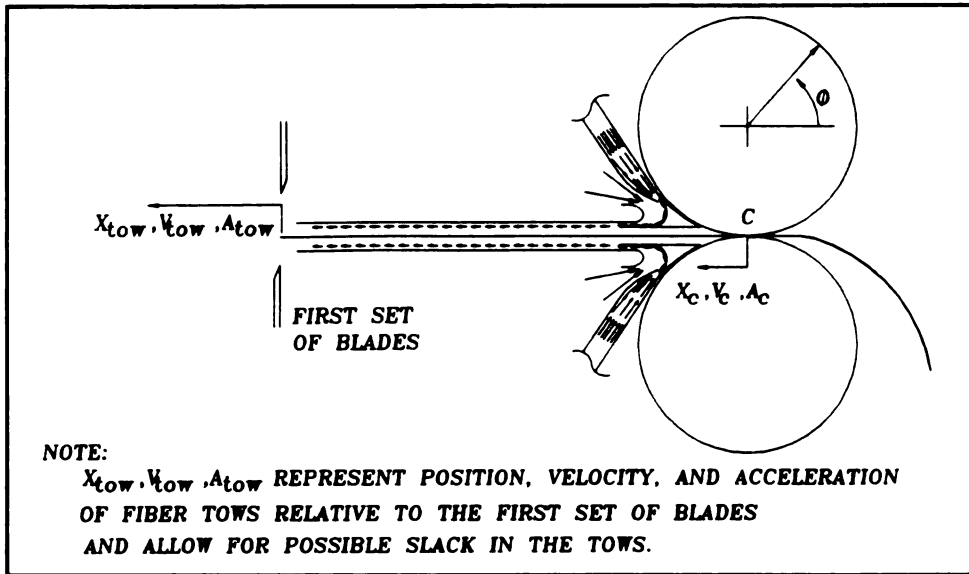


Figure 15: Schematic of tow intake process.

The acceleration of the tow at the outlet of the entraining flow tube will be determined using a numeric algorithm, for a given air velocity. This acceleration will then be integrated once to determine the tow velocity and again to determine the position of the tows relative to the outlet. Note that  $x_{tow}$  can not exceed  $x_c$  (assuming no slip). Furthermore, when  $x_{tow} = x_c$ ,  $v_{tow}$  can not exceed  $v_c$ , and  $a_{tow}$  can not exceed  $a_c$  (see figure 15). Initially, all positions, velocities, and accelerations of the tows are zero. The above is conducive to an iterative procedure which checks the constraints at each time step. A program was written for Matlab to perform this procedure. The program is entitled “INTAKE”, and is shown in appendix E. The equations which are used in the algorithm are developed, and the results are shown, in the remainder of this chapter.

The acceleration of the tows at the first set of blades (as shown in figure 15) can be expressed as follows:

$$(17) \quad a_{tow} = \frac{F_D}{m_{tow}}$$

The mass of the tow being pulled is the product of the tow's linear strand density, " $\rho_l$ ", and the length of the tow, "L". As mentioned in the introduction, 198 m (217 yards) of tow has a mass of 0.454 kg (1.00 lb<sub>m</sub>). Hence,

$$(18) \quad \rho_l = \frac{0.454 \text{ kg}}{198 \text{ m}} = 2.29 \text{ g / m}$$

We can express the drag force on the tow as follows:

$$(19) \quad F_D = 0.5 \rho_{\text{air}} (v_{\text{air}} - v_{\text{tow}})^2 A_s C_D$$

Substituting (19) into (17) yields an expression for acceleration, shown below.

$$(20) \quad a_{\text{tow}} = 0.5 \rho_{\text{air}} (v_{\text{air}} - v_{\text{tow}})^2 C_D \left( \frac{A_s}{m_{\text{tow}}} \right)$$

The surface area over which the drag force is applied, " $A_s$ ", is not well defined due to the stranded nature of the tow. Equation 20 must be simplified, in order to obtain a form which will allow the necessary parameters to be obtained experimentally. The effective surface area is expressed as the product of an effective circumference, " $\zeta$ ", and the length of the channel. Since  $A_s = (\zeta L)$  and  $m_{\text{tow}} = (\rho_l L)$ , the right hand side of (20) can be simplified to eliminate the length of tow from the equation. Hence, the acceleration of the tow can be expressed as

$$(21) \quad a_{\text{tow}} = 0.5 \rho_{\text{air}} (v_{\text{air}} - v_{\text{tow}})^2 C_D \left( \frac{\zeta}{\rho_l} \right)$$

An experiment was performed to obtain a numerical value for the product  $C_D \zeta$ . A piece of conduit, cut to 15.24 cm (6 inches), was used to simulate the entrance tube. A piece of fiber glass tow was cut to 45.72 cm (18 inches), and the strands were taped together at one end. The tow was inserted into the plenum, through the conduit, with the taped end at the bottom. The experimental setup is shown in figure 16. Holding the top

of the strands one inch above the tube outlet, the pressure difference between the plenum and the atmosphere was slowly increased until the drag force on the tow was sufficient to suspend it in the air stream. Hence, the drag force was equal to the known weight of the tow, “W”. This relationship is shown in equation 22, below.

$$(22) \quad W = F_D = 0.5 \rho_{\text{air}} (v_{\text{air}} - v_{\text{tow}})^2 L \zeta C_D$$

In the experiment,  $L = 17.8 \text{ cm}$  (i.e., 7 inches)  
 $v_{\text{tow}} = 0 \text{ m/s}$   
 $W = 0.015 \text{ N}$  (i.e., 0.00337  $\text{lb}_f$ )

Simplifying yields equation 23, shown below.

$$(23) \quad C_D \zeta = (0.0085 \text{ N/m}) \left[ \frac{1}{(0.5)(\rho_{\text{air}})(v_{\text{air}})^2} \right]$$

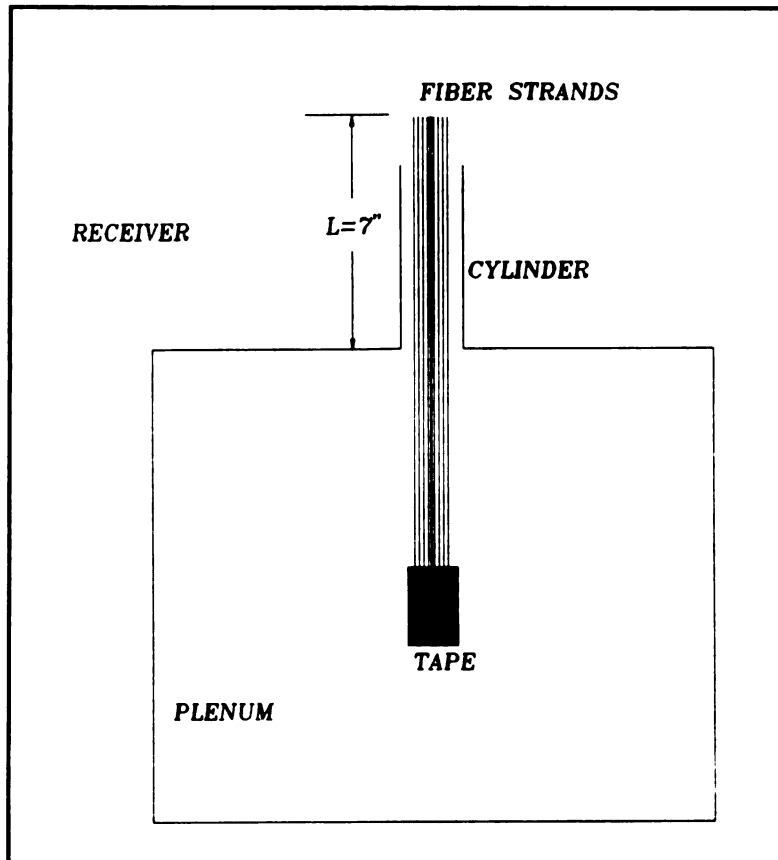


Figure 16: Schematic of experimental setup to determine drag properties.

If the air flow is approximated as an inviscid one, and gravitational effects on the flow are neglected, then Bernoulli's equation yields:

$$(24) \quad \Delta P = (0.5)(\rho_{\text{air}})(v_{\text{air}})^2$$

The pressure difference that successfully suspended the fibers strands in the air stream was measured as 3.48 MPa. Substituting (24) into (23) and simplifying yields the numerical value for  $C_D \zeta$  as shown in (25).

$$(25) \quad C_D \zeta = 0.503 \text{ mm} = 0.00165 \text{ ft}$$

The data used in the above equations reflects the median result. In each of the four other data sets taken, the value for  $C_D \zeta$  was within 10% of the value indicated in equation 25.

The linear density of the tow was determined in (18) to be 2.29 g/m ( $4.77 \times 10^{-5}$  slugs/ft). The density of air at room temperature, and atmospheric pressure, is approximately 0.00233 slugs/ft<sup>3</sup>. Using (25), the density of air, and the linear strand density of the fiber tows, we can evaluate the quantity  $\frac{0.5\rho_{\text{air}}C_D\zeta}{\rho_l} = 0.131 \text{ m}^{-1} = 0.040 \text{ ft}^{-1}$ .

Hence, we can simplify (21) to yield,

$$(26) \quad a_{\text{tow}} = (v_{\text{air}} - v_{\text{tow}})^2 (0.131 \text{ m}^{-1})$$

The position and velocity of the tows are shown graphically for four different air velocities in figures 17 and 18, respectively. As shown, when the air velocity reaches 42.7 m/s (140 fps), there is no slack in the tows. For an air velocity of 36.6 m/s (120 fps) the maximum slack is only about 6 mm (1/4 inch). Hence, the analysis presented in this chapter has shown that for an operating speed of 300 rpm (input to the Geneva mechanism) the entraining flow should have a velocity of about 42.7 m/s (140 fps). Since the analysis does not include the effects viscosity of the air jet leaving the tube, the result

should be provided with a factor of safety. An increase of 30% should provide a sufficient margin for error. Hence, we can say with confidence that an entraining flow of 55.5 m/s (182 fps) is sufficient to prevent slack in the tows.

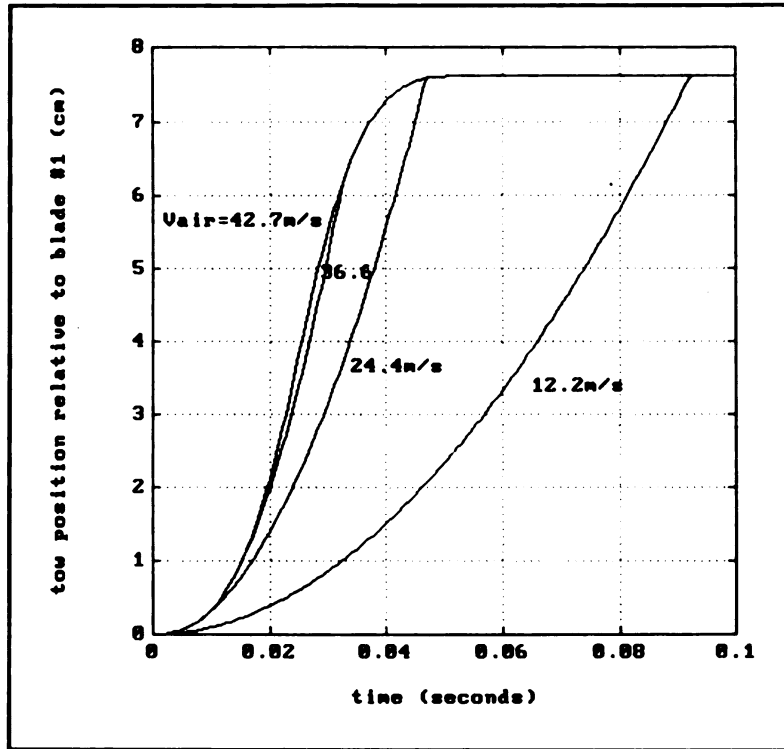


Figure 17: Position of tows as a function of time, for various air velocities.

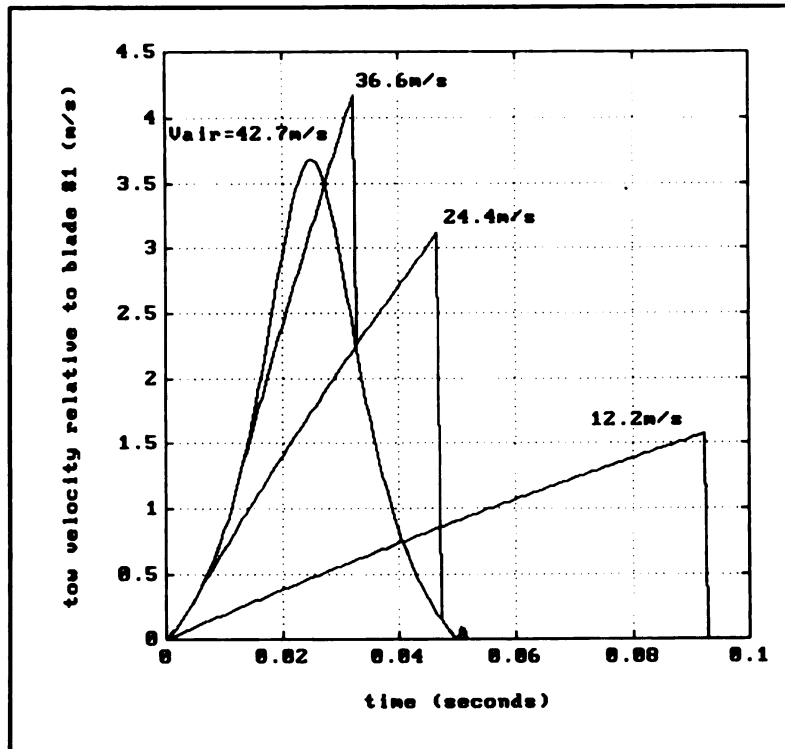


Figure 18: Velocity of tows as a function of time, for various air velocities.



## CHAPTER 4 -- ANALYSIS OF DESIGN II CUTTING MECHANISM

The system of parts used to cut the fiber glass tows is termed the “cutting mechanism”. The cutting mechanism consists of six pairs of blades which are each hinged on a common rod (similar to six pairs of scissors), five selecting pins (each controlled by a solenoid valve), 6 springs, and a cam-follower system. The blade mechanism is shown schematically in figure 19, below. This chapter details the design of the cam-follower system, and explains the choice of springs. A modern approach to the cam design is developed and executed using Matlab. The analysis is presented in three steps. First, the desired follower motion is derived. Second, the cam is designed for the desired motion. Finally, the appropriate springs are chosen.

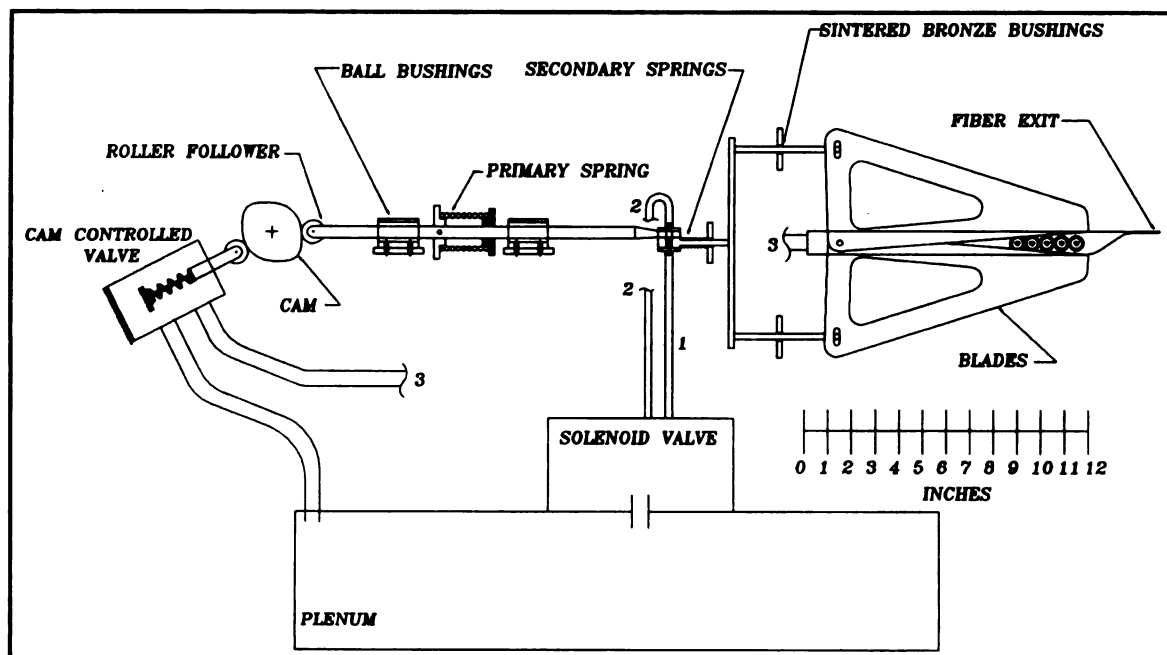


Figure 19: Schematic of cutting mechanism.

A roller follower will be used in order to reduce wear and noise. The roller will have a radius of 1.27 cm (0.5 inches). Furthermore, the motion curve will have continuous curves for position, velocity, acceleration, and jerk (also to minimize wear). The intake of the fibers requires 90 degrees of phase angle (recall one cycle corresponds to 180 degrees for the Geneva mechanism); the blades closing and opening will be allowed 45 degrees each. The cam is designed to complete two cycles per revolution, and therefore will also operate at 300 rpm. The cycle timing chart is shown in table 1 below.

PHASE ANGLE (DEGREES)	OPERATION
0 - 90	FIBER INTAKE (GENEVA ACTIVE)
90-135	BLADES CONVERGE (CUT TOWS)
110-155	IMPULSE FLOW PROPELS FIBERS OUT OF MECHANISM
135-180	BLADES RETURN TO ORIGINAL POSITION

Table 1: Cycle timing chart (design II)

### STEP 1: DERIVATION OF FOLLOWER MOTION

The above cycle timing chart requires a Dwell-Rise-Return motion program. The rise and the return are both of amplitude 6.35 mm (0.25 inches), and both occur in 45 degrees of the cam's motion (25 ms at 300 rpm). A seventh order polynomial (i.e., one having eight arbitrary coefficients) is used to determine a rise motion which is continuous, and has first, second, and third derivatives equal to zero at both end points. The polynomial is first determined in a non-dimensionalized form, to simplify the equations, then scaled to fit this problem.

If “Y” is the non-dimensionalized displacement, and “ $\bar{\theta}$ ” is the non-dimensionalized phase angle, such that  $Y \in [0,1]$  and  $\bar{\theta} \in [0,1]$ , then  $Y=f(\bar{\theta})$  and the boundary conditions are:

$$\begin{aligned}
(27) \quad & f(0)=0 \\
(28) \quad & f'(0)=0 \\
(29) \quad & f''(0)=0 \\
(30) \quad & f'''(0)=0 \\
(31) \quad & f(1)=1 \\
(32) \quad & f'(1)=0 \\
(33) \quad & f''(1)=0 \\
(34) \quad & f'''(1)=0
\end{aligned}$$

and the arbitrary 7th order polynomial is given by

$$(35) \quad Y = f(\bar{\theta}) = C_0 + C_1 \bar{\theta}^1 + C_2 \bar{\theta}^2 + C_3 \bar{\theta}^3 + C_4 \bar{\theta}^4 + C_5 \bar{\theta}^5 + C_6 \bar{\theta}^6 + C_7 \bar{\theta}^7$$

Differentiating (35) three times with respect to  $\bar{\theta}$  yields expressions for  $Y'$ ,  $Y''$ , and  $Y'''$ :

$$(36) \quad Y' = f'(\bar{\theta}) = C_1 \bar{\theta} + 2C_2 \bar{\theta}^1 + 3C_3 \bar{\theta}^2 + 4C_4 \bar{\theta}^3 + 5C_5 \bar{\theta}^4 + 6C_6 \bar{\theta}^5 + 7C_7 \bar{\theta}^6$$

$$(37) \quad Y'' = f''(\bar{\theta}) = 2C_2 + 6C_3 \bar{\theta} + 12C_4 \bar{\theta}^2 + 20C_5 \bar{\theta}^3 + 30C_6 \bar{\theta}^4 + 42C_7 \bar{\theta}^5$$

$$(38) \quad Y = f'''(\bar{\theta}) = 6C_3 + 24C_4 \bar{\theta} + 60C_5 \bar{\theta}^2 + 120C_6 \bar{\theta}^3 + 210C_7 \bar{\theta}^4$$

Substituting boundary conditions (27), (28), (29), and (30) into equations (35), (36), (37), and (38), respectively, yields

$$(39) \quad C_0 = 0$$

$$(40) \quad C_1 = 0$$

$$(41) \quad C_2 = 0$$

$$(42) \quad C_3 = 0$$

Substituting the remaining boundary conditions into equations (35) through (38) yields a system of four equations for the remaining four constants. Solving the system of equations for  $C_4$ ,  $C_5$ ,  $C_6$ , and  $C_7$ , and substituting into (35) yields equation 43, below.

$$(43) \quad Y = f(\bar{\theta}) = 35 \bar{\theta}^4 - 84 \bar{\theta}^5 + 70 \bar{\theta}^6 - 20 \bar{\theta}^7$$

This is termed a “4-5-6-7 polydyne” motion in cam texts. The next step is to scale the non-dimensionalized result in (43) to the cam in the present work. The desired rise is

0.635 cm, and it requires 45 degrees ( $\pi/4$  radians). Hence,  $0.635Y=y$  and  $\bar{\theta} = 4\theta/\pi$ .

Substituting these expressions into (43) yields the desired expression for a 45 degree rise of 0.635 cm, as shown in (44).

$$(44) \quad y = 0.635 [35(4\theta/\pi)^4 - 84(4\theta/\pi)^5 + 70(4\theta/\pi)^6 - 20(4\theta/\pi)^7]$$

In the above equation,  $y$  is measured in cm and  $\theta$  in radians. Equation 44 is valid on the interval from  $\theta=0$  to  $\theta=\pi/4$ . Simplifying (44) yields:

$$(45) \quad y = 58.409 \theta^4 - 178.486 \theta^5 + 189.379 \theta^6 - 68.893 \theta^7$$

The displacement curve for the return motion is a mirror image of that for the rise motion, about the value  $\theta = \pi/4$ . The position, velocity, and acceleration curves for the rise and return motion (for an input speed of 300 rpm) are shown in the following three figures.

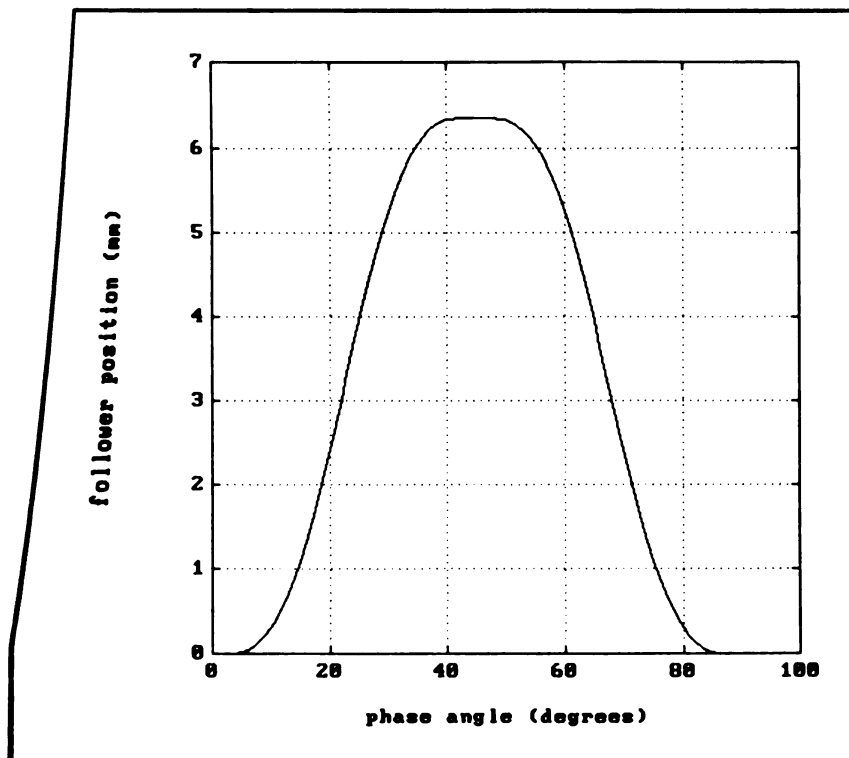


**Figure 20:** Position curve of follower during rise and return.

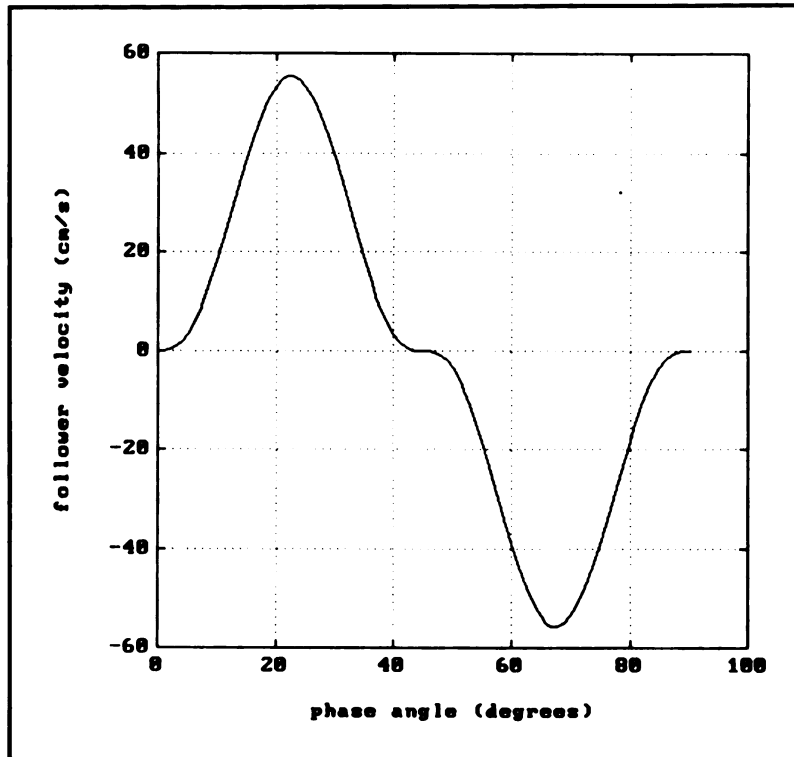


Figure 21: Velocity curve of follower during rise and return.

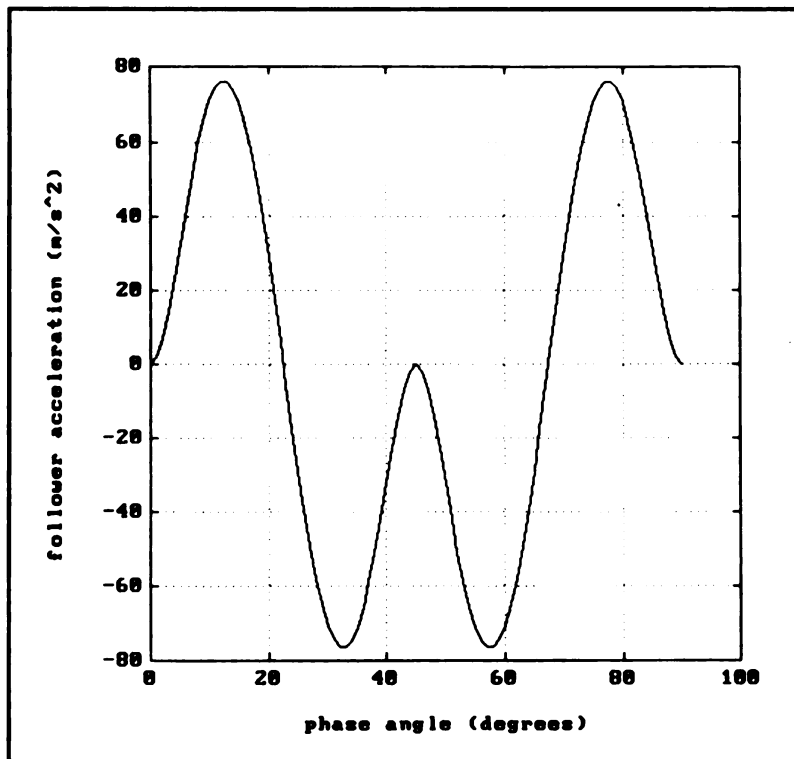


Figure 22: Acceleration curve of follower during rise and return.

## **STEP 2: CAM DESIGN**

The motion program for the follower has been determined. The next step is to derive the “pitch curve”. The pitch curve is defined as the locus of points, through which the center of the roller follower passes, during each revolution of the cam. For any given phase angle,  $\theta$ , the pitch curve has a radius of  $R + y$ , where  $R$  is the base circle radius and  $y$  is the amplitude of the follower motion at that phase angle. Once the pitch curve is found, conventional methods use a graphical technique to determine the cam profile. This graphical technique is summarized below:

**Step 1:** Draw a number of circles with their centers located on the pitch curve, each having a radius equal to that of the roller follower.

**Step 2:** Draw a curve on the inside of the pitch curve which is tangent to all of the circles which were drawn in step 1. This curve is the cam profile.

Obviously, the accuracy of the cam profile is directly proportional to the number of circles drawn in step 1. This technique is sufficient to give a qualitative representation of the cam profile, but it is not very accurate. This process can be done quickly and accurately using a personal computer. The numeric process will first be described, then executed using a Matlab program.

A curve which is tangent to a circle at a given point, is perpendicular to a radius of that circle, passing through that point. Consider curve D, which is tangent to three circles of equal radii, as shown in figure 23. The Radii of circles A, B, and C, which pass through the points tangent to D, are all normal to curve D. Next, circles A', B', and C' are drawn having the radii of circles A, B, and C, respectively, as their diameters. Curve E is drawn tangent to circles A', B', and C' at the centers of circles A, B, C. Hence, curve E passes

through the centers of circles A, B, and C and is perpendicular to their radii, as shown. If curve E is a pitch curve, then curve D must be the corresponding cam profile, as defined by the graphical method.

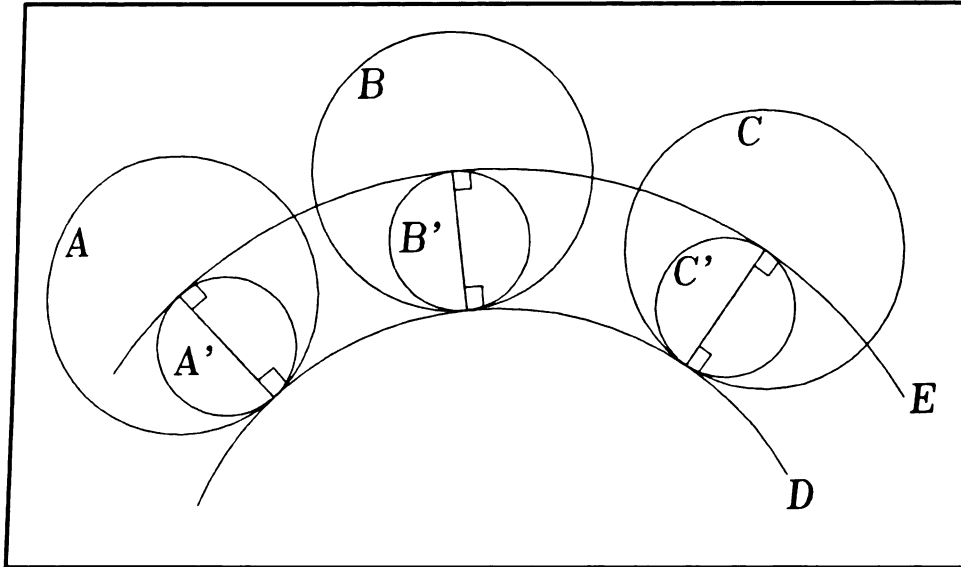


**Figure 23: Illustration of cam profile relation to pitch curve.**

The numerical method uses this principle to find the cam profile at any desired number of points (the Matlab program was written to locate 360 points). Two steps are required to locate a point on the cam profile for each point on the pitch curve. First, the slope of the pitch curve is determined using the Richardson extrapolation technique (a detailed explanation of the Richardson extrapolation technique is given in appendix C). Second, a vector is constructed, having a length equal to the roller radius and a direction normal to the pitch curve. This vector locates a point on the cam profile. The graphical interpretation of this process is shown in figure 24. The Matlab program used to determine the cam profile is entitled “CAM”, and is shown in Appendix E.

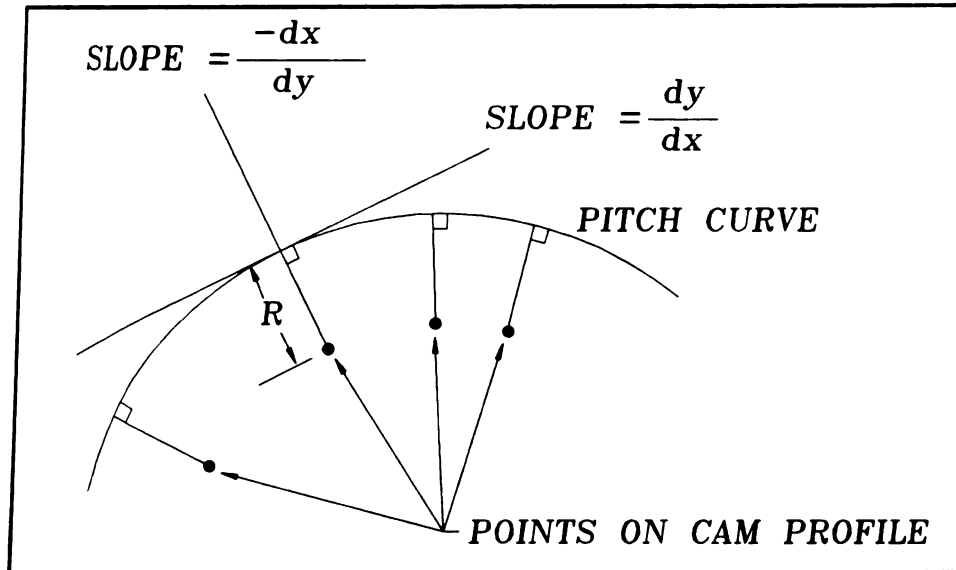


Figure 24: Illustration of cam profile determination, given a pitch curve.

When designing cam-follower systems, using a roller type follower, an important parameter is the “pressure angle”. The pressure angle is a measure of the angle between the force vector, applied by the cam, and the direction of motion executed by the follower. The pressure angle should be kept less than 30 degrees for high speed operation. The pressure angle decreases when the radius of the base circle increases. The pressure angle was calculated in the “CAM” program. Table 2 shows the maximum pressure angle for various base circle radii, and a 1.27 cm (0.5 inch) roller radius.

BASE CIRCLE RADIUS	MAXIMUM PRESSURE ANGLE (degrees)
2.54 cm (1.00 in.)	31.8550
3.175 cm (1.25 in.)	26.9256
3.81 cm (1.50 in.)	23.2416
4.445 cm (1.75 in.)	20.4058
5.08 cm (2.00in.)	18.1658

Table 2: Maximum pressure angles for various base circle radii.



As previously mentioned, the cam should be symmetric in order two complete two cycles per revolution. Figure 25 shows the pitch curve and the cam profile for a base circle of 4.44 cm (1.75 inches), as determined by the numeric method.

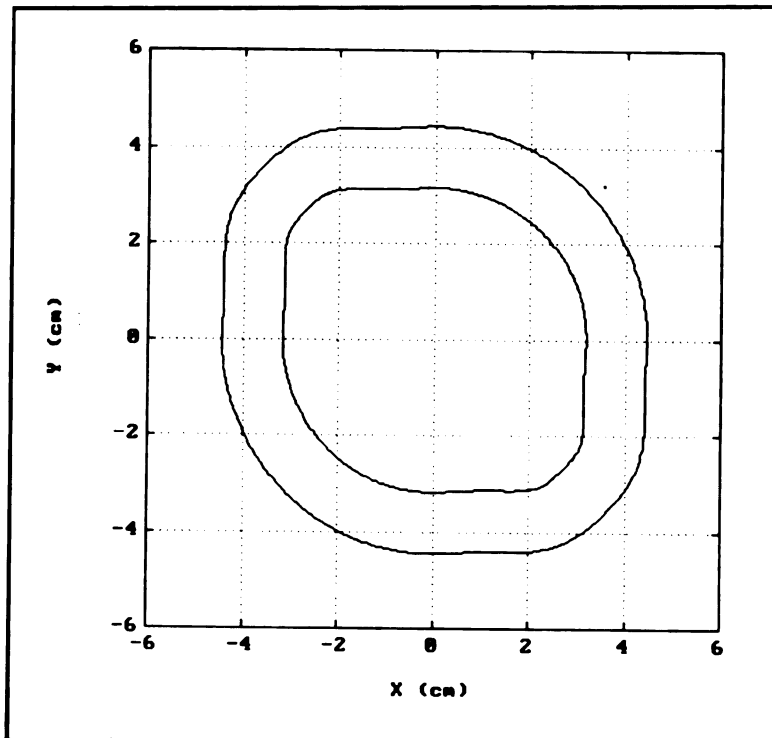


Figure 25: Pitch curve (outside) and cam profile (inside).

### STEP 3: SPRING SELECTION

After designing the cam, the next step is to determine the appropriate spring constants and preloads (i.e., initial displacements). When designing springs, there are usually two important considerations: geometric constraints and loading requirements. There are 5 secondary springs used to retract the blade actuation links. The geometric constraints are of primary concern for the secondary springs. The links are spaced on links are spaced on 1/2 inch intervals. The diameter of each rod is 1/4 inch, and the rods

are spaced at 1/2 inch intervals. Hence, the secondary spring must have an inner diameter greater than 1/4" and an outer diameter less than 1/2 inch. The primary spring is not subject to any binding geometric constraints, but is responsible for holding the follower mechanism firmly against the cam for the duration of each cycle.

The motion program of the follower was developed in step one. Using the kinematics of the follower, and estimating the masses of the moving parts, the forces can be determined. Hence, the loading requirements for the springs may be determined. The cutting mechanism will be considered in three parts. First, the force on the blades will be determined, then the force on the blade actuation link, and finally, the force exerted on the follower (in its axial direction) by the cam. Consider the free body diagram of a blade, shown in figure 26 below.

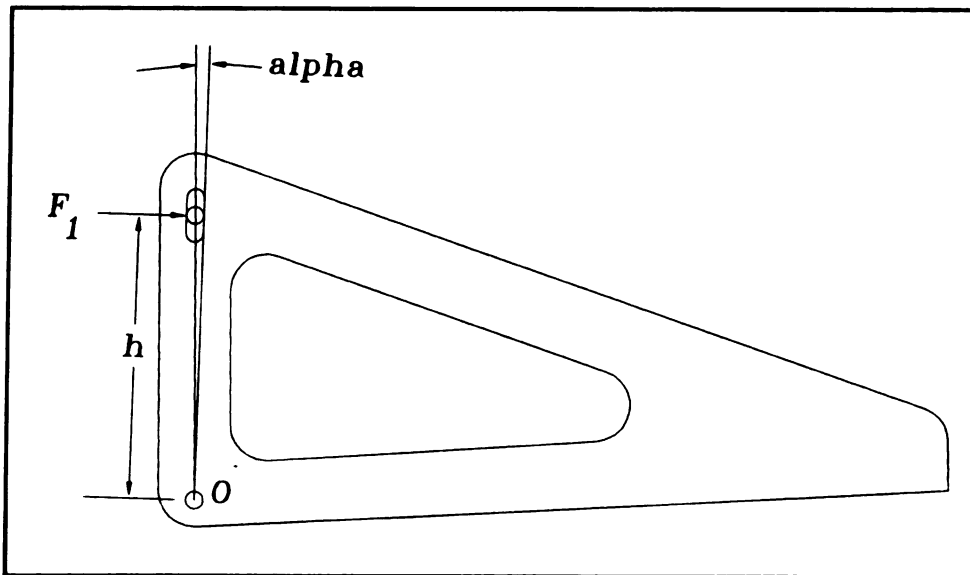


Figure 26: Free body diagram of a blade.

From the free body diagram shown above, summing moments about point O yields:

$$(46) \quad F_1 h = I_o \ddot{\alpha}$$

From the geometry of the problem, we know

$$(47) \quad \tan(\alpha) = (x_f - 3.175)/h, \text{ where } x_f \text{ is measured in mm.}$$

Since  $\alpha$  is small,  $\alpha \approx \tan(\alpha)$ . Using this approximation, and differentiating (49) twice yields

$$(48) \quad \ddot{\alpha} = a_f / h$$

Substituting (48) into (46) yields (49).

$$(49) \quad F_1 = \frac{I_o}{h^2} a_f$$

Estimating  $I_o \approx 60.3 \text{ kg}\cdot\text{cm}^2$  (i.e.,  $0.64 \text{ slug in}^2$ ) and  $h \approx 10 \text{ cm}$  (i.e., 4 inches) allows the evaluation of (49), as shown in figure 27, below.

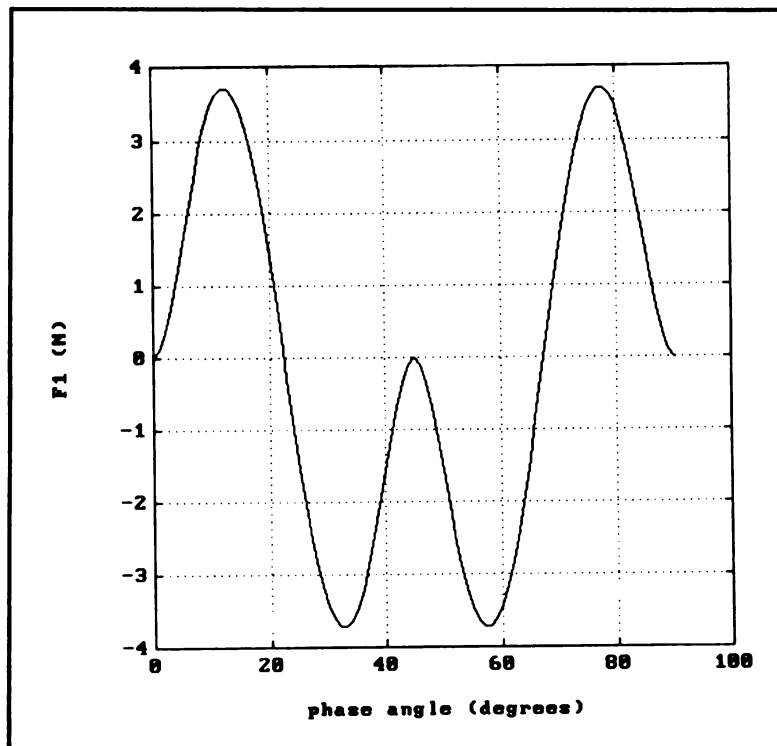


Figure 27:  $F_1$  vs.  $\theta$ .

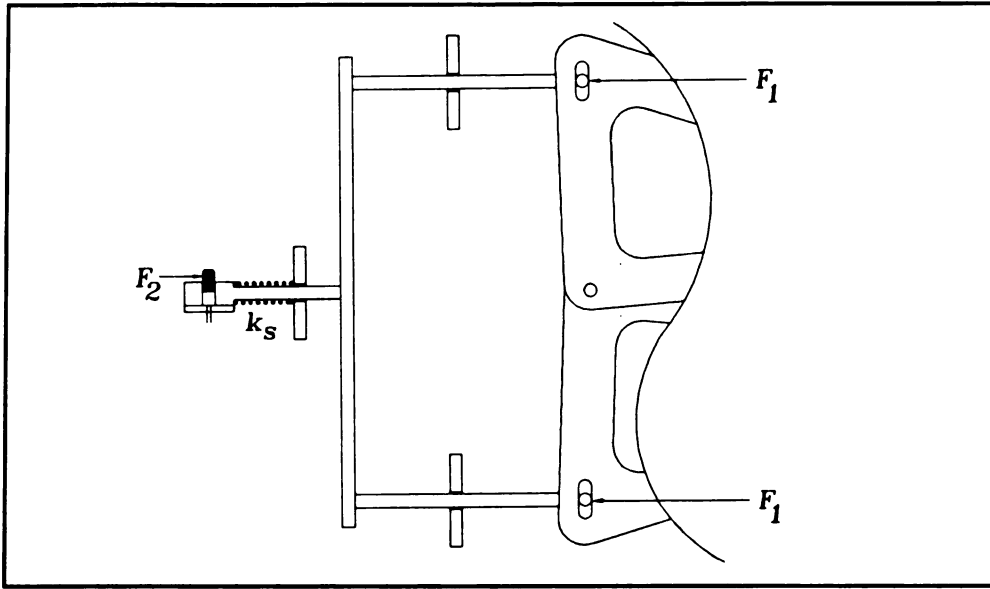


Figure 28: Free body diagram of blade actuation link.

In figure 28,  $F_1$  denotes the reversed inertial force of the blade (as defined by D'Alembert's principle). Denoting the mass of the blade actuation link as  $m_2$ , and summing the forces in the x-direction yields (50).

$$(50) \quad F_2 = m_2 a_f + k_s(x_f + x_{o,s}) + 2F_1$$

To evaluate (50), values are needed for  $m_2$ ,  $k_s$ , and  $x_{o,s}$ . As previously mentioned, the geometric constraints must be considered for the secondary springs. From the tables in Mechanical Springs, by A. H. Wahl, a compression spring with inner diameter of 5/16" and wire diameter of 1/16", has a spring rate per coil of 429 lb<sub>f</sub> per inch (i.e., 752 N/cm). For a 12 turn spring, there are about 10 active coils. Hence, the spring constant,  $k_s$ , is equal to 752/10=75.2 N/cm. Choosing an initial displacement of 3.175 mm (1/8 inch) results in a fluctuating load from 24.0 N to 71.2 N (i.e., 5.4 lb<sub>f</sub> to 16.1 lb<sub>f</sub>). Hence, the

initial displacement and spring constant have been determined. The mass is estimated as  $m_2 \approx 0.25 \text{ kg}$  (i.e., 0.017 slugs).  $F_2$  can now be evaluated, as shown in figure 29.

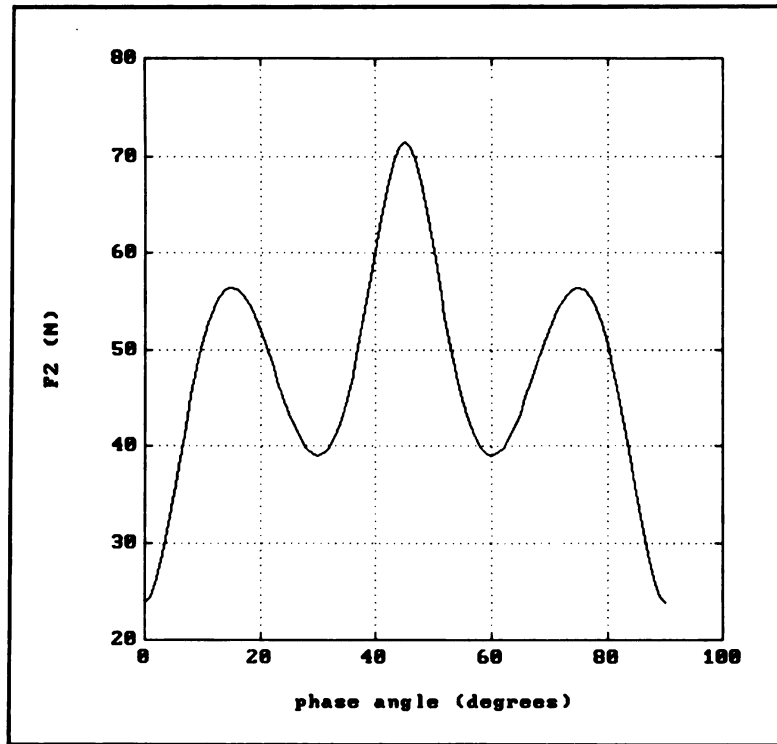


Figure 29:  $F_2$  vs.  $\theta$ .

Next, consider the free body diagram of the follower, shown below in figure 30.

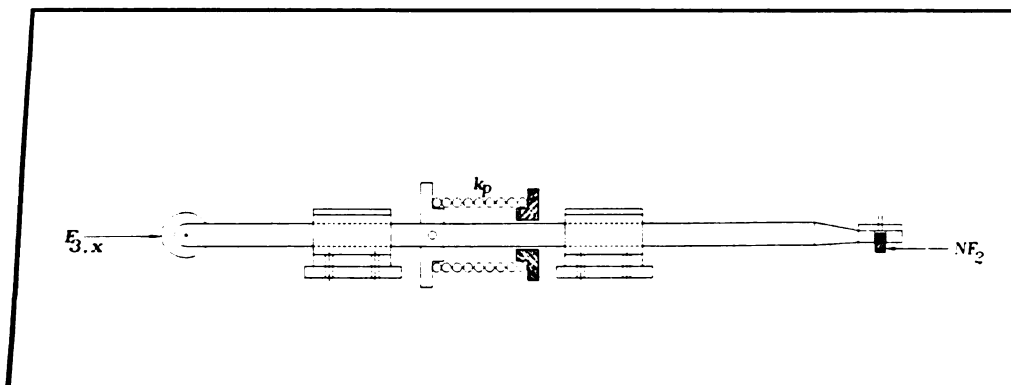


Figure 30: Free body diagram of follower.

If the number of active blades is denoted by “N”, and the mass of the follower by “ $m_3$ ”, then using D’Alambert’s principle in the x-direction yields (51).

$$(51) \quad F_{3,x} = m_3 a_f + k_p(x_f + x_{o,p}) + NF_2$$

The primary spring should be stiff enough to ensure contact between the follower and the cam, and maintain a minimum force of 89N (20 lbf) at the contact point in the x-direction (i.e.,  $F_{3,x} \geq 20 \text{ lbf}$ ). After some trial and error with the Matlab program,  $k_p$  was chosen as 70.25 N/cm (40 lbf/in) and  $x_{o,p}$  was chosen as 1.27 cm (0.5 inches). The evaluation of  $F_3$  for all blades active (i.e.,  $N=6$ ) is shown in figure 31.

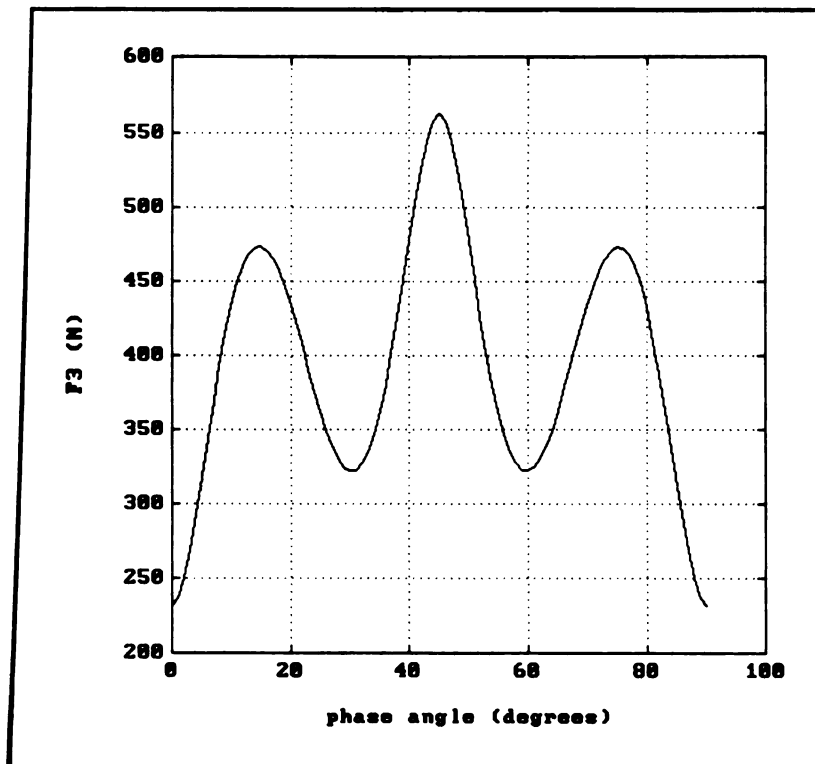


Figure 31:  $F_3$  vs.  $\theta$ .

The appropriate primary spring should have a spring constant of 40 lb<sub>f</sub>/in and an inside diameter of 9/16 inches. From the spring tables (Wahl, p.82), a steel compression spring with outer diameter of 0.75 inches and wire diameter of 0.095 inches has a spring rate per coil of 417 lb<sub>f</sub>. Hence, a 12 coil spring (i.e., about 10 active coils) has a spring rate of 41.7 lb<sub>f</sub>/in (i.e., 73.23 N/cm).

The cutting mechanism may now be completely designed. The cam has been designed and the springs have been selected. Roller bearings (i.e., ball bushings) should be used to support the follower; sintered bronze bushings can be used to support the moving push rods (see figure 19). The inertial forces are small due to the small amplitude of the follower motion. Hence, balancing should not be necessary. The analysis of the blade mechanism is complete. The following chapter examines the delivery process.

## CHAPTER 5 -- ANALYSIS OF DESIGN II DELIVERY CHANNEL

Experiments were conducted to observe the fibers' behavior in a rectangular channel. The motivation for using a rectangular delivery channel, rather than a cylindrical tube, was to deliver the fibers with their direction of motion normal to their longitudinal axis (as described in chapter 1). It is a well known fluid flow phenomenon that cylinders will align themselves perpendicular to a uniform flow. This phenomenon was to be exploited with the cut tow segments inside of a narrow channel. However, as this chapter will illustrate, the fiber glass tows did not behave like cylinders.

The experimental apparatus consisted of a channel that was 8.9 cm (3.5 inches) wide (recall that the longest cut tow segments are to be 3 inches), a blower, a screen, and a high speed video camera. The channel height was varied to examine how it affected the moving fibers' behavior. The channel had a glass top; the fibers were observed at 1000 frames per second, using the high speed video camera. The tows moved under the influence of the blower, which was positioned at one end of the channel. The channel entrance was blocked with a flat plate, which was quickly removed to simulate an impulse jet.

Channel heights of 7/8", 3/8", and 1/16" were observed. The average flow speed in the channel was measured to be 17.1 m/s (56 fps), and did not vary significantly for the various channel heights. Various frames from the video are presented, in the following figures, to illustrate the effects of the channel height on the behavior of the moving fibers.



Figure 32, below, illustrates how uniform cylinders act in the channel. Arrows are placed in the figures of this chapter to point to the cylinders (or fibers). The “uniform cylinders” were raw spaghetti noodles. Three short noodles were placed side by side. The impulse flow hit the noodles, causing them to proceed down the channel. As expected, the noodles tended to remain perpendicular to their directions of motion.

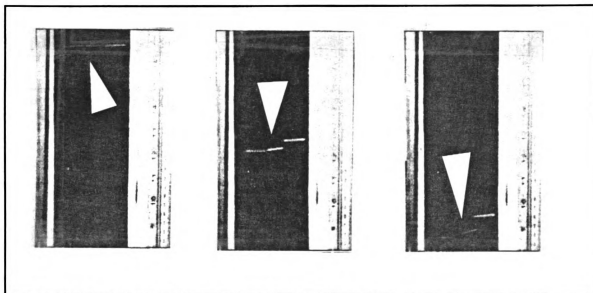


Figure 32: Three short noodles moving in 3/8" tall channel.

The noodles also displayed the desired behavior as they were sprayed onto a screen. Figure 33 shows the initial and final position of a three inch long cylinder being forced out of the channel. The screen had several pieces of tape attached to display the desired final orientation.

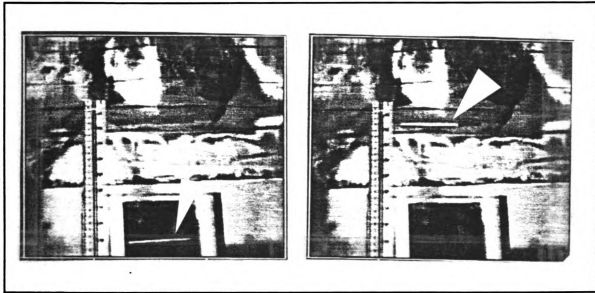


Figure 33: One 3 inch noodle, discharged to screen (channel height 1/16").

Unfortunately, the fiber tows did not behave like cylinders. The strands tended to separate very quickly, and did not remain perpendicular to the direction of the flow. This is illustrated in figure 34, below, for one 3 inch tow segment.

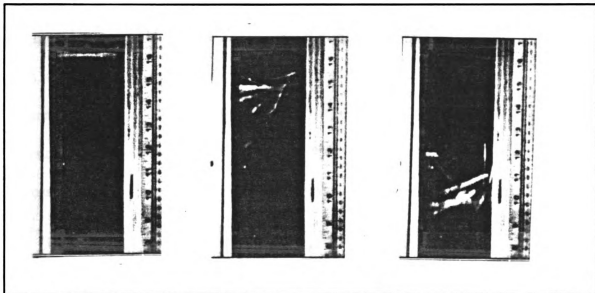


Figure 34: One 3 inch tow segment (channel height 3/8").

Although the tow segments did not behave as expected, the end result was acceptable. Figure 35 shows how a three inch tow segment impacted the screen when discharged from the channel having a height of  $3/8$  inch. The strands favored the desired orientation, but were not aligned as well as anticipated.



Figure 35: One 3 inch tow segment, screen impact (channel height  $3/8$ "")

The best results came when the channel height was reduced to approximately  $1/16$  inch, and the tow segments were started only a few inches from the channel exit. The sequence of events shown in figure 36 is ideal. Unfortunately, due to the spatial constraints imposed by the intake and cutting methods, the initial channel height must be at least one inch. However, it should still be beneficial to contract the channel to a narrow exit. Further research must be done to determine the best nozzle design.

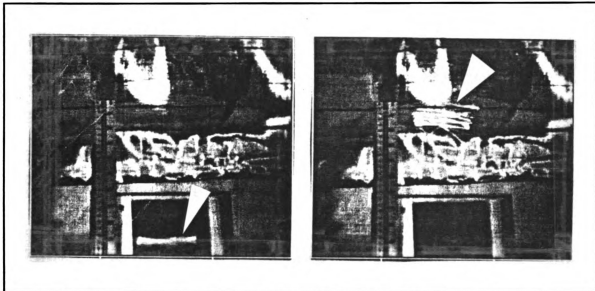


Figure 36: One 3" tow segment screen impact (channel height 1/16")

Other trials were executed using short fibers. In general, the shorter fibers had a much more random distribution on the screen. Like the longer strands, however, the short strands impacted the screen in a more desirable fashion when the most narrow channel was used.

The use of a narrow rectangular channel will deliver the cut tow segments in a manner suitable for direction controlled preforming. As mentioned, further research will be required to determine the optimum design of the constricting channel. The experiment also showed that the tow segments separate quickly in the air flow. Hence, a short channel should be used. The schematic, shown in figure 19, shows the anticipated constricting delivery channel, qualitatively (i.e., the appropriate general shape and length).

## **CHAPTER 6 -- CONCLUSIONS AND RECOMMENDATIONS**

**A feasible design has been developed for a fiber chopper which is able to cut fiber tows to variable lengths, and deliver them in a manner suitable for direction controlled preforming. The length of cut fibers may be selected during each cycle; changing the length tow segments does not delay the deposition process. The device will be capable of delivering 1.15 lb<sub>m</sub> of fiber per minute. The following conclusions are supported by the preceding chapters, as well as the following appendices:**

- 1. A narrow channel may be used to control the orientation of the strands on the preform.**
- 2. In order to change the length of cut tow segments without delaying the deposition process, the tows must be pulled into the device and cut by two distinctly controllable mechanisms (i.e., cannot use pinch rollers with embedded blades).**
- 3. To allow a short stroke of the blade mechanism, and prevent vibration, the intake process should not involve any parts moving between the blades and the tows.**
- 4. For the Geneva mechanism controlled intake process, the entraining air flow should have a velocity of 55.5 m/s (182 fps) in order to prevent slack in the tows (for an input rotational speed of 300 rpm).**
- 5. When cutting the tows with a shearing action, the two edges should remain in contact. A scissor action is preferable to a stationary edge with a corresponding descending blade.**
- 6. In order to control which blades are active, and which blades are not, solenoid valves are used to control a selecting pin. When the pin connects the blade actuation link to the follower, the corresponding blade is active.**

7. A numeric algorithm has been developed to design a cam, for use with a roller follower, given the desired follower motion.
8. The cut tow segments do not behave like cylinders in an air stream.
9. The flow characteristics for the fiber tow in an entraining flow were determined. The product of the drag coefficient,  $C_D$ , and the effective circumference,  $\zeta$ , was determined to be 0.503 mm (0.00165 ft).
10. Composite parts using properly oriented fibers are significantly better than those with random fibers, as shown in appendix A.

The design process, as shown in figure 4, is currently in its second iteration, and is not complete. Recommendations for future work are listed below.

1. Manufacture a prototype of design II.
2. The design of the contracting delivery channel must be examined. It would be beneficial to manufacture the prototype with a removable delivery channel. Hence, several channels could be tested with the device.
3. In the analysis, the mass of the moving parts was estimated to find the primary spring constant. After these parts are manufactured for the prototype, the exact mass should be determined, and the calculations for the spring constant should be repeated using the Matlab program, "CAM", provided in appendix E.

## **APPENDIX A**

## APPENDIX A -- FINITE ELEMENT ANALYSIS OF COMPOSITE BEAM

A case study on a beam is presented to show the advantage of using directed fibers. A beam with oriented fibers is illustrated in figure 37, below. For the model problem, the beam is fixed at both ends and supports a load of 5000 Newtons, which is equally distributed across the top surface. The beam has a fiber volume fraction of 0.4 and an elastic modulus of 8.6 GPa (for the isotropic beam). A schematic of the model problem is shown in figure 38.

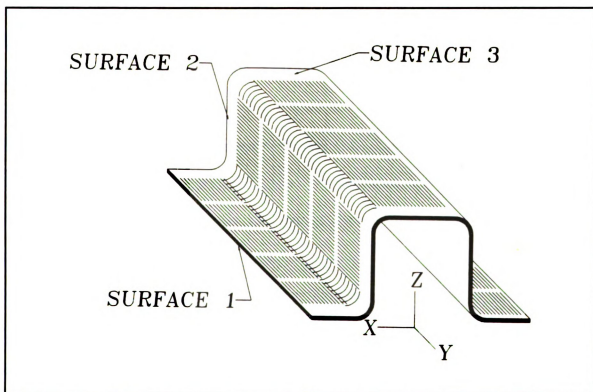
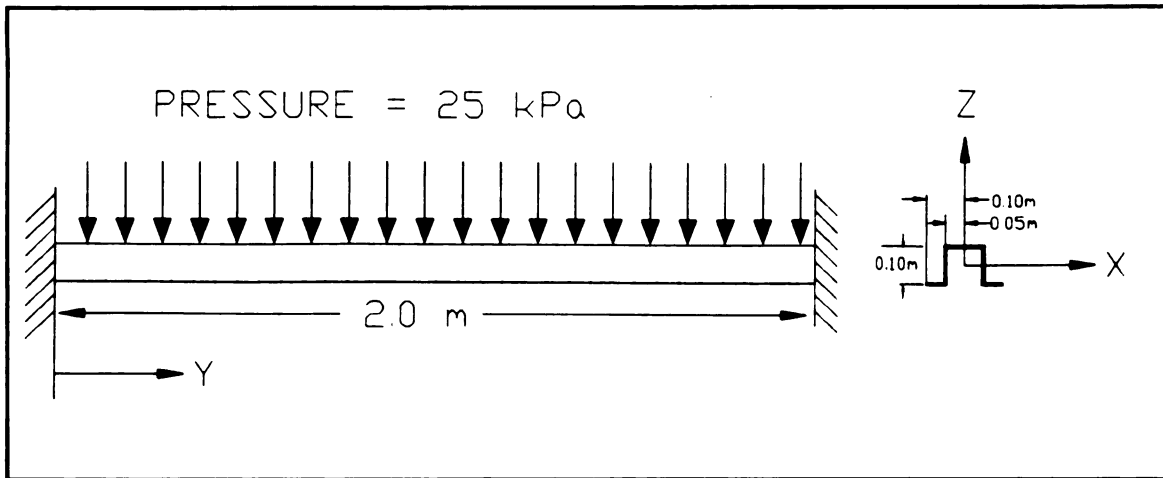


Figure 37: Schematic of the beam with oriented fibers.





**Figure 38: Schematic of model problem.**

The displacement of the neutral axis, in the z-direction, can be found easily (for the isotropic problem) with conventional methods. Since the beam is fixed at both ends, and the force is equally distributed, the problem is statically indeterminate. Therefore, the solution is found using the principle of superposition. Knowing the solution to the isotropic problem provides assurance that the finite element approximation is accurate, as will be shown.

The finite element analysis was performed using the Mentat II (version 2.1.1) software by MARC Analysis Research Corp. The problem is defined such that there is symmetry about two planes. Hence, only one quarter of the beam must be modeled for analysis, with the added boundary conditions. In order to insure the convergence of the finite element model, four meshes were used. All meshes used 9-noded, quadrilateral, shell elements. Meshes of 15, 30, 80, and 320 elements were used, on the isotropic model.

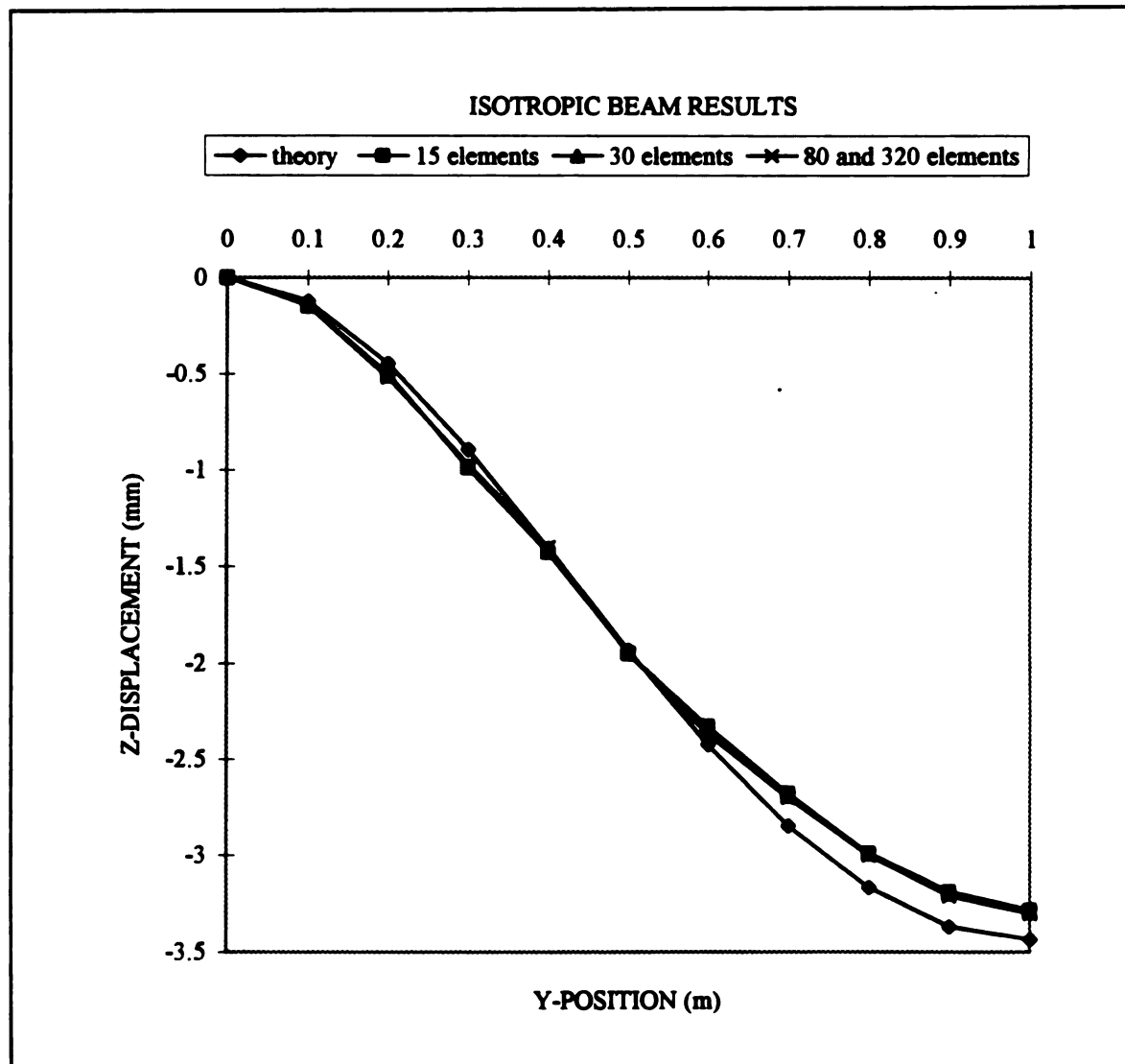


Figure 39: Displacement of isotropic beam, calculated with various models.

<u># of elements</u>	<u>Extreme Z-Displacement (mm)</u>
15	-3.283
30	-3.293
80	-3.303
320	-3.306
theory	-3.438

Table 3: Convergence of results for isotropic problem.

The displacement of the lower edge of the beam, in the z-direction, is plotted in figure 39 for each of the meshes. The displacement of the neutral axis is also shown, for the result obtained using the conventional approach. The finite element solution converges to within 4% of the theoretical solution. The four percent error is reasonable, considering the difference between the displacement of the neutral axis and the outer edge of the beam cross-section. Extreme values for the displacement are shown in table 3. The difference between the 320 element mesh and the 80 element mesh is only about 0.1%, but the required computation time is much greater for the 320 element mesh. Therefore, the 80 element mesh is used for the orthotropic beam study.

Equations from a paper by Ericson & Berglund are used to estimate the orthotropic properties of the composite beam. In "Processing and Mechanical Properties of Oriented Preformed Glass Mat Reinforced Thermoplastics", Ericson & Berglund give predictions for the elastic, transverse, and shear moduli as functions of a fiber length efficiency coefficient. They define the fiber length efficiency coefficient as "a measure of the load transfer capability of discontinuous fibers". The coefficient was varied to support experimental data. For chopped fibers of about one inch, the fiber length efficiency coefficient was determined to be 0.7.

The elastic modulus of the composite in the axial direction of the fibers, for the model problem, was found to be 21.47 GPa. In the transverse direction, the elastic modulus is only 0.47 GPa. Recall, that the modulus for the isotropic material is 8.6 GPa. These properties were assigned to the 80 element mesh, using three different combinations of fiber orientation. The deflection of the beam is shown for the various fiber orientations

in figure 40, and the maximum deflections are given in table 4. The notation used to indicate the fiber orientation (e.g., X-Z-X) refers to the axial direction of the fibers on surfaces 1, 2, and 3, respectively (as shown in figure 34). Hence, in figure 37, the beam is shown with a Y-Y-Y fiber orientation.

It has been demonstrated that direction controlled preforming can have enormous advantages over random fiber distributions. For cases in which the loading will be in only one direction (such as the model problem presented), substantial material savings can be realized. In the case study, deformation in the z-direction was reduced by 60% (with respect to the isotropic beam) when the fibers were properly oriented. It should be noted, however, that improperly oriented fibers result in much larger deformations. The worst case scenario for the composite beam problem resulted in a 400% increase in deformation (see table 4).

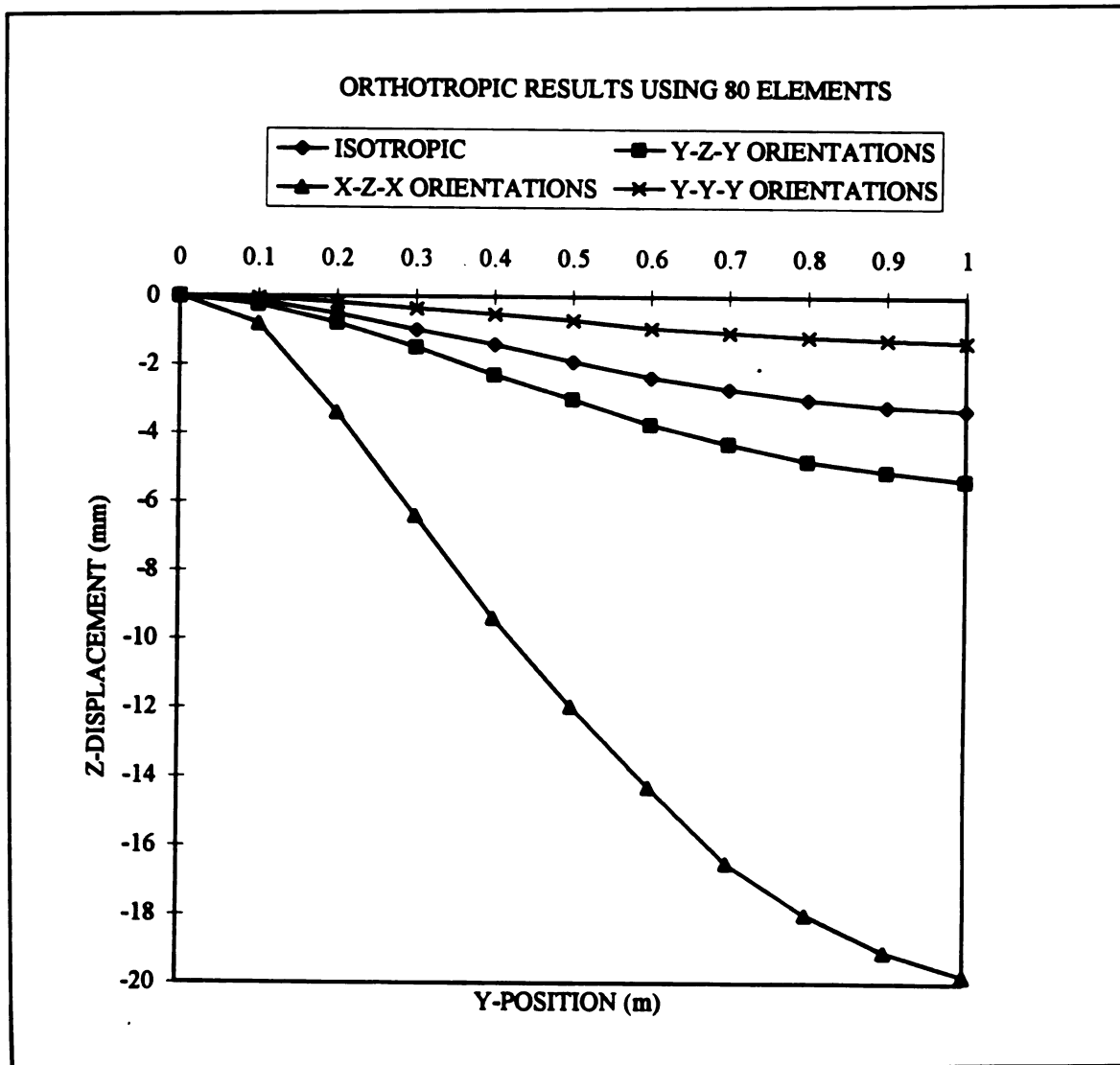


Figure 40: Displacement of beams with various fiber orientations.

<i>fiber orientation</i>	<i>Extreme Z-Displacement (mm)</i>
Y-Y-Y	-1.311
random	-3.303
Y-Z-Y	-5.354
X-Z-X	-19.79

Table 4: Extreme displacements for various fiber orientations.

## **APPENDIX B**

## **APPENDIX B -- SYNTHESIS OF INITIAL DESIGN**

In this appendix, the synthesis of design I is presented. Design I is shown schematically; detailed drawings are not given. Appendix C examines the blade mechanism for design I in considerable detail. As described in chapter 1, the process should be a cyclic one, consisting of three phases (intake, cut, and delivery). The delivery process was described in the introduction; recall that the strands' orientations are controlled by using a narrow channel to deliver them. The syntheses of the fiber intake and cutting processes for design I are the focus of this appendix.

In present fiber choppers, the fibers are drawn into the device and cut by the same mechanism (i.e., a pair of pinch rollers, one of which is embedded with blades). The fibers must be pulled into the device and cut by two distinct mechanisms to independently control the rate of fiber intake and the length of cut fibers. A pair of grippers and three distinctly controlled air flows were proposed to pull the fibers into the device and position them for the cutting process. A schematic of the intake mechanism for design I is shown in figure 41.

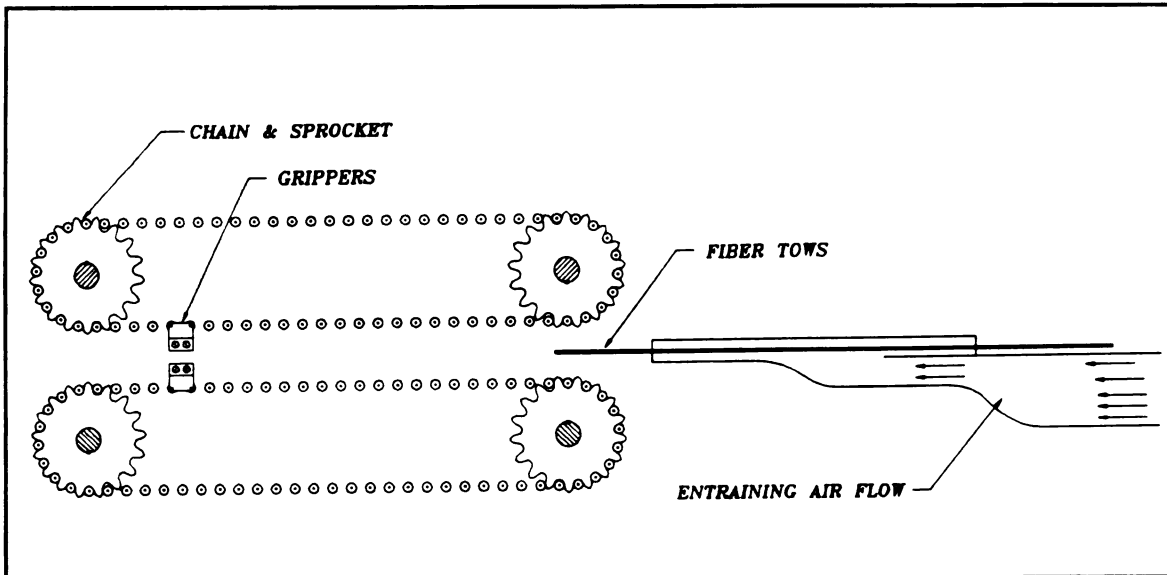


Figure 41: Schematic of fiber intake mechanism, design I.

The channel through which the fibers were to be fed into the device would provide an entraining airflow. This entraining airflow was to be used to hold the fibers straight so that the grippers could grab the tow in the same position, consistently, over the course of many cycles. The other two airflows were to be used to secure the fibers to the cutting surface before the cut, and to propel the fibers out of the device. The cutting surface was designed to be perforated, thus allowing air to flow through it. A sub-atmospheric pressure in the chamber beneath the cutting surface, combined with a downward flow around the blades, would secure the tows on the cutting surface. After the tows had been cut, the chamber beneath the cutting surface would be pressurized to help lift the fibers off the cutting surface. In addition, an airflow was to be initiated in the fiber exit channel to spray the fibers out of the device in the desired fashion. This airflow could have been classified as part of the fiber delivery process. However, it is mentioned here, in the context of the other airflows, to illustrate the order of events.



The grippers were designed to be attached to chains, as shown in figure 41. The grippers would have moved relative to the chains; they would have been forced together to grab the tows and forced apart to release them. An electro-magnetic force would be used to bring the grippers together and apart. This force could be generated by an electric current, flowing through the grippers, as they passed through a magnetic field. The physical law that applies to this process is given by:

$$(52) \quad \vec{F} = \vec{i} \ell \times \vec{B}$$

where,  $\vec{F} \equiv$  Force generated on the gripper (Newtons)

$\vec{i} \equiv$  current passing through gripper (Amps)

$\ell \equiv$  length of gripper (meters)

$\vec{B} \equiv$  Magnetic field (Teslas)

Obviously, if the direction of the electric current is reversed, in equation 52, the resulting force is also reversed. This would have been a convenient way to force the grippers both together and apart, with the spatial constraints imposed by the cutting blades.

The system of parts designed to cut the fiber tows was called the "blade mechanism". A shearing action was to be used to sever the fiber tows once they were drawn into the device. The tows were to be held in place by the aforementioned downward airflow passing through the perforated cutting surface. The shearing force was to be generated by a sharp edged blade, which would descend through the tow, against the cutting surface.

To modify the length of fibers at each cut, a row of six blades on 1/2 inch intervals was to be used (see figure 42). Any desired combination of the six blades could have been selected for use, during each cycle of operation. Recall that three inches of each tow are pulled into the device for each cycle. It follows that any combination of multiples of 1/2

inch that add up to 3 inches may be cut during each cycle of operation. For example, the device could cut (6) 1/2 inch pieces, (1) 3 inch piece, (3) 1 inch pieces, (1) 1 inch and (4) 1/2 inch pieces, etc.

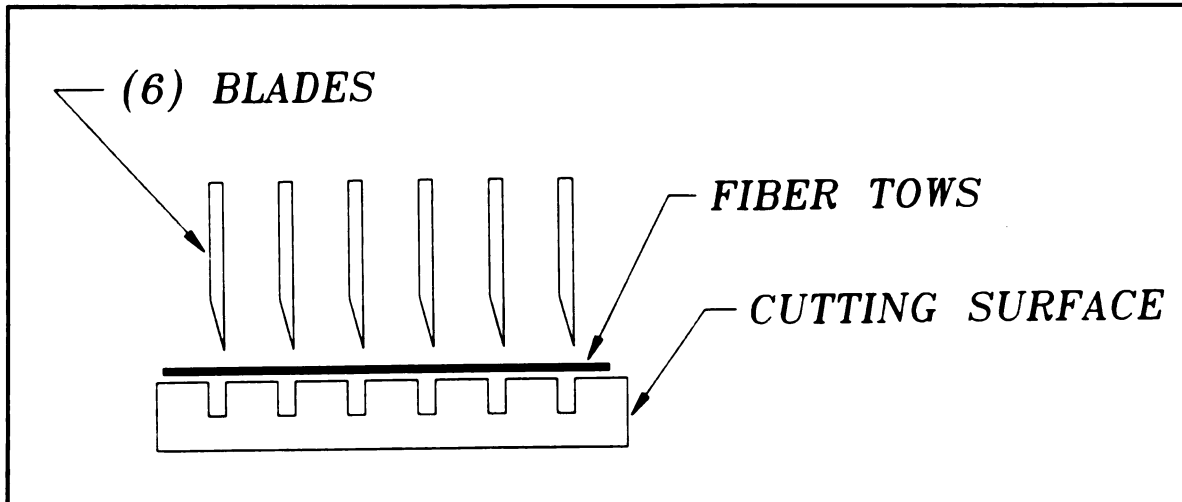


Figure 42: Multiple blade arrangement, design I.

To select any combination of the six blades, for every cycle of operation, sliding pins were to be used. The pins could have been moved by initiating a high air pressure in the appropriate line. Each pin would come to rest in one of two possible positions, during each cycle. Figure 43 shows a schematic of this blade selection process. As shown, if the pin was in the left position, the blade would have been held fixed to the stationary structure of the device, and termed “inactive”. Conversely, if the pin was in the right position, the blade would have been held fixed to the moving cradle, and termed “active”.

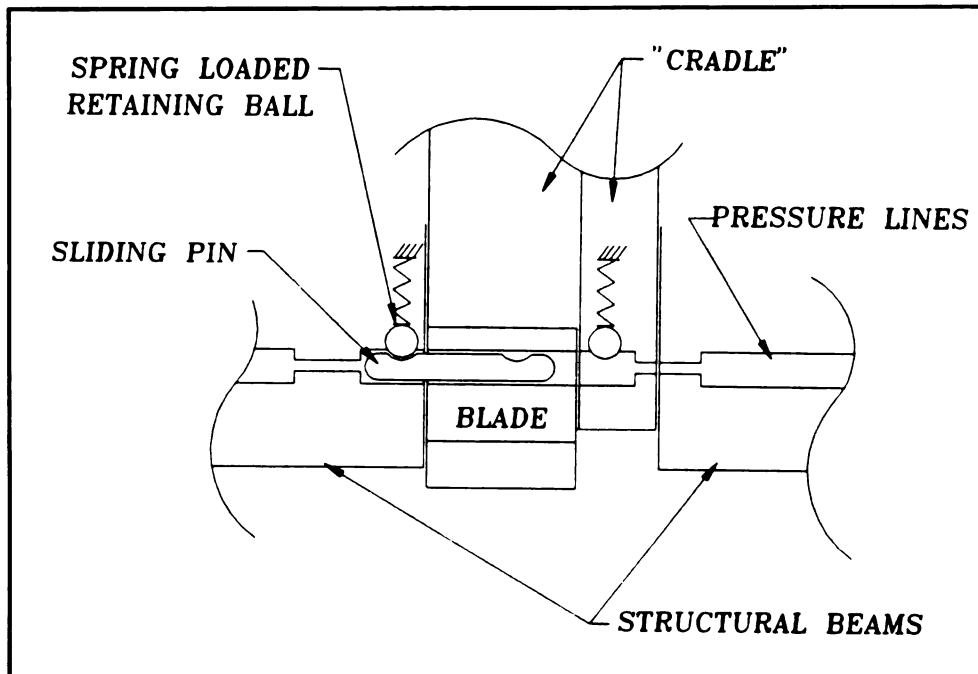


Figure 43: Blade selection process.

The cradle was required to remain stationary during the blade selection process, because it obviously required a non-zero time to move the pin from one position to the other. Hence, the motion of the cradle would consist of three stages. First, the cradle would descend (for the active blades to cut the tows). Second, the cradle would return to its original position. Finally, the cradle would remain stationary for the blade selection process. In mechanism texts, this type of motion is termed “Rise-Dwell-Return (RDR)”, for obvious reasons.

One method for achieving an RDR motion is explained and illustrated in Mechanism Synthesis and Analysis, by Soni. This method is illustrated in figure 44 and is explained as follows in the text (Soni, p.361):

1. Consider a coupler curve with a straight line segment  $x$ , see curve in figure 4.
2. Place a slider pair with its axis parallel to line  $x$ . Place a revolute pair at joint C as shown in figure 4.
3. The coupler curve is approximately symmetric. Place a prism pair with its axis

coincident with the line of symmetry.

4. When coupler point C traces the straight line segment, the output slider pair experiences a dwell.

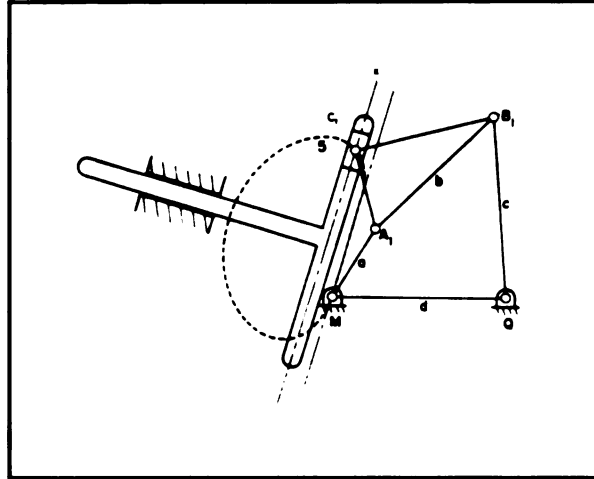


Figure 44: Mechanism used to obtain an RDR motion (Soni, p.361)

There are several four bar linkages that contain a “straight” line segment in their coupler curves. One such linkage is illustrated in the literature (Soni, p. 323), and is shown in figure 45, below. Note that the location of the best coupler point, C, (i.e., the one that results in the best straight line segment in the coupler curve) is not given. In the literature, several coupler curves are drawn; the distance “e” appears to be between 1.0 and 1.5 units. Using Matlab, the coupler curves were determined numerically, and the best distance, e, was found (this analysis is shown in appendix C).

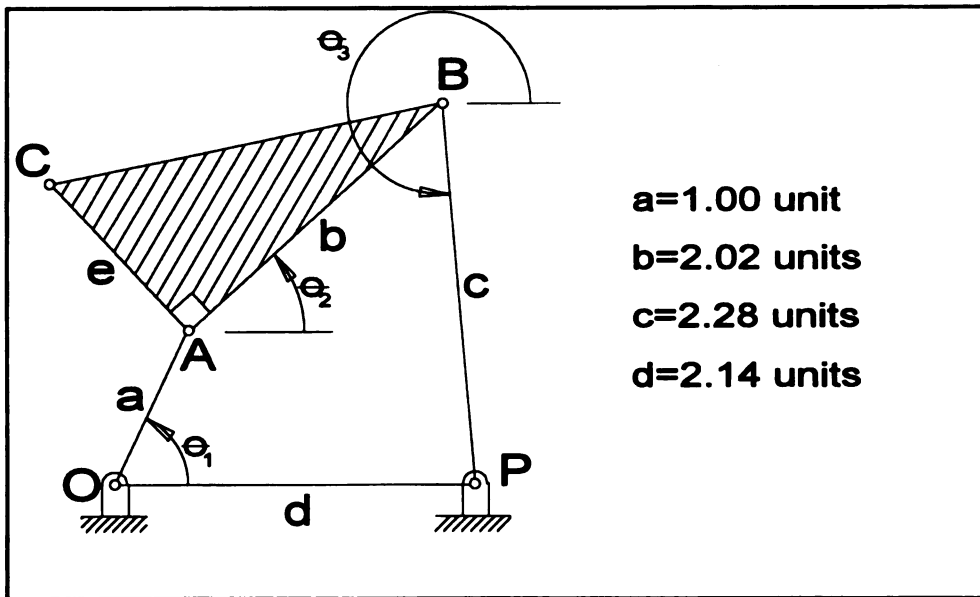


Figure 45: Schematic of four bar linkage used to obtain a “straight” coupler curve.

Thus far, the intake, cut, and delivery phases of the process in design I, have been presented as if they were to be distinct; however, these phases would need to have been blended together in order to work properly with each other. In other words, these phases were not to occur one after the other, but overlap and accommodate each other. The required sequence of events is shown below:

**EVENT #    DESCRIPTION OF EVENT**

- 1      Blade mechanism begins dwell period.
- 2      Blades for next cut are selected or deselected for next cut by a pressure in the appropriate tubes.
- 3      Blade mechanism finishes dwell period and begins descent.
- 4      Entraining airflow is started.
- 5      The electro-magnetic grippers are started as they pass over the tows.
- 6      The entraining airflow is terminated.
- 7      The chamber beneath the cutting surface is evacuated.

- 8      The downward flow around the blades begins.
- 9      The grippers reach the end of the cutting surface, and the electric current is reversed causing them to release the tows.
- 10     The combination of the downward flow around the blades and the evacuated chamber below the perforated cutting surface secures the fiber tow to the cutting surface.
- 11     The electric current through the grippers is terminated.
- 12     The blades reach maximum depth after cutting tow.
- 13     Downward flow and chamber evacuation terminated.
- 14     High speed flow is initiated in the bottom passage, drawing the fibers out of the cutting chamber and propelling them onto the preform.

The above sequence of events was later refined; the events were timed relative to the phase of the crank. To determine the process timing, the blade motion was analyzed, and the number of pitches in the chains were determined. The analysis of the blade mechanism is described in the following appendix. It was determined that a standard 3/8" pitch (68 pitches long) chain, with 17 tooth sprockets would yield the appropriate timing.

Having synthesized a feasible process for the device, the next step was to put the parts together. The device is shown schematically in figures 46 and 47. The device is about 4 feet tall and 3 feet wide, although dimensions are not shown.

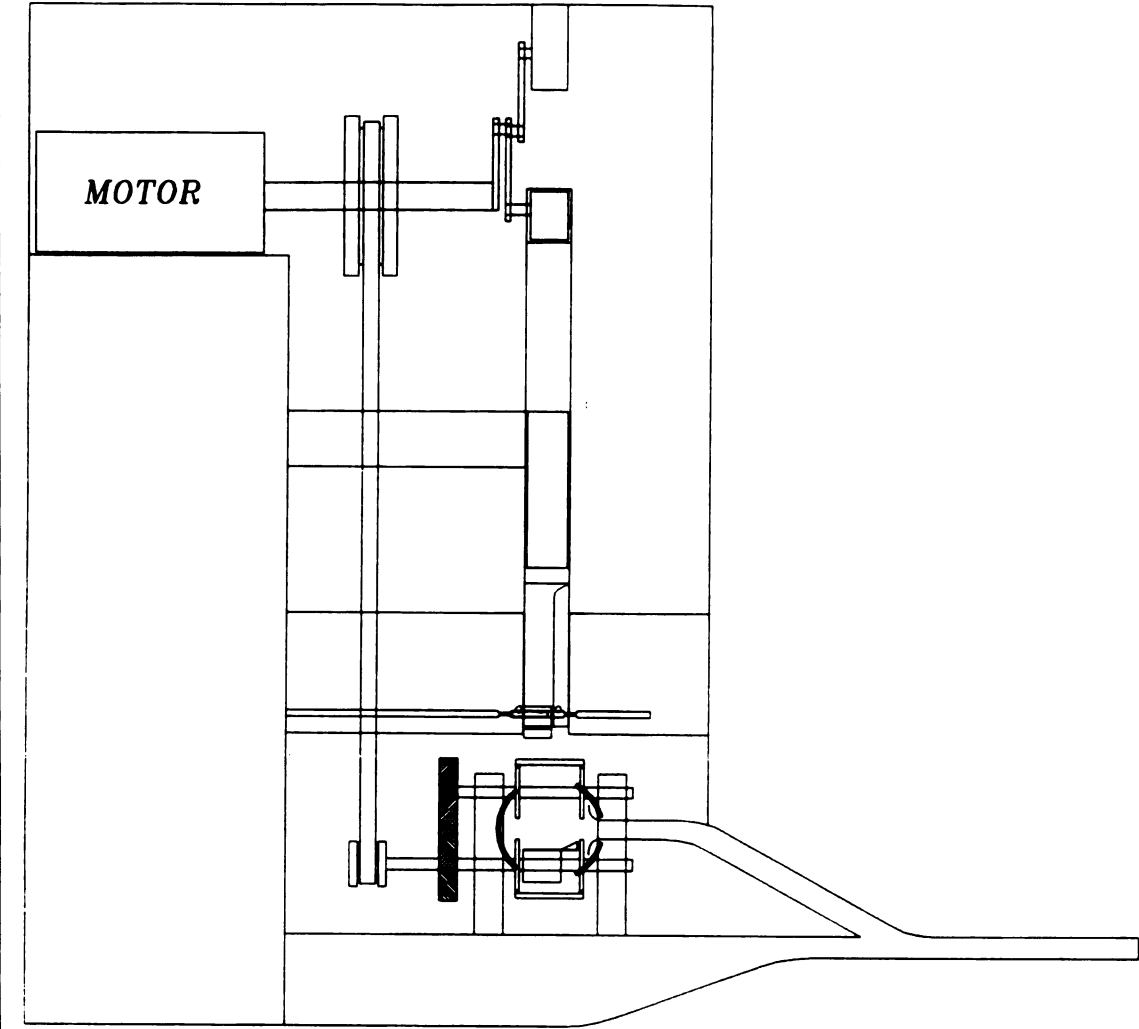


**Figure 46: Schematic of design I -- front view.**

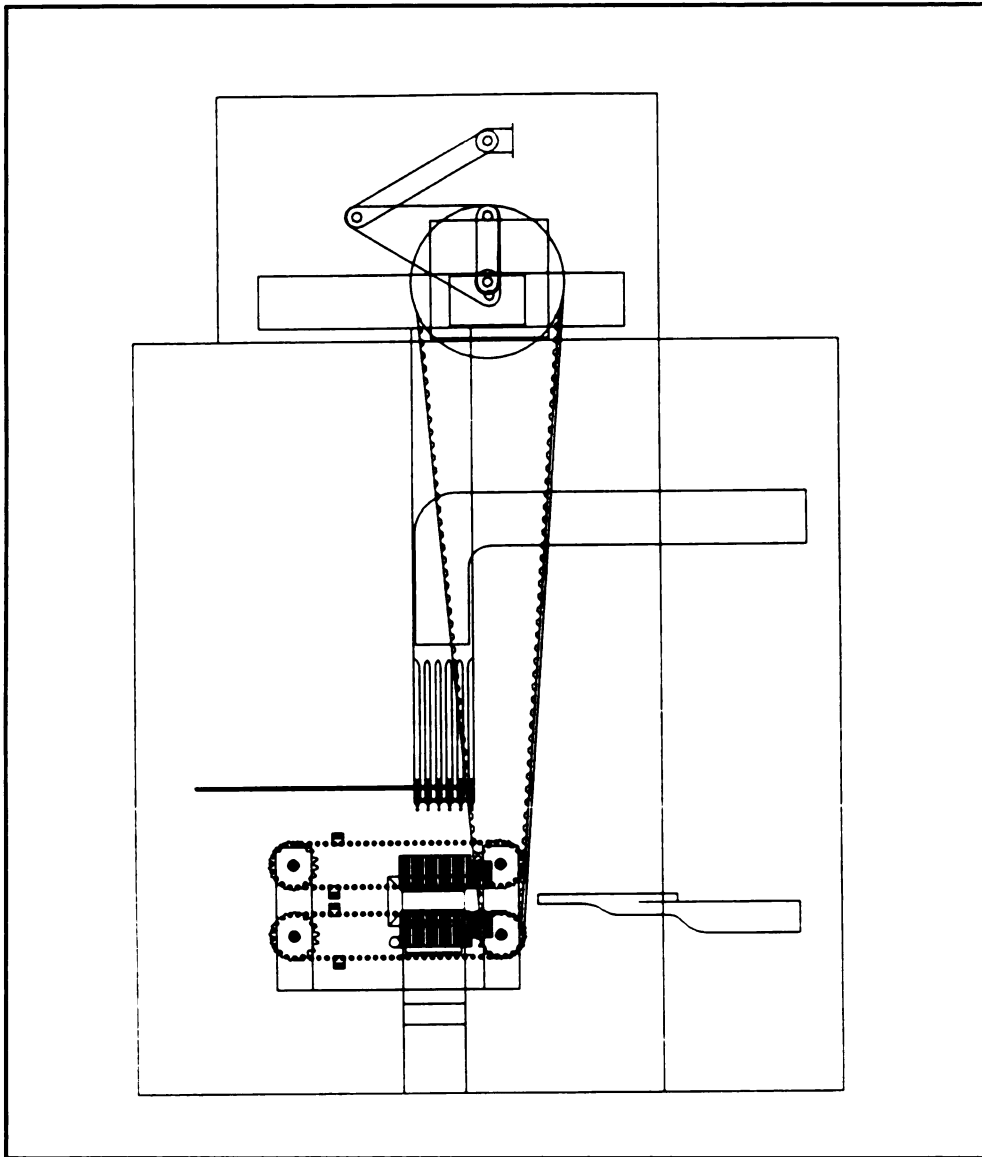


Figure 47: Schematic of design I -- right side view.



## **APPENDIX C**

## **APPENDIX C -- ANALYSIS OF INITIAL DESIGN BLADE MECHANISM**

The cradle must translate 13.33 cm (5.25 inches) to provide the appropriate clearance for the intake mechanism (i.e., the grippers; see figure 47). The cradle should undergo a rise-dwell-return, vertical motion. The dwell period would provide the time required to select the active blades, as was explained in appendix B. The analysis of the mechanism will consist of the following four steps:

1. Determine the length, AC (as defined in figure 45), which results in the best coupler curve (the one with the straightest line segment).
2. Scale and rotate the mechanism such that the straight portion of the coupler curve is parallel to the x-axis and the amplitude of motion is 5.25 inches.
3. Perform the kinematic analysis on the mechanism, using the parameters established in step 2. Determine the position, velocity, and acceleration of points A, B, and C for each degree of crank phase.
4. Estimate masses and moments of inertia of the moving parts. Use d'Alembert's principle to estimate the forces present in the pin joints.

### **STEP 1: Determine length AC**

The vector equation that describes the 4-bar linkage is usually called the "loop closure equation". The loop closure equation for the mechanism, as shown in figure 45, is

$$(53) \quad \vec{R}_{AO} + \vec{R}_{BA} + \vec{R}_{CB} = \vec{R}_{PO}$$

BASIS: vector 2-space with origin at O.

$\hat{i}$  is a unit vector in the X-direction

$\hat{j}$  is a unit vector in the Y-direction

Taking the dot product of  $\hat{i}$  and the loop closure equation yields:

$$(54) \quad AO \cos(\theta_1) + BA \cos(\theta_2) + PB \cos(\theta_3) = PO$$

Similarly, taking the dot product of  $\hat{j}$  and the loop closure equation yields:

$$(55) \quad AO \sin(\theta_1) + BA \sin(\theta_2) + PB \sin(\theta_3) = 0$$

where,  $AO = 1.00$  units  
 $BA = 2.02$  units  
 $PB = 2.28$  units  
 $PO = 2.14$  units

Note that (54) and (55) are a system of two non-linear equations with three unknowns. Hence, the equations should be solved for a function that determines two of the angles when given the other. This is not as simple as it sounds, however, because sine and cosine functions do not have unique inverses. In order to compute  $\theta_2$  and  $\theta_3$ , given  $\theta_1$  a program was written using Matlab. This program was used, and all angles were found for each degree of  $\theta_1$ . The points on the coupler curve are characterized by the following equation:

$$(56) \quad \vec{R}_{CO} = \vec{R}_{AO} + \vec{R}_{CA}$$

Note that the “coupler curve” is the path traced by point C in each revolution of the crankshaft.

Since  $\theta_2$  and  $AO$  are known for all values of  $\theta_1$  (degrees)  $\in [1, 2, 3, \dots, 360]$ ,  $\vec{R}_{CO}$  can be determined (at each degree of  $\theta_1$ ) for given values of  $CA$ . This was done for

various values of CA. The results are plotted in the following figures.

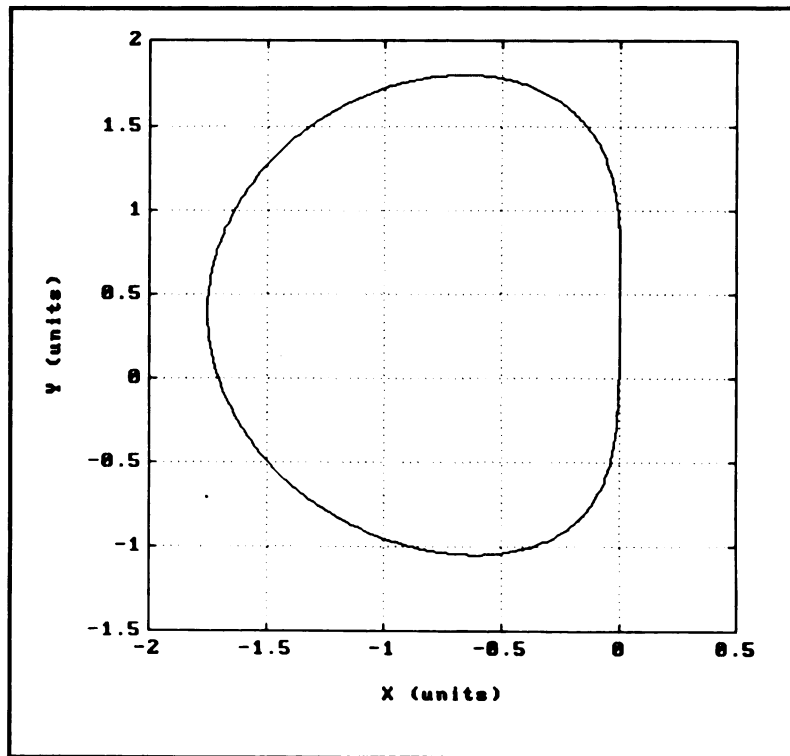


Figure 48: Coupler curve generated when  $CA = 1.00$ .

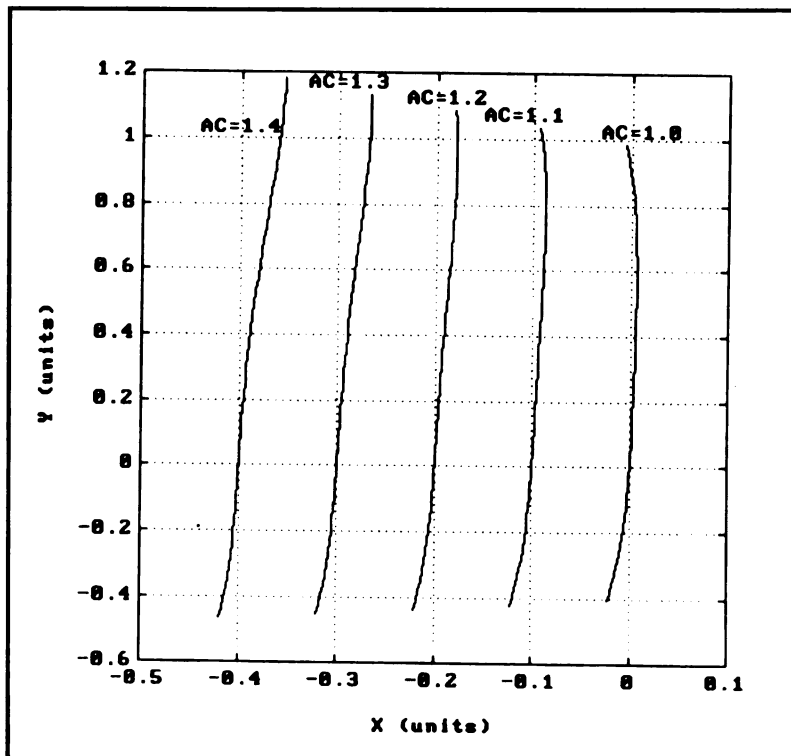


Figure 49: "Straight" portions of coupler curves for various values of CA.

It was determined that  $CA = 1.2$  units was the best value from figure 49.

**STEP 2:** Determine the scaling and orientation of the mechanism.

The orientation of the mechanism is determined by the straight line segment of the coupler curve. The mechanism should be oriented such that the straight portion of the coupler curve is horizontal (i.e., along the X-axis). Since the motion of the blades will be constrained to move in the Y-direction, orienting the straight portion of the coupler curve in the X-direction results in a dwell in the blades' motion. In other words, the  $\hat{j}$  component of the coupler curve is approximately constant.

Again using Matlab, a best fit line was constructed through the appropriate segment of the coupler curve. The angle of this line, as measured from the X-axis, was found to be 1.5462 radians. This implies that the mechanism should be rotated, about the origin O, by 1.5954 radians counter clockwise.

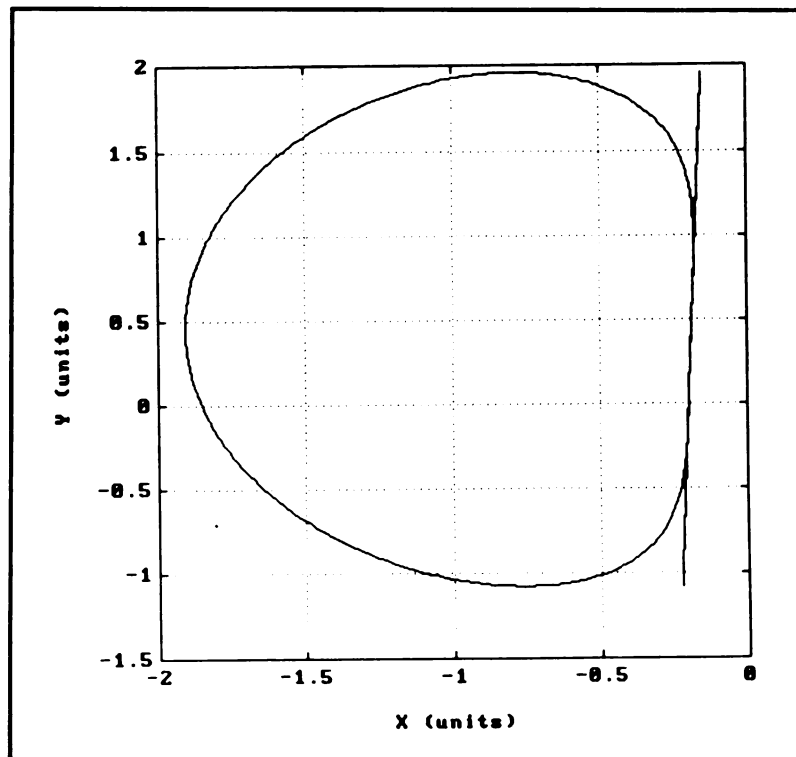


Figure 50: Coupler curve with best fit line ( $CA = 1.20$  units).

The distance of the coupler curve from the best fit line was also calculated at each degree of  $\theta_1$ . The maximum value of this distance (i.e., the amplitude of motion) was found to be 1.7185 units.

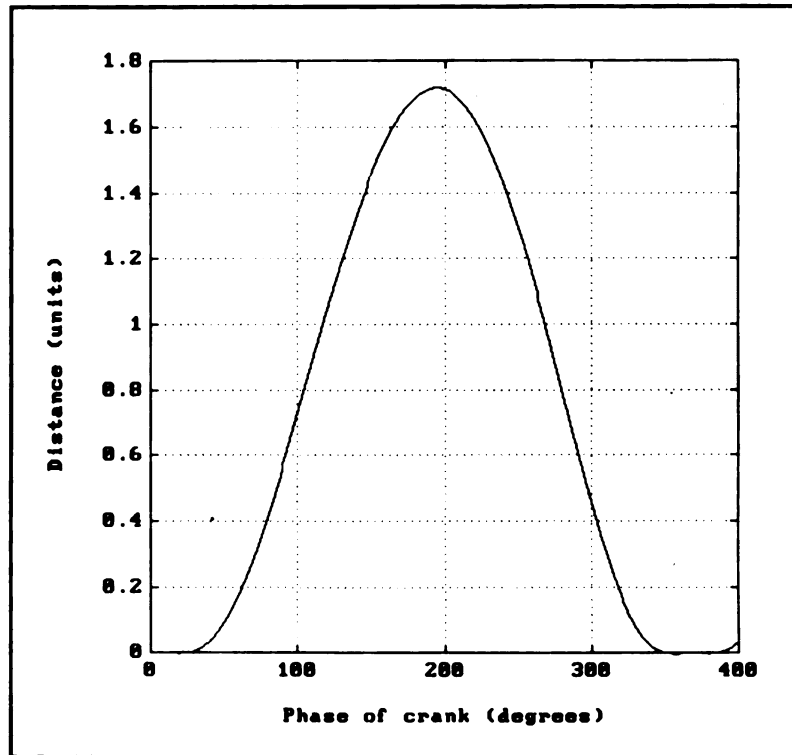


Figure 51: Distance of coupler curve from best fit line ( $CA = 1.20$  units).

To achieve the desired amplitude of 13.33 cm (5.25 inches), the mechanism must be scaled by a factor of 7.760 cm (3.055 inches) per unit. After scaling and rotating appropriately, the point, P, is located at  $[(-4.03 \text{ mm}) \hat{i}, (16.60 \text{ cm}) \hat{j}]$ . The properly oriented and scaled mechanism is shown schematically in figure 49.

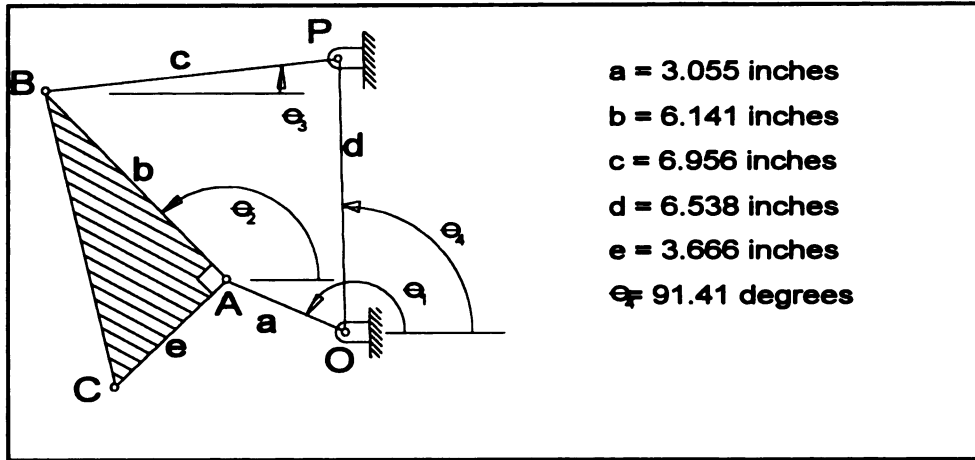


Figure 52: Properly scaled and oriented mechanism.

**STEP 3:** Determine positions, velocities, and accelerations of point A, B, and C.

Just as in step 1, the analysis begins by separating the loop closure equation into its orthogonal components. Taking the dot product of  $\hat{i}$  and the loop closure equation yields:

$$(57) \quad AO \cos(\theta_1) + BA \cos(\theta_2) + PB \cos(\theta_3) = -4.03 \text{ mm}$$

Similarly, taking the dot product of  $\hat{j}$  and the loop closure equation yields:

$$(58) \quad AO \sin(\theta_1) + BA \sin(\theta_2) + PB \sin(\theta_3) = 16.60 \text{ mm}$$

The analysis is now repeated for the scaled, rotated mechanism. The angles,  $\theta_2$  and  $\theta_3$  are evaluated at each degree of  $\theta_1$ . Hence, the known angles are held in a  $360 \times 3$  matrix.

Furthermore, the  $\hat{i}$  and  $\hat{j}$  components of the position vectors related to the points A, B, and C are known for each degree of  $\theta_1$ . These positions are determined as follows:

$$(59) \quad R_{A,I} = AO \cos(\theta_1)$$

where the scalar,  $R_{A,I}$ , denotes the dot product  $\vec{R}_{AO} \cdot \hat{i}$ .

$$(60) \quad R_{A,J} = AO \sin(\theta_1)$$

$$(61) \quad R_{B,I} = R_{A,I} + BA \cos(\theta_2)$$

$$(62) \quad R_{B,J} = R_{A,J} + BA \sin(\theta_2)$$

$$(63) \quad R_{CJ} = R_{AJ} + CA \cos(\theta_2 + \pi/2)$$

$$(64) \quad R_{CJ} = R_{AJ} + CA \sin(\theta_2 + \pi/2)$$

Differentiating the above position equations with respect to time yields the velocity equations, shown below.

$$(65) \quad V_{AJ} = -\dot{\theta}_1 AO \sin(\theta_1)$$

$$(66) \quad V_{AJ} = \dot{\theta}_1 AO \cos(\theta_1)$$

$$(67) \quad V_{BJ} = V_{AJ} - \dot{\theta}_2 BA \sin(\theta_2)$$

$$(68) \quad V_{BJ} = V_{AJ} + \dot{\theta}_2 BA \cos(\theta_2)$$

$$(69) \quad V_{CJ} = V_{AJ} - \dot{\theta}_2 CA \sin(\theta_2 + \pi/2)$$

$$(70) \quad V_{CJ} = V_{AJ} + \dot{\theta}_2 CA \cos(\theta_2 + \pi/2)$$

Similarly, differentiating the velocity equations with respect to time yields the acceleration equations.

$$(71) \quad A_{AJ} = -\ddot{\theta}_1 AO \sin(\theta_1) - (\dot{\theta}_1)^2 AO \cos(\theta_1)$$

$$(72) \quad A_{AJ} = \ddot{\theta}_1 AO \cos(\theta_1) - (\dot{\theta}_1)^2 AO \sin(\theta_1)$$

$$(73) \quad A_{BJ} = A_{AJ} - \ddot{\theta}_2 BA \sin(\theta_2) - (\dot{\theta}_2)^2 BA \cos(\theta_2)$$

$$(74) \quad A_{BJ} = A_{AJ} + \ddot{\theta}_2 BA \cos(\theta_2) - (\dot{\theta}_2)^2 BA \sin(\theta_2)$$

$$(75) \quad A_{CJ} = A_{AJ} - \ddot{\theta}_2 CA \sin(\theta_2 + \pi/2) - (\dot{\theta}_2)^2 CA \cos(\theta_2 + \pi/2)$$

$$(76) \quad A_{CJ} = A_{AJ} + \ddot{\theta}_2 CA \cos(\theta_2 + \pi/2) - (\dot{\theta}_2)^2 CA \sin(\theta_2 + \pi/2)$$

The above equations indicate that only four derivatives are required to calculate all the desired velocities and accelerations, namely  $\dot{\theta}_1$ ,  $\dot{\theta}_2$ ,  $\ddot{\theta}_1$ , and  $\ddot{\theta}_2$ . The angles are known for a given set of input values for  $\theta_1$ . Hence, using numerical methods, it is possible to calculate  $d\theta_2/d\theta_1$ . However, to determine  $\dot{\theta}_1$  and  $\dot{\theta}_2$ , it is required to choose a value for  $\dot{\theta}_1$ . It is anticipated that the device will operate at approximately 5 Hz. Since,  $\theta_1$  represents the phase of the crankshaft,  $\dot{\theta}_1$  reflects the operating speed of the device. Therefore,  $\dot{\theta}_1 = 10\pi$  (rad/sec) or 1800 (deg/sec). Note that assuming a constant value for  $\dot{\theta}_1$  implies  $\ddot{\theta}_1$  is identically zero, which simplifies some of the acceleration equations. It is essential that the numerical differentiation scheme used is accurate, since the accelerations



are used to determine the forces present in the device.

The central finite difference method is often used to estimate the derivative of an unknown function, for which several values are known. A better method is called the Richardson extrapolation. Given the following table of values,

u:	(x-h)	(x - h/2)	(x)	(x + h/2)	(x + h)
f(u)	f(x-h)	f(x - h/2)	f(x)	f(x + h/2)	f(x + h)

Table 5: Typical values to be differentiated numerically.

Consider the following Taylor series expansions f:

$$(77) \quad f(x + h) = f(x) + hf'(x) + \frac{h^2 f''(x)}{2!} + \frac{h^3 f'''(x)}{3!} + \frac{h^4 f^{(iv)}(x)}{4!} + \dots$$

and

$$(78) \quad f(x - h) = f(x) - hf'(x) + \frac{h^2 f''(x)}{2!} - \frac{h^3 f'''(x)}{3!} + \frac{h^4 f^{(iv)}(x)}{4!} - \dots$$

hence,

$$(79) \quad f(x + h) - f(x - h) = 2 \left( hf'(x) + \frac{h^3 f'''(x)}{3!} + \frac{h^5 f^{(v)}(x)}{5!} + \dots \right)$$

therefore,

$$(80) \quad f'(x) = \frac{f(x + h) - f(x - h)}{2h} - \frac{h^2 f'''(x)}{2(3!)} + \frac{h^4 f^{(v)}(x)}{2(5!)} + \dots$$

The first term on the right hand side of equation 28 is the equation used by the central finite difference approximation. Note that for small values of h the error term is on the order of  $h^2$ . Holding f and x fixed, we define a function of h, by the formula

$$(81) \quad \phi(h) = \frac{f(x + h) - f(x - h)}{2h}$$

hence,

$$(82) \quad \phi(h) = f'(x) - a_2 h^2 - a_4 h^4 - a_6 h^6 - \dots$$

and,

$$(83) \quad \phi\left(\frac{h}{2}\right) = f'(x) - a_2 \left(\frac{h}{2}\right)^2 - a_4 \left(\frac{h}{2}\right)^4 - a_6 \left(\frac{h}{2}\right)^6 - \dots$$

where  $a_2$ ,  $a_4$ , and  $a_6$  are constants that depend on  $f$  and  $x$ .

It is possible to eliminate the highest order error term with simple algebra.

$$(84) \quad \frac{4\phi\left(\frac{h}{2}\right) - \phi(h)}{3} = f'(x) + \frac{a_4 h^4}{4} + \frac{5a_6 h^6}{16} + \dots$$

The error is now on the order of  $h^4$  (although it should be noted that this  $h$  is twice the value of the  $h$  that would logically be used for the central difference method; so for relatively large values of  $h$ , the central difference method could actually be more accurate). For a more detailed explanation of the Richardson extrapolation technique (which the authors termed a “miraculous discovery”), see pp. 137-141 of Numerical Methods and Computing by Cheney & Kincaid.

Since the angles are calculated (in radians) at each degree of  $\theta_1$ , the central finite difference method would yield an error term on the order of  $(\pi/180)^2 = 0.00030$  radians per degree when calculating  $d\theta_2/d\theta_1$ . Then, using the chain rule, this is scaled by  $d\theta_1/dt$ , which is 1800 degrees/sec, hence the total error for  $\dot{\theta}_2$  would be on the order of 0.55 rad/sec. This error would of course be compounded when the angular acceleration,  $\ddot{\theta}_2$ , was computed.

Similarly, using the first order Richardson extrapolation, the error for  $d\theta_2/d\theta_1$  is on

the order of  $(2\pi/180)^4 = 0.0000015$  rad/degree, and the total error for  $\dot{\theta}_2$  is on the order of 0.0027 rad/sec. This is a substantially more accurate method, and the excess computation time is only a few seconds on a personal computer. The following figures show the paths, velocities, and accelerations of points A, B, and C over the course of one cycle (as calculated for a device operating speed of 5 Hz.)

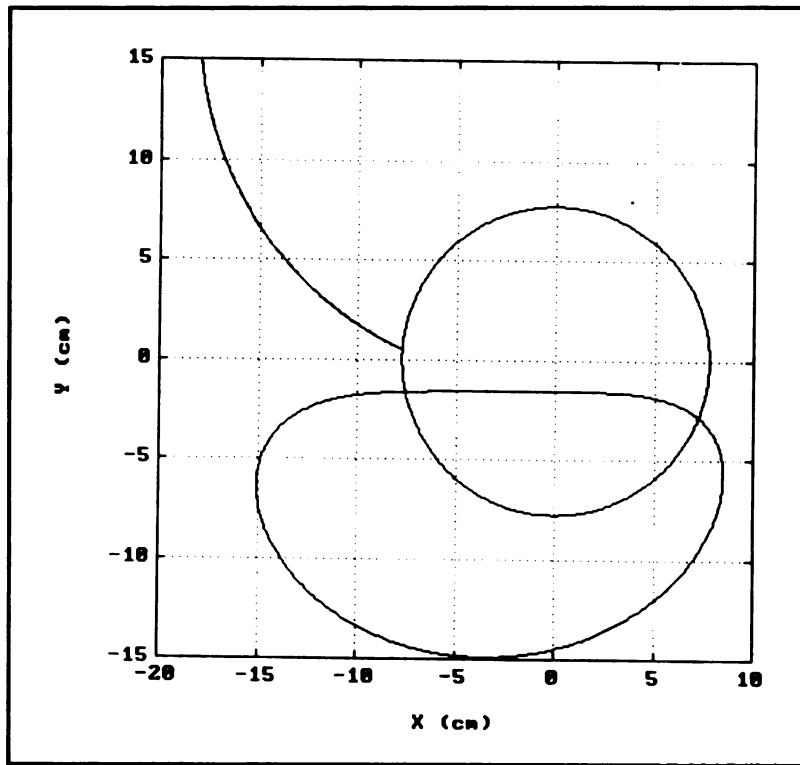


Figure 53: Trajectories of points A, B, and C.

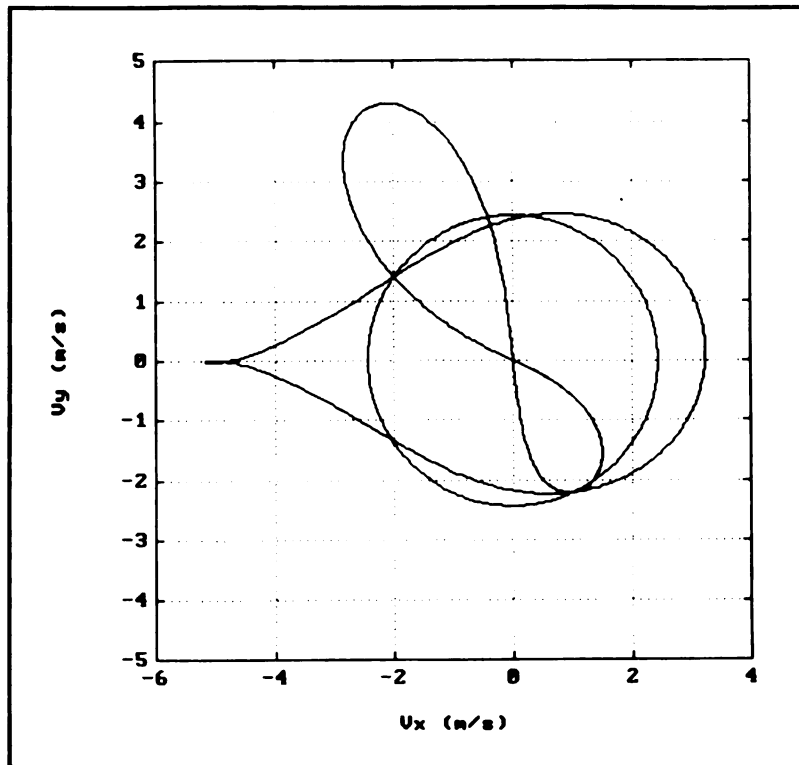


Figure 54: Parametric Velocity curves of points A, B, and C.

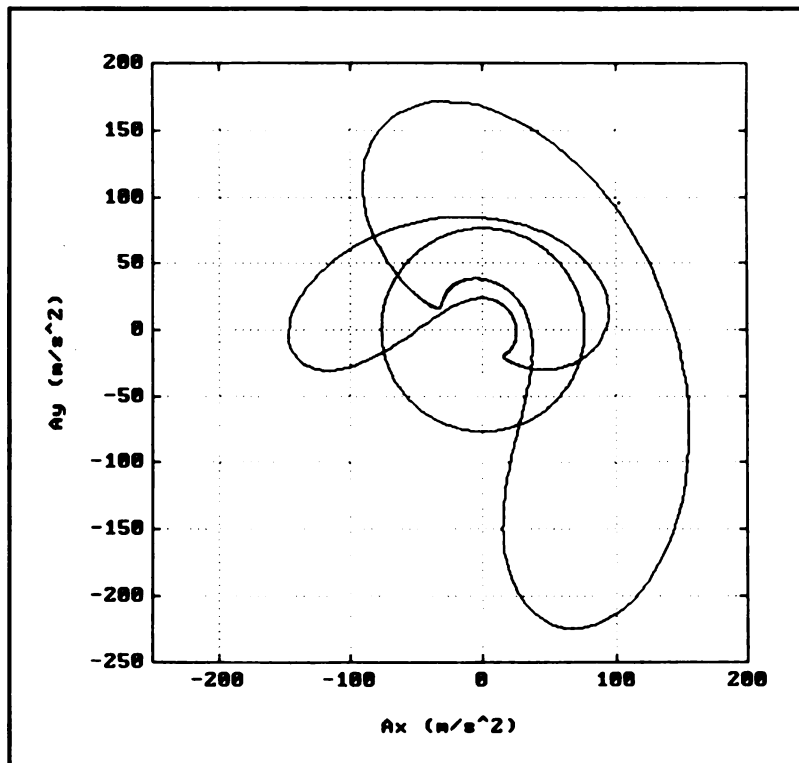


Figure 55: Parametric acceleration curves of points A, B, and C.

**STEP 4:** Determine the forces present in the pin joints.

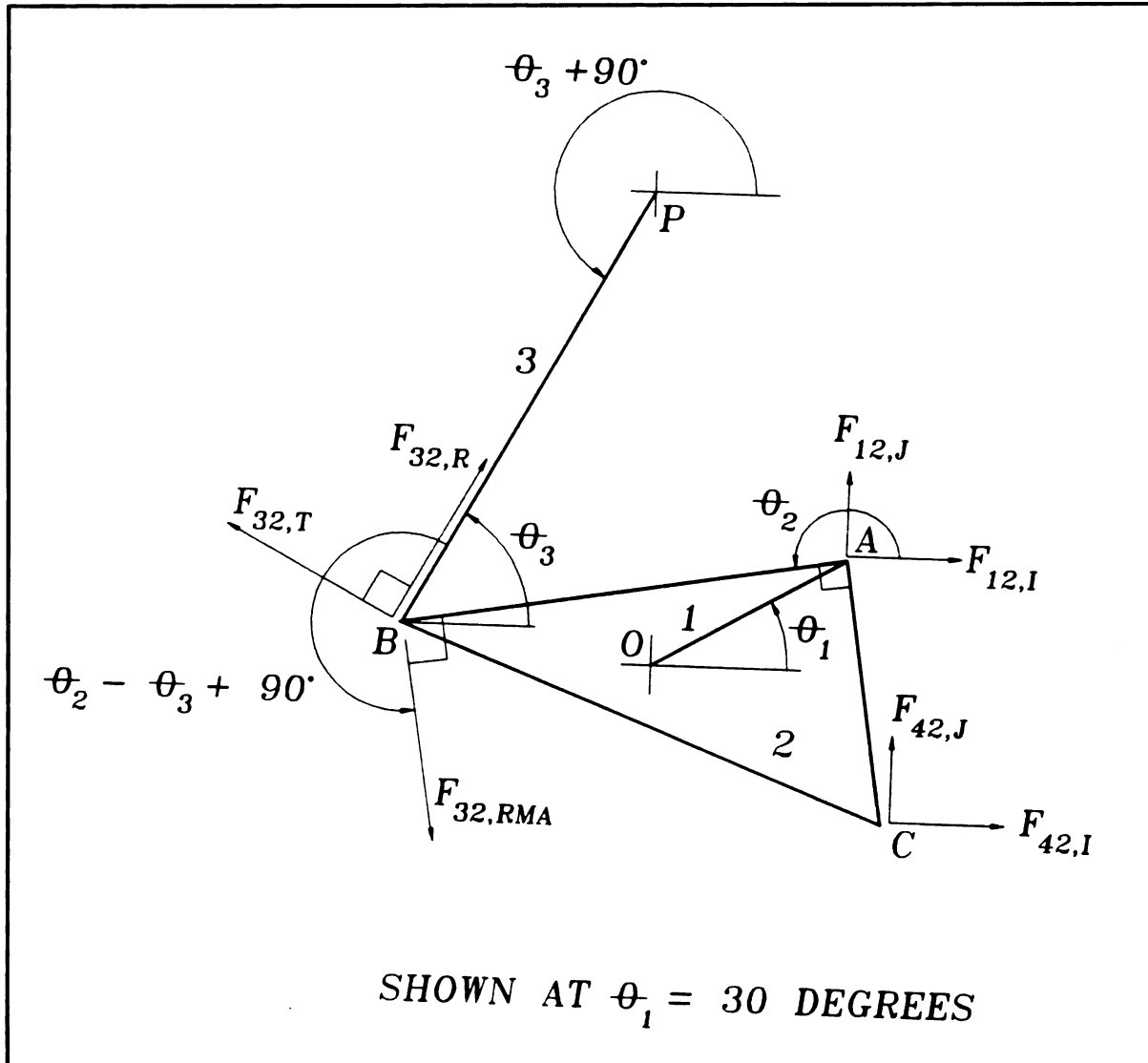


Figure 56: Free body diagram of the coupler (link 2).

First, conservative estimates are made for the masses of the moving parts. The moments of inertia of link 2 about point A, and link 3 about point P are calculated. The force transmitted from link 2 to link 4 is determined using d'Alembert's Principle. The tangential component of force from link 2 to link 3 is known (using  $M = J\ddot{\theta}_3$ ). Consider the motion of link 2 to be the sum of a translation of point A and a rotation about point A.

Summing moments about point A will determine the radial component of the force at point B. Finally, summing forces in the x and y directions, and again using d'Alembert's principle, the forces at point A are determined.

From the kinematics, the following values are known:

$$\theta_1, \theta_2, \theta_3, \ddot{\theta}_1, \ddot{\theta}_2, \ddot{\theta}_3, R_{A,I}, R_{A,J}, R_{B,I}, R_{B,J}, R_{C,I}, R_{C,J}, A_{A,I}, A_{A,J}, A_{B,I}, A_{B,J}, A_{C,I}, A_{C,J}$$

Knowing the above positions and accelerations, and estimating the masses and moments of inertia, is sufficient to determine all forces. The procedure is outlined below.

Estimated masses:

$$\begin{aligned} m_2 &= 227 \text{ g} = 0.5 \text{ lb}_m \\ m_3 &= 114 \text{ g} = 0.25 \text{ lb}_m \\ m_4 &= 681 \text{ g} = 1.5 \text{ lb}_m \\ m_5 &= 9.08 \text{ kg} = 20 \text{ lb}_m \end{aligned}$$

Moments of Inertia:

$$(85) \quad J_{3,P} = (1/12)[(m_3) [(1'')^2 + (8'')^2]/144 \text{ ft}^2] + [(m_3) [(3.5/12 \text{ ft})^2]$$

$$(86) \quad J_{2,A} = (1/18)[(m_2) [(4.7'')^2 + (7.2'')^2]/144 \text{ ft}^2] + [(m_2) [(2.1/12 \text{ ft})^2]$$

Consider the forces transmitted from the coupler to the 2-axis slider. The mass of the 2-axis slider is divided into two parts. The masses of the parts that are constrained to move in the  $\hat{j}$  direction only constitute  $m_5$ . The parts which make up the slider that moves horizontally, relative to  $m_5$ , constitute  $m_4$ . Therefore, using d'Alembert's principle, consider the forces from link 2 to link 4, in the  $\hat{i}$  direction:

$$(87) \quad F_{24,I} = (m_4) A_{C,I}$$

Similarly, in the  $\hat{j}$  direction,

$$(88) \quad F_{24,J} = (m_4 + m_5) A_{C,J}$$

The next step is to calculate the component of force at point B that is tangent to link 3.

Applying d'Alembert's principle to the rotational motion of link 3 about point P yields,

$$(89) \quad M_{3,P} = F_{23,T} (BP) = J_{3,P} \ddot{\theta}_3$$

Hence,

$$(90) \quad F_{23,T} = J_{3,P} \ddot{\theta}_3 / BP$$

Note that the angle of link 3, as measured from a vector in the  $\hat{i}$  direction originating from point P, is  $(\pi + \theta_3)$ . Hence, upon differentiation, the  $\pi$  drops out, and the angular acceleration about point P is just  $\ddot{\theta}_3$ . Note that  $F_{23,T}$  is constantly changing direction, and must be converted into its  $\hat{i}$  and  $\hat{j}$  components at each degree independently. This is done as follows:

$$(91) \quad F_{23,T,I} = F_{23,T} \cos(\theta_3 + \pi/2)$$

$$(92) \quad F_{23,T,J} = F_{23,T} \sin(\theta_3 + \pi/2)$$

Now consider link 2. Since the analysis is restricted to 2-space, and there are three points where force can be applied to link 2, there are 6 orthogonal components required to adequately describe all three forces. Presently, three of the six have been determined; namely  $F_{24,I}$ ,  $F_{24,J}$ , and  $F_{23,T}$ . Considering the forces to be acting on link 2, the forces should take on the opposite of their previously calculated values (i.e.,  $F_{42,I} = -F_{24,I}$ ). Note that the assumption of massless pins, with negligible friction forces, has been made here. The present study is interested in the inertial forces of the links. Consider the motion of link 2 to be described by the sum of a translation of point A and a rotation about point A. The remaining component of force at point B can be found. The portion of the radial component of force at point B, which contributes to the moments about point A is found.

Then, knowing that the total radial component of force must be perpendicular to the tangential component, a vector triangle is formed, and the desired force is calculated.

$$(93) \quad \sum M_A = J_{2,A} \ddot{\theta}_2 = F_{32,RMA}(AB) + [F_{32,T,I} (R_{A,J} - R_{B,J})] + [F_{32,T,J} (R_{B,I} - R_{A,I})] + [F_{42,I} (R_{A,J} - R_{C,J})] + [F_{42,J} (R_{C,I} - R_{A,I})]$$

therefore,

$$(94) \quad F_{32,RMA} = \{ J_{2,A} \ddot{\theta}_2 - [F_{32,T,I} (R_{A,J} - R_{B,J})] - [F_{32,T,J} (R_{B,I} - R_{A,I})] - [F_{42,I} (R_{A,J} - R_{C,J})] - [F_{42,J} (R_{C,I} - R_{A,I})] \} / AB$$

where  $F_{32,RMA}$  is the component of the radial force at C which contributes to the moment of link 2 about point A. Knowing that the direction of the total radial component of force is  $\theta_3$ , it is possible to determine the  $\hat{i}$  and  $\hat{j}$  components of the radial force at C.

$$(95) \quad F_{32,R,I} = (F_{32,RMA}) \cos(\theta_3) / [\cos(\theta_2 + \pi/2 - \theta_3)]$$

and,

$$(96) \quad F_{32,R,J} = (F_{32,RMA}) \sin(\theta_3) / [\cos(\theta_2 + \pi/2 - \theta_3)]$$

Therefore, all forces are known at points B and C, the forces are summed and in both the  $\hat{i}$  and  $\hat{j}$  directions and the forces at point A are easily calculated. Applying d'Alembert's principle to link 2 yields the forces at point A

$$(97) \quad F_{12,I} = m_2 A_{2,I} - F_{32,T,I} - F_{32,R,I} - F_{42,I}$$

and,

$$(98) \quad F_{12,J} = m_2 A_{2,J} - F_{32,T,J} - F_{32,R,J} - F_{42,J}$$

It is desirable to convert the forces at A from  $\hat{i}$  and  $\hat{j}$  components to radial and tangential components, thus making it more convenient when selecting bearings for the crankshaft, and the motor.



$$(99) \quad F_{12,R} = F_{12,I} \cos(-\theta_1) + F_{12,J} \cos(\pi/2 - \theta_1)$$

$$(100) \quad F_{12,T} = F_{12,I} \sin(-\theta_1) + F_{12,J} \sin(\pi/2 - \theta_1)$$

The equations derived in this section are placed in a Matlab program, and the forces are calculated for each degree of  $\theta_1$ . The results are plotted for  $F_{42,I}$ ,  $F_{42,J}$ ,  $F_{42}$ ,  $F_{32,T}$ ,  $F_{32,R}$ ,  $F_{32}$ ,  $F_{12,T}$ ,  $F_{12,R}$ ,  $F_{12}$ , all as functions of  $\theta_1$

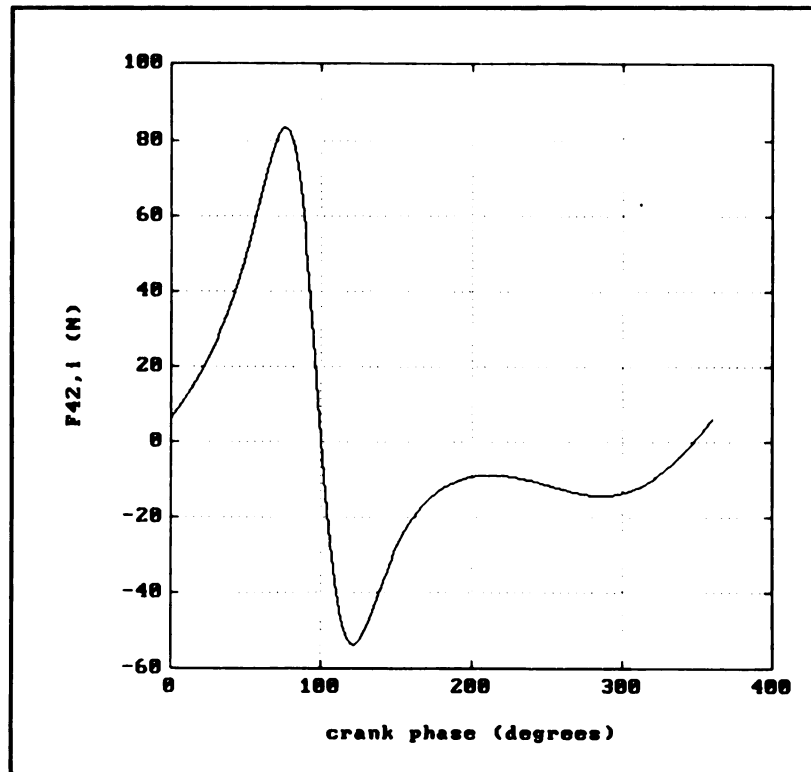
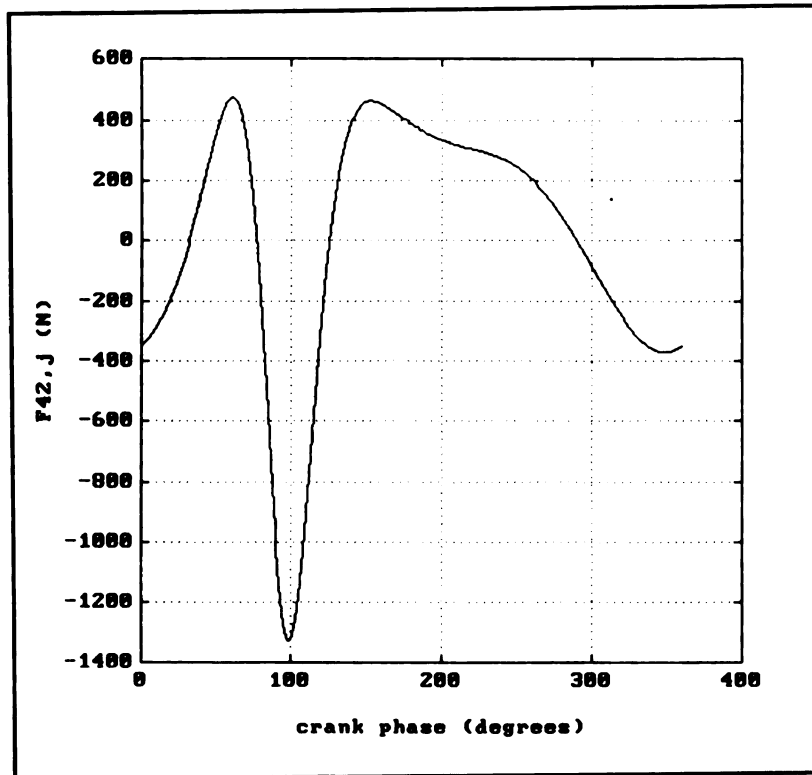
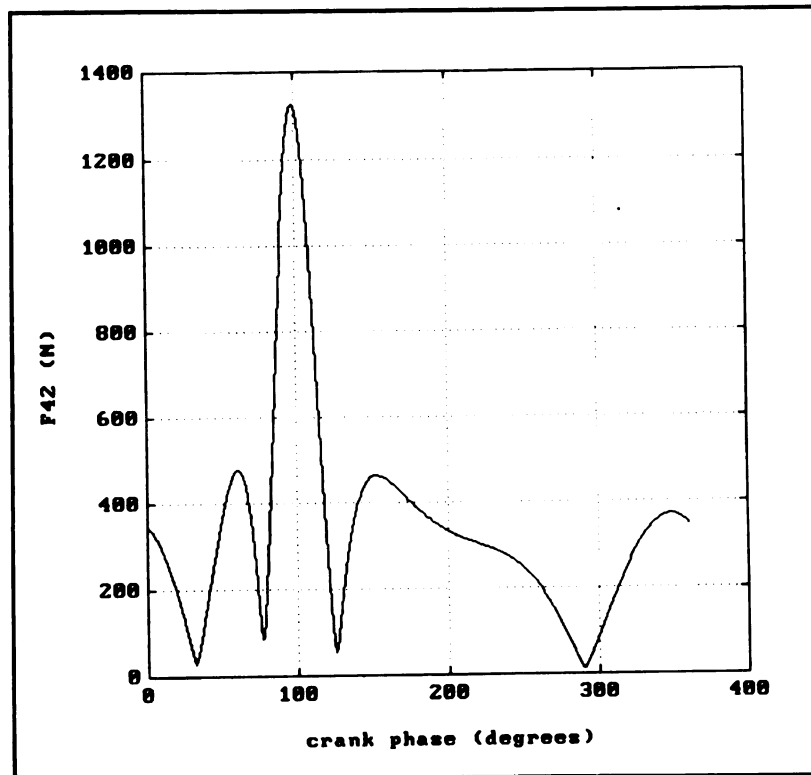
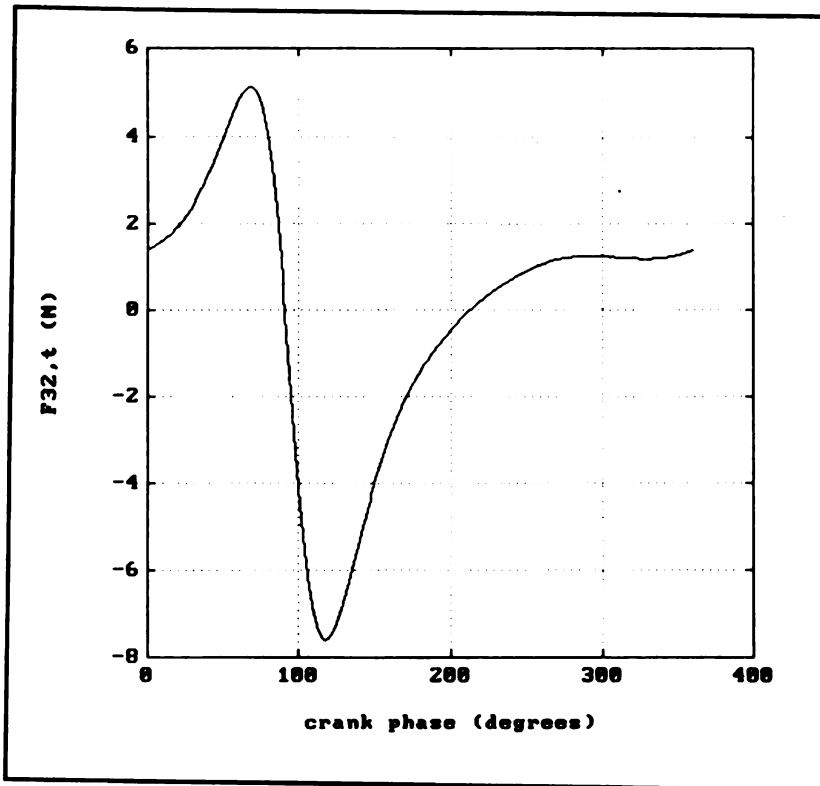
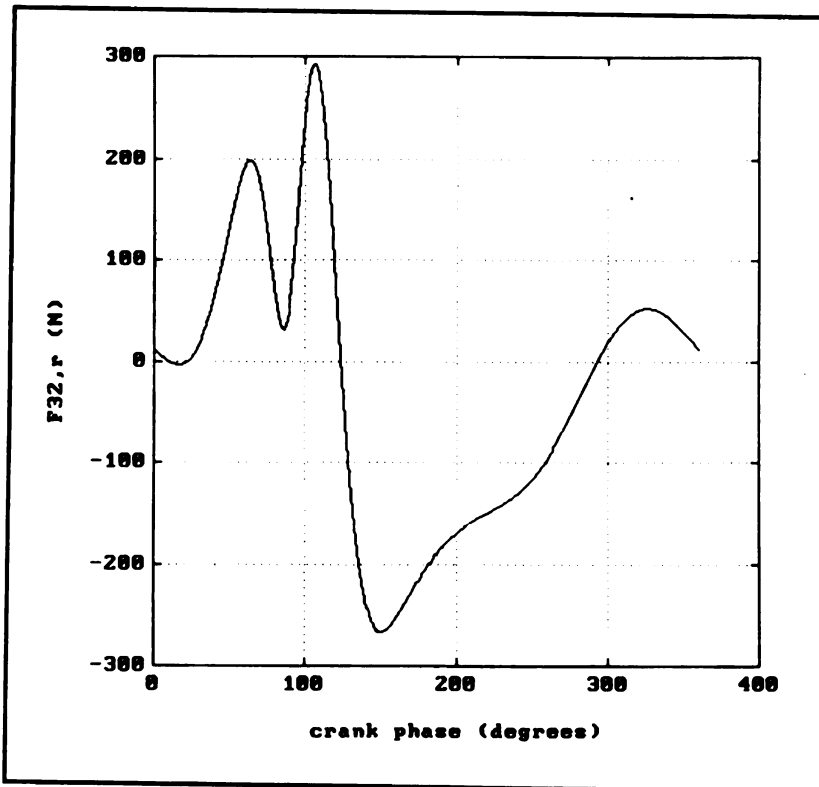


Figure 57:  $F_{42,I}$  vs.  $\theta_1$

Figure 58:  $F_{42,J}$  vs.  $\theta_1$ Figure 59:  $|F_{42}|$  vs.  $\theta_1$

Figure 60:  $F_{32,T}$  vs.  $\theta_1$ Figure 61:  $F_{32,R}$  vs.  $\theta_1$

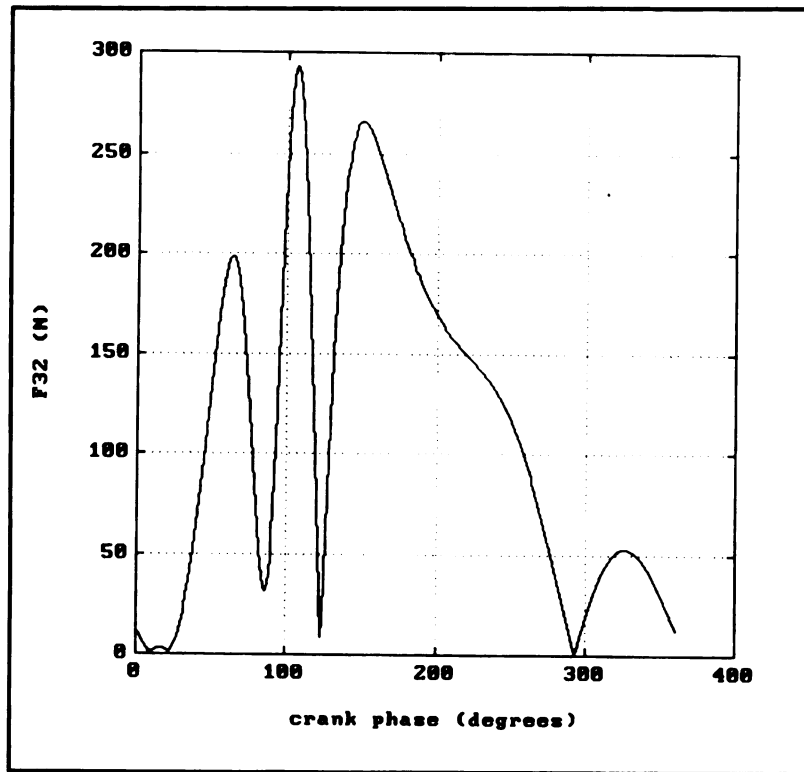


Figure 62:  $|F_{32}|$  vs.  $\theta_1$

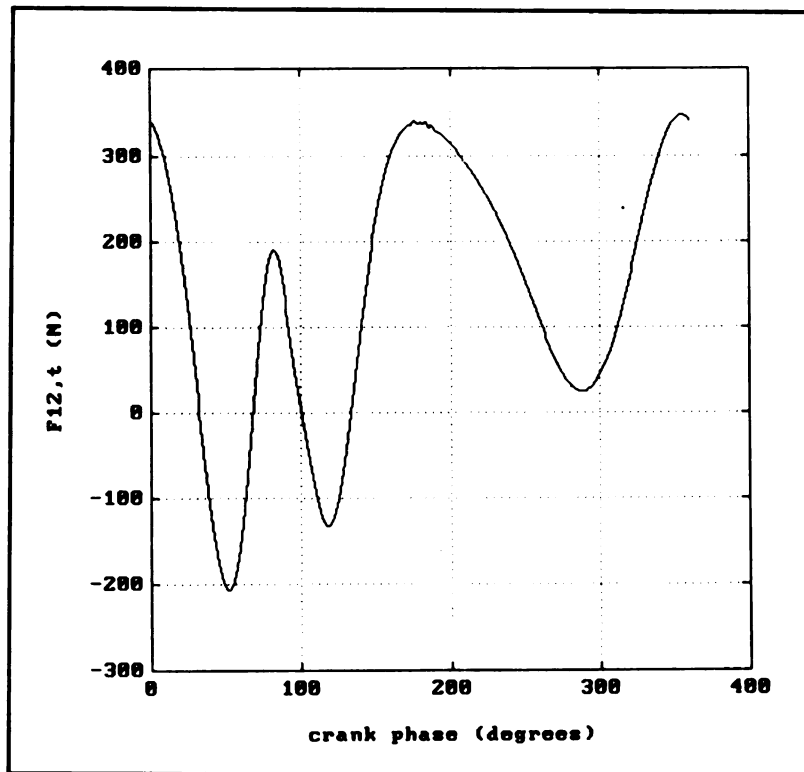
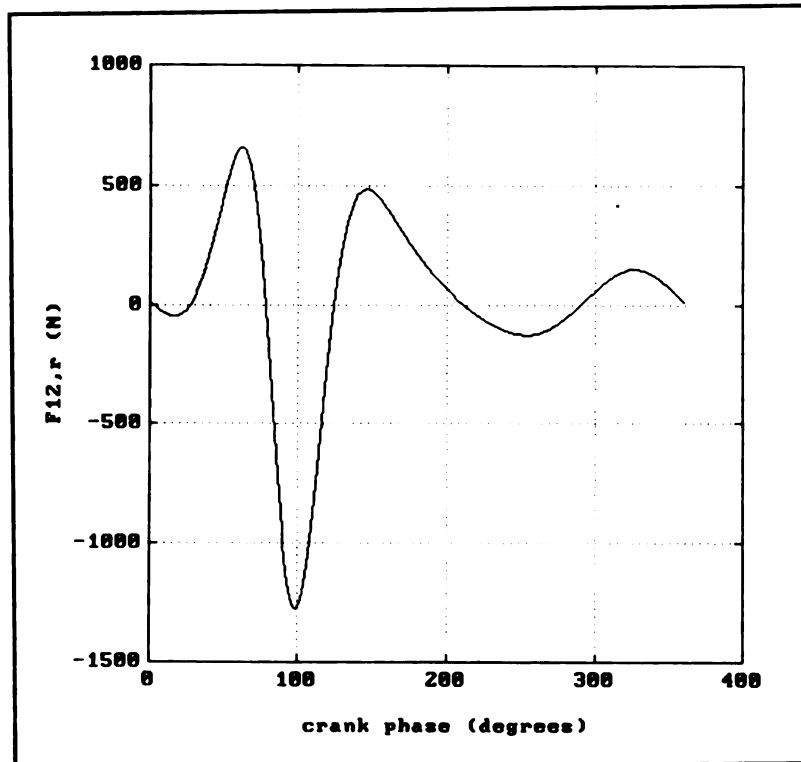
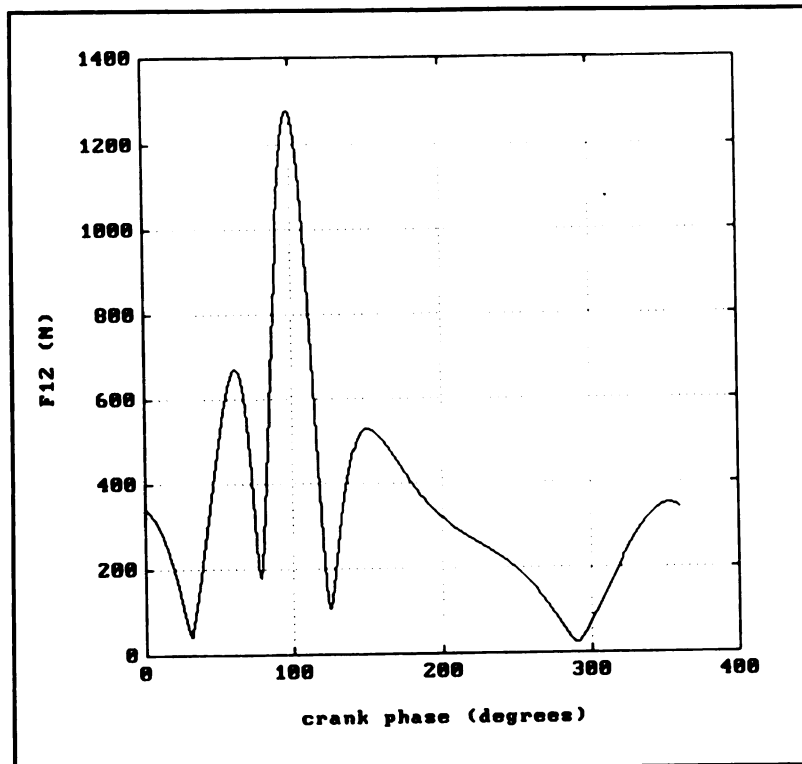


Figure 63:  $F_{12,t}$  vs.  $\theta_1$

Figure 64:  $F_{12,R}$  vs.  $\theta_1$ Figure 65:  $|F_{12}|$  vs.  $\theta_1$

A six part linkage has been analyzed which uses a rotational input motion to generate a rise-dwell-return motion. Sufficient time is allowed for the blade selection process during the dwell portion of the cycle. The ability to select or deselect the blades at each cycle of operation allows the device to cut fibers at variable 1.27 cm (1/2 inch) intervals. Therefore, the length of fibers is alterable without any delay in the operation of the device, which is a feature that is not available in existing devices. All the inertial forces present in the blade mechanism have been calculated (using estimates for masses). Hence, the appropriate bearings and motor can be chosen.

## **APPENDIX D**

## **APPENDIX D -- EVALUATION OF INITIAL DESIGN**

A prototype was manufactured to test the blade mechanism. It was anticipated that all of the parts used in the prototype, except the blade, would be useable in the final design. The blade selection process was not part of the experimental setup. After the prototype was manufactured, two major problems were discovered. First, the stroke of the blade was relatively large (5.25 inches), which resulted in violent vibrations of the apparatus at high speeds. Second, the blade did not cut the tow cleanly.

In order to reduce the vibration of the apparatus there are four options. First, the stroke of the cradle could be reduced. Second, the mass of the cradle could be reduced. Third, the operating speed of the apparatus could be reduced. Finally, another mass could be made to move opposite the cradle to balance the device. Any combination of these would aid in the reduction of vibration.

The blade must be held firmly against the cutting surface without crashing on the descent to cut the tow cleanly. In order to do this, a new cutting method is in order. Rather than the blade moving against a shearing surface, as commonly done with metals, a scissor-like mechanism could be used. The major benefit of a scissor-like action is that the two blades are always in contact, with crash being prevented by the "leading edges".

Unfortunately, the use of a new cutting method, will also necessitate a completely new fiber intake process, and minor modifications to the delivery process. The fiber intake process proposed in design I, although not specifically tested, had some inherent flaws.



The biggest problem is that the grippers moved around the incoming tows, and were located between the tows and the blades. This is why the blades were required to travel the relatively large distance (5.25 in.). In order to pull the fiber tows into position in an intermittent fashion, while not using any mechanism that will travel under the blades, an entraining flow may be used. That is, the tows may be pulled in three inches at a point located outside of the "cutting chamber". The entraining flow can then be used to force the excess 3" of slack tow in position for the cut. The suggestions put forth here are explained in greater detail in chapter 2 ("Synthesis of Design 2").

## **APPENDIX E**

## APPENDIX E -- MATLAB PROGRAMS

Several programs, written for Matlab, were referred to in the analysis. Those programs are presented in this chapter. Chapter 3 used programs “geneva” and “intake” to analyze the fiber intake process. Chapter 4 used the program “cam” to design the cam system and determine the required spring constant for the primary spring. Appendix C used programs “rdr1a”, “rdr1b”, and “bladmech” to analyze the kinematics and forces of the blade mechanism in the initial design. This appendix consists of the listing of the programs used.

### “GENEVA” :

**% DEFINE VARIABLES**

```
theta=zeros(91,1);
z=zeros(91,1);
phi=zeros(91,1);
Xr=zeros(91,1);
Vr=zeros(91,1);
Ar=zeros(91,1);
phidot=zeros(91,1);
phidotdot=zeros(91,1);
phase=zeros(91,1);
```

**% PARAMETERS**

```
rad= pi/180;
R=0.159 ; % feet (radius of pinchroller driven by geneva)
```

**% CALCULATE QUANTITIES AT EVERY DEGREE OF INPUT MOTION**

**for i=1:91**

```
theta(i)=(i+134)*rad;
z(i)=(3+2.828427*cos(theta(i)))^0.5;
phi(i)=asin(sin(theta(i))/z(i));
Xr(i)=R*12*(pi/4 - phi(i));%inches
```

```

thetadot=10 * pi; % radians/second
phidot(i)= thetadot / cos(phi(i)) * (1/z(i) * cos(theta(i)) + ...
    1/z(i)^3 * 1.4142136 * (sin(theta(i)))^2);
Vr(i)=-R*phidot(i);%feet per second
phidotdot(i)=1/cos(phi(i)) * (phidot(i)^2 * sin(phi(i)) + ....
    thetadot^2*sin(theta(i))/z(i) * (6.0/z(i)^4 * ....
    sin(theta(i))^2 + 3*1.4142136/z(i)^2 * cos(theta(i)) - 1.0));
Ar(i)=-R * phidotdot(i);%feet per second^2
phase(i) = i-1;
end

```

```
axis('square')
```

```

% PLOT POSITION CURVE
%axis([ 0 90 0 3])
%plot (phase, 2.54*Xr)
%grid
%xlabel('phase angle - 135 (deg.)')
%ylabel('tow position relative to roller (cm)')

```

```

% PLOT VELOCITY CURVE
%axis([0 90 0 14])
plot (phase,0.305 * Vr)
grid
xlabel('phase angle - 135 (deg.)')
ylabel('tow velocity at roller (m/s)')

```

```

%PLOT ACCELERATION CURVE
%axis([0 90 -1000 1000])
%plot (phase,0.305 * Ar)
%grid
%xlabel('phase angle - 135 (deg.)')
%ylabel('tow acceleration at roller (m/s^2)')

```

### “INTAKE” :

```

% Define variables
theta=zeros(91,1);
z=zeros(91,1);
phi=zeros(91,1);
Xr=zeros(91,1);
Vr=zeros(91,1);
Ar=zeros(91,1);
Xtow=zeros(181,3);
Vtow=zeros(181,3);
Atow=zeros(181,3);
phidot=zeros(91,1);
phidotdot=zeros(91,1);
phase=zeros(91,1);

```

```

% PARAMETERS
rad= pi/180;

```

```

R=0.159 ; % feet (radius of pinchroller driven by geneva)
Vtow(1,:)=[0,0,0];
Xtow(1,:)=[0,0,0];
deltat=0.1/180;% time step in seconds
Vair=[40, 80, 120];% feet per second

```

**% CALCULATE MOTION OF GENEVA MECHANISM**

```

for i=1:91
    theta(i)=(i+134)*rad;
    z(i)=(3+2.828427*cos(theta(i)))^0.5;
    phi(i)=asin(sin(theta(i))/z(i));
    Xr(i)=R*12*(pi/4 - phi(i));%inches
    thetadot=10 * pi; % radians/second
    phidot(i)= thetadot / cos(phi(i)) * (1/z(i) * cos(theta(i)) + ...
        1/z(i)^3 * 1.4142136 * (sin(theta(i)))^2);
    Vr(i)=-R*phidot(i);%feet per second
    phidotdot(i)=1/cos(phi(i)) * (phidot(i)^2 * sin(phi(i)) + ....
        thetadot^2*sin(theta(i))/z(i) * (6.0/z(i)^4 * ....
        sin(theta(i))^2 + 3*1.4142136/z(i)^2 * cos(theta(i)) - 1.0));
    Ar(i) =-R * phidotdot(i);%feet per second^2
    phase(i) = i-1;
end

```

```

for i=1:91
    Xr2(i)=Xr(i);
    Xr2(i+90)=3.0;
    Vr2(i)=Vr(i);
    Vr2(i+90)=0;
    Ar2(i)=Ar(i);
    Ar2(i+90)=0;
end

```

**%CALCULATE MOTION OF TOW UNDER THE INFLUENCE OF THE ENTRAINING FLOW**

**%NOT ALLOWING THE TOW TO EXCEED THE BOUNDARY CONDITIONS IMPOSED BY THE  
%GENEVA MECHANISM.**

```

for i=1:180
    for j=1:3
        Atow(i,j)=0.040*(Vair(j)-Vtow(i,j))^2;% feet per second^2
        if Xtow(i,j) >= Xr2(i)
            Xtow(i,j)=Xr2(i);
            if Vtow(i,j) >= Vr2(i)
                Vtow(i,j)=Vr2(i);
                Atow(i,j)=Ar2(i);
            end
        end
        Vtow(i+1,j)=Vtow(i,j)+Atow(i,j)*deltat;%feet/sec
        Xtow(i+1,j)=Xtow(i,j)+Vtow(i+1,j)*deltat*12;%inches
    end
end
Atow(181,:)=Atow(180,:);

```

```

axis('square')

t91=0:1/1800:0.05;
t181=0:1/1800:0.1;

% PLOT POSITION CURVE
%axis([ 0 0.1 0 3])
plot (t181,2.54*Xtow,t91,2.54*Xr)
grid
%title ('Position Curves during Return')
xlabel('time (seconds)')
ylabel('tow position relative to blade #1 (cm)')
text(.002,5.5,'Vair=42.7m/s')
text(.029,4.8,'36.6')
text(.034,3.5,'24.4m/s')
text(.065,3.25,'12.2m/s')

% PLOT VELOCITY CURVE
%axis([0 0.1 0 14])
%plot (t181,.305*Vtow,t91,.305*Vr)
%grid
%title ('Tow velocities at Roller and outlet (operating speed 300 rpm)')
%xlabel('time (seconds)')
%ylabel('tow velocity relative to blade #1 (m/s)')
%text(.001,3.8,'Vair=42.7m/s')
%text(.033,4.2,'36.6m/s')
%text(.048,3.15,'24.4m/s')
%text(.073,1.6,'12.2m/s')

%PLOT ACCELERATION CURVE
%axis([0 0.1 -1000 1000])
%plot (phase,Ar)
%grid
%title ('Tow acceleration at Roller (operating speed 300 rpm)')
%xlabel('phase angle - 135 (deg.)')
%ylabel('acceleration (ft/s^2)')

```

### “CAM” :

```

% DEFINE VARIABLES
y=zeros(361,1);
rise=zeros(46,1);
retrn=zeros(46,1);
theta=zeros(361,1);
pitchr=zeros(361,1);
camr=zeros(361,1);
force=zeros(91,1);
x=zeros(91,1);
v=zeros(91,1);
a=zeros(91,1);

```

```

% PARAMETERS
rad= pi/180;
baser=1.75;
rollerr=0.5;
m=8/32.2;%slugs
thetadot = 10 * pi ; %radians per second
xi=0.5;%inches (initial spring compression)
klact=160;%Lbs/in (primary spring constant)

for i=1:46
    angle=(i-1)*rad;
    rise(i)= (22.9958 * angle^4) - (70.27 * angle^5) + ....
              (74.5588 * angle^6) - (27.1232 * angle^7);%inches

    vrise(i)= ((4*22.9958 * angle^3) - (5*70.27 * angle^4) + ....
              (6*74.5588 * angle^5) - ....
              (7*27.1232 * angle^6))*thetadot/12;%fps

    arise(i)= ((3*4*22.9958 * angle^2) - (4*5*70.27 * angle^3) + ....
              (5*6*74.5588 * angle^4) - ....
              (6*7*27.1232 * angle^5))*thetadot^2/12;%fps^2

    retrn(47-i)=rise(i);
    vretrn(47-i)=-vrise(i);
    aretrn(47-i)=arise(i);
end

for i=1:46
    x(i)=rise(i);
    x(i+45)=retrn(i);
    v(i)=vrise(i);
    v(i+45)=vretrn(i);
    a(i)=arise(i);
    a(i+45)=aretrn(i);
    phase(i)=i-1;
    phase(i+45)=i+44;
end

for i=1:361
    pitchr(i)=baser;
    theta(i)=i*rad;
end

topdwell=baser+0.5;
pitchr(90:135)=baser+rise;
pitchr(135:180)=baser+retrn;

for i=181:360
    pitchr(i)=pitchr(i-180);
end

pitchr(361)=pitchr(1);

```

```

for i=1:361
    pitchx(i)=pitchr(i) .* cos(theta(i));
    pitchy(i)=pitchr(i) .* sin(theta(i));
end

dpy(1)=(4*(pitchy(2)-pitchy(360))/2-(pitchy(3)-pitchy(359))/4)/3;
dpx(1)=(4*(pitchx(2)-pitchx(360))/2-(pitchx(3)-pitchx(359))/4)/3;

dpy(2)=(4*(pitchy(3)-pitchy(1))/2-(pitchy(4)-pitchy(360))/4)/3;
dpx(2)=(4*(pitchx(3)-pitchx(1))/2-(pitchx(4)-pitchx(360))/4)/3;

for i=3:359
    dpy(i)=(4*(pitchy(i+1)-pitchy(i-1))/2-(pitchy(i+2)-pitchy(i-2))/4)/3;
    dpx(i)=(4*(pitchx(i+1)-pitchx(i-1))/2-(pitchx(i+2)-pitchx(i-2))/4)/3;
end

dpy(360)=(4*(pitchy(1)-pitchy(359))/2-(pitchy(2)-pitchy(358))/4)/3;
dpx(360)=(4*(pitchx(1)-pitchx(359))/2-(pitchx(2)-pitchx(358))/4)/3;

dpy(361)=dpy(1);
dpx(361)=dpx(1);

for i=1:361;
    if dpx(i)==0
        if dpy(i)>0
            gamma(i)=pi/2;
        else
            gamma(i)=-pi/2;
        end
    else
        gamma(i)=atan(dpy(i)/dpx(i));
        if dpx(i)<0
            gamma(i)=gamma(i)+pi;
        end
    end
end

for i=1:361
    camx(i)=pitchx(i) + rollerr*cos(gamma(i)+pi/2);
    camy(i)=pitchy(i) + rollerr*sin(gamma(i)+pi/2);
end

maxpressure=0;

for i=1:361
    pressure(i)=180/pi *( pi/2 - gamma(i) + theta(i));
    if pressure(i) > 180
        pressure(i)=pressure(i)-360;
    end
    if pressure(i)>maxpressure
        maxpressure=pressure(i);
        position=i;
    end
end

```



end

maxpressure  
position

```
Io=0.641;%slug in^2
h=4;%inches
F1=((Io/h)/12)*a;%lbf
m2=0.017;%slugs
ks=42.9;%lbf/in
x0s=0.125;%in.
F2=m2*a + ks*(x+x0s)+2*F1;%lbf
m3=0.037;%slugs
x0p=0.5;%in.
N=6;%#of active blades
%kpreq=(50 - m3.*a - N*F2)./(x+x0p);
kp=40;%lbf
F3=m3*a + kp*(x+x0p)+ N*F2;%lbf
```

axis('square');

%PLOT POSTION CURVE FOR RISE AND RETURN MOTION

```
%axis([0 90 0 0.3])
%plot(phase,25.4*x)
%grid
%xlabel('phase angle (degrees)')
%ylabel('follower position (mm)')
```

%PLOT VELOCITY CURVE FOR RISE AND RETURN MOTION

```
%axis([0 90 -2 2])
%plot(phase,30.5*v)
%grid
%xlabel('phase angle (degrees)')
%ylabel('follower velocity (cm/s)')
```

%PLOT ACCELERATION CURVE FOR RISE AND RETURN MOTION

```
%axis([0 90 -250 250])
%plot(phase,.305*a)
%grid
%xlabel('phase angle (degrees)')
%ylabel('follower acceleration (m/s^2)')
```

%PLOT PITCH CURVE AND CAM PROFILE

```
%axis([-6 6 -6 6])
%plot(2.54*pitchx,2.54*pitchy,2.54*camx,2.54*camy)
%grid
%xlabel('X (cm)')
%ylabel('Y (cm)')
```

%PLOT F1

```
%axis([0 90 -4 4])
%plot(phase, 4.45*F1)
%grid
```

```
%xlabel('phase angle (degrees)')
%ylabel('F1 (N)')
```

```
%PLOT F2
%axis([0 90 -4 4])
%plot(phase, 4.45*F2)
%grid
%xlabel('phase angle (degrees)')
%ylabel('F2 (N)')
```

```
%PLOT F3
%axis([0 90 80 120])
plot(phase,4.45*F3)
grid
xlabel('phase angle (degrees)')
ylabel('F3 (N)')
```

### “RDR1A” :

```
% PROGRAM RDR1A.M

% This program calculates the coupler curve of a four bar (crank-rocker)
% mechanism. In addition, it does a least square fit to the
% straight line portion of the coupler curve, and measures the distance
% from the straight line as a function of the crank phase.

% Define variables
theta=zeros(360,3);
global count theta1 temp2 tempa;

% Solve for the angles of links a,b,c in the X-Y plane for point 1
% by calling program 'rdr1b.m'
theta1=2 * pi * (1)/360;
theta(1,1)=2 * pi * (1)/360;
theta(1,3)=fzero('rdr1b',-1.1,.0001);
theta(1,2)=temp2;

% Iteratively search for solution at each subsequent crank degree
% Starting each search at the previous solution (this calls sub-
% program 'thesis1.m' 359 times).
for i=2:400
    m=i-1;
    theta1=2 * pi * (i)/360;
    theta(i,1)=theta1;
    theta(i,3)=fzero('rdr1b',theta(m,3),.00001);
    theta(i,2)=temp2;
m
end

% Define position of coupler point, and calculate its position in the X-Y
% plane for all values of crank phase
```

```

% e=[1.0 1.1 1.2 1.3 1.4];
e=[1.2]

x(:,1)=cos(theta(:,1))+e(1).*cos(pi/2 + theta(:,2));
y(:,1)=sin(theta(:,1))+e(1).*sin(pi/2 + theta(:,2));

% x(:,2)=cos(theta(:,1))+e(2).*cos(pi/2 + theta(:,2));
% y(:,2)=sin(theta(:,1))+e(2).*sin(pi/2 + theta(:,2));

% x(:,3)=cos(theta(:,1))+e(3).*cos(pi/2 + theta(:,2));
% y(:,3)=sin(theta(:,1))+e(3).*sin(pi/2 + theta(:,2));

% x(:,4)=cos(theta(:,1))+e(4).*cos(pi/2 + theta(:,2));
% y(:,4)=sin(theta(:,1))+e(4).*sin(pi/2 + theta(:,2));

% x(:,5)=cos(theta(:,1))+e(5).*cos(pi/2 + theta(:,2));
% y(:,5)=sin(theta(:,1))+e(5).*sin(pi/2 + theta(:,2));

% Construct a best fit line through the appropriate portion
% of the coupler curve
xfit1=x(360:385,1); yfit1=y(360:385,1);
fit1a=polyfit(yfit1,xfit1,1);
fit1=polyval(fit1a,y(:,1));

% Measure angle of best fit line wrt y-axis and
% distance of coupler curve from best fit line
slope1 = (y(380)-y(355))/(fit1(380)-fit1(355));
angle1=atan(slope1)
delx1=fit1-x;
distfromline1=delx1 .* cos(pi/2 - angle1);
theta=1:400;

% Plot all desired results
axis('square');

%COUPLER CURVE
%plot(x,y)
%xlabel('X (units)')
%ylabel('Y (units)')
%grid

% STRAIGHT PORTIONS OF COUPLER CURVES
% plot(x(345:390,:),y(345:390,:))
% text(-0.44,1,'AC=1.4')
% text(-0.33,1.14,'AC=1.3')
% text(-0.23,1.09,'AC=1.2')
% text(-0.15,1.04,'AC=1.1')
% text(-0.03,0.99,'AC=1.0')
% xlabel('X (units)')
% ylabel('Y (units)')
% grid

```

```

% COUPLER CURVE WITH BEST FIT LINE
% plot(x,y,fit1,y(:,1))
% xlabel('X (units)')
% ylabel('Y (units)')
% grid

% COUPLER CURVE DISTANCE FROM BEST FIT LINE
% plot(theta,distfromline1)
% title ('Distance of Coupler Curve From Best Fit Line (AC=1.2)')
% xlabel('Phase of crank (degrees)')
% ylabel('Distance (units) ')
% grid

```

### “RDR1B” :

% THIS SUBROUTINE SOLVES FOR THE ANGLES OF EACH LINKS b and c  
% IN THE X-Y PLANE, GIVEN THE PHASE OF THE CRANK LINK a.

```
function q=rdr1b1(theta3)
```

```

% SOLVE FOR THETA2 IN TERMS OF THETA1 AND THETA3.
cosine2=(2.14 - cos(theta1) - 2.28 * cos(theta3))/2.02;
sin2=(-sin(theta1) - 2.28 * sin(theta3))/2.02;

```

```
%DETERMINE WHICH QUADRANT ANGLE (theta2) LIES IN
```

```
if cosine2<0
```

```
    if sin2<0
```

```
        qd=3;
```

```
    else
```

```
        qd=2;
```

```
    end
```

```
else
```

```
    if sin2<0
```

```
        qd=4;
```

```
    else
```

```
        qd=1;
```

```
    end
```

```
end
```

```

% IF ANGLE IS PI/2 ArcTan IS UNDEFINED, SO PREVENTATIVE STATEMENTS
FOLLOW

```

```
if cosine2^2 < .0000000005
```

```
    temp2=pi/2
```

```
else
```

```
    temp2=atan(sin2/cosine2);
```

```
end
```

```

% IF ANGLE LIES IN QUADRANTS 2 OR 3, THE ArcTan MUST BE CORRECTED
ACCORDINGLY

```

```
if qd==2
```

```
    if temp2<0
```

```
        temp2=temp2 + pi;
```

```

    else
        temp2=temp2 - pi;
    end
end
if qd==3
    if temp2<0
        temp2=temp2 + pi;
    else
        temp2=temp2 - pi;
    end
end
end

```

```

% SOLVE FOR THETA3
cosine3=(2.14-cos(theta1)-2.02 * cos(temp2)) / 2.28;
sin3=(-sin(theta1) - 2.02 * sin(temp2)) / 2.28;

```

```

%DETERMINE WHICH QUADRANT ANGLE LIES IN
if cosine3<0
    if sin3<0
        qd=3;
    else
        qd=2;
    end
else
    if sin3<0
        qd=4;
    else
        qd=1;
    end
end
end

```

```

% IF ANGLE IS PI/2 ArcTan IS UNDEFINED, SO PREVENTATIVE STATEMENTS
FOLLOW
if cosine3 ^2<.0000000005
    temp3=pi/2;
else
    temp3=atan(sin3/cosine3);
end
end

```

```

% IF ANGLE LIES IN QUADRANTS 2 OR 3, THE ArcTan MUST BE CORRECTED
if qd==2
    if temp3<0
        temp3=temp3 + pi;
    else
        temp3=temp3 - pi;
    end
end
if qd==3
    if temp3<0
        temp3=temp3 + pi;
    else
        temp3=temp3 - pi;
    end
end
end

```

q=theta3-temp3;

### "BLADMECH" :

% results for theta were found using the program "rdr1a.m"  
 % for the following parameters:  
 % point d located at (-.1586,6.5354)  
 % OA=3.0548, AB=6.1407, BD=6.9560, AC=3.666  
 % Angles in Radians, Positions in inches, Velocities in fps  
 % Accelerations in feet per second squared.

omega=zeros(362,3);  
 alpha=zeros(362,3);

%theta=[theta1 theta2 theta3]

theta =	[1.745329251994330e-002	3.113720802476451e+000	1.136739381546554e+000
	3.490658503988658e-002	3.122202165496739e+000	1.136323236548638e+000
	5.235987755982989e-002	3.130641921151158e+000	1.135830029883163e+000
	6.981317007977317e-002	3.139035448859498e+000	1.135258836626968e+000
	8.726646259971646e-002	3.147380068515256e+000	1.134608606946408e+000
	1.047197551196598e-001	3.155673036487348e+000	1.133878239631274e+000
	1.221730476396031e-001	3.163911542966456e+000	1.133066580469717e+000
	1.396263401595464e-001	3.172092709212307e+000	1.132172420575618e+000
	1.570796326794897e-001	3.180213584699805e+000	1.131194494667796e+000
	1.745329251994329e-001	3.188271144162147e+000	1.130131479300721e+000
	1.919862177193762e-001	3.196262284529220e+000	1.128981991046653e+000
	2.094395102393195e-001	3.204183821759752e+000	1.127744584629416e+000
	2.268928027592629e-001	3.212032487566008e+000	1.126417751010338e+000
	2.443460952792061e-001	3.219804926030102e+000	1.124999915427313e+000
	2.617993877991495e-001	3.227497690111411e+000	1.123489435388328e+000
	2.792526803190927e-001	3.235107238044986e+000	1.121884598621355e+000
	2.967059728390360e-001	3.242629929631415e+000	1.120183620983044e+000
	3.141592653589793e-001	3.250062022419213e+000	1.118384644329339e+000
	3.316125578789226e-001	3.257399667781523e+000	1.116485734351847e+000
	3.490658503988658e-001	3.264638906889739e+000	1.114482649414900e+000
	3.665191429188092e-001	3.271775666613308e+000	1.112377758468086e+000
	3.839724354387525e-001	3.278805755199339e+000	1.110166652417288e+000
	4.014257279586957e-001	3.285724858108370e+000	1.107847070201894e+000
	4.188790204786391e-001	3.292528533529091e+000	1.105416663428202e+000
	4.363323129985823e-001	3.299212207937705e+000	1.102872994173305e+000
	4.537856055185257e-001	3.305771171572669e+000	1.100213532775147e+000
	4.712388980384691e-001	3.312200573860740e+000	1.097435655660016e+000
	4.886921905584123e-001	3.318495335571678e+000	1.094536522306337e+000
	5.061454830783557e-001	3.324650357403438e+000	1.091513386403284e+000
	5.235987755982989e-001	3.330660369701675e+000	1.088363375965598e+000
	5.410520681182421e-001	3.336519912791531e+000	1.085083471870345e+000
	5.585053606381856e-001	3.342223363259218e+000	1.081670551473304e+000
	5.759586531581287e-001	3.347764929511204e+000	1.078121387095939e+000
	5.934119456780722e-001	3.353138647459263e+000	1.074432644723272e+000
	6.108652381980152e-001	3.358338376372979e+000	1.070600882951486e+000

6.283185307179585e-001	3.363357794946879e+000	1.066622552228696e+000
6.457718232379018e-001	3.368190397635479e+000	1.062493994437298e+000
6.632251157578452e-001	3.372829491316214e+000	1.058211442871709e+000
6.806784082777886e-001	3.377269824377672e+000	1.053771022671161e+000
6.981317007977317e-001	3.381501064260582e+000	1.049168751773486e+000
7.155849933176750e-001	3.385517562716573e+000	1.044400542462585e+000
7.330382858376183e-001	3.389311852013211e+000	1.039462203589380e+000
7.504915783575615e-001	3.392876267721335e+000	1.034349443553694e+000
7.679448708775050e-001	3.396202949059866e+000	1.029057874142413e+000
7.853981633974483e-001	3.399283840229550e+000	1.023583015327557e+000
8.028514559173916e-001	3.402110692872228e+000	1.017920301136487e+000
8.203047484373348e-001	3.404675069804374e+000	1.012065086715066e+000
8.377580409572781e-001	3.406968350186278e+000	1.006012656713407e+000
8.552113334772213e-001	3.408981736708175e+000	9.997582351323364e-001
8.726646259971647e-001	3.410706273504033e+000	9.932969967770005e-001
8.901179185171080e-001	3.412132826781648e+000	9.866240804716429e-001
9.075712110370514e-001	3.413252127849044e+000	9.797346041963543e-001
9.250245035569945e-001	3.414054778267443e+000	9.726236823121054e-001
9.424777960769382e-001	3.414531267717754e+000	9.652864450441800e-001
9.599310885968813e-001	3.414671994765778e+000	9.577180603958352e-001
9.773843811168247e-001	3.414467290769588e+000	9.499137586629300e-001
9.948376736367678e-001	3.413907447173963e+000	9.418688597159400e-001
1.012290966156711e+000	3.412982746433827e+000	9.335788032073064e-001
1.029744258676654e+000	3.411683496800837e+000	9.250391818489060e-001
1.047197551196598e+000	3.410000071193158e+000	9.162457778856113e-001
1.064650843716541e+000	3.407922950347260e+000	9.071946028656651e-001
1.082104136236484e+000	3.405442770421140e+000	8.978819407760668e-001
1.099557428756428e+000	3.402550375179488e+000	8.883043945705017e-001
1.117010721276371e+000	3.399236872841988e+000	8.784589360677769e-001
1.134464013796314e+000	3.395493697615119e+000	8.683429591395756e-001
1.151917306316258e+000	3.391312675854758e+000	8.579543360371789e-001
1.169370598836201e+000	3.386686096720775e+000	8.472914766272893e-001
1.186823891356144e+000	3.381606787085590e+000	8.363533902173579e-001
1.204277183876087e+000	3.376068190346325e+000	8.251397495513462e-001
1.221730476396031e+000	3.370064448665443e+000	8.136509564485946e-001
1.239183768915974e+000	3.363590488029041e+000	8.018882084429970e-001
1.256637061435917e+000	3.356642105367090e+000	7.898535656591881e-001
1.274090353955861e+000	3.349216056829127e+000	7.775500170399019e-001
1.291543646475804e+000	3.341310146155647e+000	7.649815449176692e-001
1.308996938995747e+000	3.332923311934684e+000	7.521531868090887e-001
1.326450231515690e+000	3.324053788830350e+000	7.390710932059730e-001
1.343903524035634e+000	3.314706877910334e+000	7.257425800506152e-001
1.361356816555577e+000	3.304883495149655e+000	7.121761745180725e-001
1.378810109075520e+000	3.294587918888089e+000	6.983816526930575e-001
1.396263401595464e+000	3.283825930507706e+000	6.843700677287414e-001
1.413716694115407e+000	3.272604862982351e+000	6.701537671149371e-001
1.431169986635350e+000	3.260933637140549e+000	6.557463977683671e-001
1.448623279155294e+000	3.248822784085077e+000	6.411628977909372e-001
1.466076571675237e+000	3.236284452372915e+000	6.264194739246732e-001
1.483529864195180e+000	3.223332231713883e+000	6.115333930509848e-001
1.500983156715123e+000	3.209981603493183e+000	5.965234175254956e-001
1.518436449235067e+000	3.196249478339136e+000	5.814093080311460e-001
1.535889741755010e+000	3.182154207294182e+000	5.662118152373485e-001
1.553343034274953e+000	3.167715535267049e+000	5.509526154941951e-001

1.570796326794897e+000	3.152954503169598e+000	5.356561977666531e-001
1.588249619314840e+000	3.137893333528359e+000	5.203417376985768e-001
1.605702911834783e+000	3.122555302353677e+000	5.050349618335861e-001
1.623156204354726e+000	3.106964595632331e+000	4.897600004375186e-001
1.640609496874670e+000	3.091146157223823e+000	4.745412358638604e-001
1.658062789394613e+000	3.075125527051174e+000	4.594031452751142e-001
1.675516081914556e+000	3.058928673626127e+000	4.443701417010587e-001
1.692969374434500e+000	3.042581823407379e+000	4.294664157653381e-001
1.710422666954443e+000	3.026111289771274e+000	4.147157806275132e-001
1.727875959474386e+000	3.009543304331320e+000	4.001415225825591e-001
1.745329251994330e+000	2.992903853220070e+000	3.857662595844191e-001
1.762782544514273e+000	2.976218520751353e+000	3.716118097232363e-001
1.780235837034216e+000	2.959512342623315e+000	3.576990713985560e-001
1.797689129554159e+000	2.942809670515540e+000	3.440479166060353e-001
1.815142422074103e+000	2.926134049591361e+000	3.306770984071397e-001
1.832595714594046e+000	2.909508110053564e+000	3.176041732938512e-001
1.850049007113989e+000	2.892953473533109e+000	3.048454388071958e-001
1.867502299633933e+000	2.876490674729310e+000	2.924158864313154e-001
1.884955592153876e+000	2.860139098378117e+000	2.803291694743203e-001
1.902408884673819e+000	2.843916931312633e+000	2.685975853712373e-001
1.919862177193763e+000	2.827841129103943e+000	2.572320716088175e-001
1.937315469713706e+000	2.811927396536037e+000	2.462422142802678e-001
1.954768762233649e+000	2.796190180978591e+000	2.356362681311854e-001
1.972222054753592e+000	2.780642677576330e+000	2.254211868556123e-001
1.989675347273536e+000	2.765296845072201e+000	2.156026623405328e-001
2.007128639793479e+000	2.750163431021117e+000	2.061851715349861e-001
2.024581932313422e+000	2.735252005127374e+000	1.971720296314119e-001
2.042035224833366e+000	2.720570999447729e+000	1.885654482870454e-001
2.059488517353309e+000	2.706127754238084e+000	1.803665976766676e-001
2.076941809873252e+000	2.691928568279906e+000	1.725756712495433e-001
2.094395102393195e+000	2.677978752597618e+000	1.651919521579885e-001
2.111848394913139e+000	2.664282686565504e+000	1.582138804279155e-001
2.129301687433082e+000	2.650843875497956e+000	1.516391200491329e-001
2.146754979953025e+000	2.637665008916172e+000	1.454646252712360e-001
2.164208272472969e+000	2.624748018784571e+000	1.396867054971153e-001
2.181661564992912e+000	2.612094137108635e+000	1.343010882678504e-001
2.199114857512855e+000	2.599703952380291e+000	1.293029799284696e-001
2.216568150032799e+000	2.587577464446053e+000	1.246871236524979e-001
2.234021442552742e+000	2.575714137455511e+000	1.204478545835004e-001
2.251474735072685e+000	2.564112950623006e+000	1.165791519237645e-001
2.268928027592628e+000	2.552772446602806e+000	1.130746878635230e-001
2.286381320112572e+000	2.541690777337916e+000	1.099278732990592e-001
2.303834612632515e+000	2.530865747294937e+000	1.071319003349234e-001
2.321287905152458e+000	2.520294854042266e+000	1.046797816047689e-001
2.338741197672401e+000	2.509975326167147e+000	1.025643864777093e-001
2.356194490192345e+000	2.499904158558798e+000	1.007784742430914e-001
2.373647782712288e+000	2.490078145110924e+000	9.931472438691602e-002
2.391101075232231e+000	2.480493908917763e+000	9.816576408848840e-002
2.408554367752175e+000	2.471147930054078e+000	9.732419307683564e-002
2.426007660272118e+000	2.462036571041708e+000	9.678260599361441e-002
2.443460952792061e+000	2.453156100114076e+000	9.653361241327212e-002
2.460914245312004e+000	2.444505886301469e+000	9.656985029468640e-002
2.478367537831948e+000	2.436075694697460e+000	9.688401929698012e-002
2.495820830351891e+000	2.427864831845420e+000	9.746886838444842e-002



2.513274122871834e+000	2.419869381588660e+000	9.831722550004697e-002
2.530727415391778e+000	2.412085420944609e+000	9.942200373695234e-002
2.548180707911721e+000	2.404507516894784e+000	1.007762104112003e-001
2.565634000431665e+000	2.397134815807062e+000	1.023729547878432e-001
2.583087292951608e+000	2.389961913429032e+000	1.042054545806888e-001
2.600540585471551e+000	2.382984971833208e+000	1.062670413385955e-001
2.617993877991494e+000	2.376200196350856e+000	1.085511648241494e-001
2.635447170511438e+000	2.369603842273355e+000	1.110513964834276e-001
2.652900463031381e+000	2.363192220661526e+000	1.137614320985637e-001
2.670353755551324e+000	2.356961703343240e+000	1.166750937080441e-001
2.687807048071268e+000	2.350908727174175e+000	1.197863308731183e-001
2.705260340591211e+000	2.345029797631310e+000	1.230892213624582e-001
2.722713633111154e+000	2.339321491803607e+000	1.265779713212463e-001
2.740166925631097e+000	2.333780460839437e+000	1.302469149852660e-001
2.757620218151041e+000	2.328403431905626e+000	1.340905139952744e-001
2.775073510670984e+000	2.323187209708584e+000	1.381033563620141e-001
2.792526803190927e+000	2.318128677623786e+000	1.422801551275878e-001
2.809980095710870e+000	2.313224798475970e+000	1.466157467646531e-001
2.827433388230814e+000	2.308472615008748e+000	1.511050893509225e-001
2.844886680750757e+000	2.303869250078891e+000	1.557432605527923e-001
2.862339973270700e+000	2.299411906607398e+000	1.605254554485560e-001
2.879793265790644e+000	2.295097867316487e+000	1.654469842185519e-001
2.897246558310587e+000	2.290924494278933e+000	1.705032697267644e-001
2.914699850830531e+000	2.286889228303668e+000	1.756898450158024e-001
2.932153143350474e+000	2.282989588179231e+000	1.810023507348043e-001
2.949606435870417e+000	2.279223169794542e+000	1.864365325176740e-001
2.967059728390360e+000	2.275587645154508e+000	1.919882383270824e-001
2.984513020910303e+000	2.272080761306201e+000	1.976534157778986e-001
3.001966313430247e+000	2.268700339189695e+000	2.034281094521038e-001
3.019419605950190e+000	2.265444272426164e+000	2.093084582157836e-001
3.036872898470134e+000	2.262310526054494e+000	2.152906925474846e-001
3.054326190990076e+000	2.259296114996488e+000	2.213711318860404e-001
3.071779483510020e+000	2.256401202027628e+000	2.275461820049017e-001
3.089232776029963e+000	2.253622919899827e+000	2.338123324190600e-001
3.106686068549906e+000	2.250960444996485e+000	2.401661000195562e-001
3.124139361069850e+000	2.248410070410401e+000	2.466040032039936e-001
3.141592653589793e+000	2.245971220940157e+000	2.531229205569658e-001
3.159045946109737e+000	2.243642324003975e+000	2.597196502043971e-001
3.176499238629680e+000	2.241421867573171e+000	2.663930618401985e-001
3.193952531149623e+000	2.239308398827331e+000	2.731360945405429e-001
3.211405823669566e+000	2.237300522604108e+000	2.799477541493283e-001
3.228859116189509e+000	2.235398571637061e+000	2.868251117951350e-001
3.246312408709453e+000	2.233597882829904e+000	2.937653011963003e-001
3.263765701229397e+000	2.231898934510367e+000	3.007675167552613e-001
3.281218993749340e+000	2.230300548979817e+000	3.078250111441411e-001
3.298672286269283e+000	2.228802579041687e+000	3.149376642321272e-001
3.316125578789226e+000	2.227402198026055e+000	3.221023248763004e-001
3.333578871309169e+000	2.226099149177374e+000	3.293163902165043e-001
3.351032163829113e+000	2.224892449994538e+000	3.365773276405454e-001
3.368485456349056e+000	2.223781163873479e+000	3.438826537296892e-001
3.385938748868998e+000	2.222764398890974e+000	3.512299325923928e-001
3.403392041388942e+000	2.221841306607638e+000	3.586167742561118e-001
3.420845333908886e+000	2.221011080889876e+000	3.660408331165768e-001
3.438298626428829e+000	2.220272956750415e+000	3.734998064438704e-001

3.455751918948773e+000	2.219626209206956e+000	3.809914329446026e-001
3.473205211468716e+000	2.219070152158409e+000	3.885134913794163e-001
3.490658503988659e+000	2.218604137278078e+000	3.960637992350639e-001
3.508111796508603e+000	2.218227552923131e+000	4.036402114502384e-001
3.525565089028546e+000	2.217939823059602e+000	4.112406191943475e-001
3.543018381548489e+000	2.217740406202173e+000	4.188629486984030e-001
3.560471674068432e+000	2.217628794367903e+000	4.265051601371954e-001
3.577924966588375e+000	2.217604512043085e+000	4.341652465619050e-001
3.595378259108319e+000	2.217667115162373e+000	4.418412328823288e-001
3.612831551628262e+000	2.217816190099285e+000	4.495311748978769e-001
3.630284844148206e+000	2.218051352667254e+000	4.572331583765131e-001
3.647738136668149e+000	2.218372247130297e+000	4.649452981808103e-001
3.665191429188092e+000	2.218778545222472e+000	4.726657374403072e-001
3.682644721708035e+000	2.219269945175228e+000	4.803926467693391e-001
3.700098014227978e+000	2.219846170751818e+000	4.881242235295439e-001
3.717551306747922e+000	2.220506970287939e+000	4.958586911362309e-001
3.735004599267866e+000	2.221252115737780e+000	5.035942984078059e-001
3.752457891787808e+000	2.222081401724706e+000	5.113293189574629e-001
3.769911184307752e+000	2.222994644595836e+000	5.190620506263282e-001
3.787364476827695e+000	2.223991681479768e+000	5.267908149572593e-001
3.804817769347638e+000	2.225072369346802e+000	5.345139567084985e-001
3.822271061867582e+000	2.226236584071014e+000	5.422298434063575e-001
3.839724354387525e+000	2.227484219493578e+000	5.499368649361193e-001
3.857177646907469e+000	2.228815186486810e+000	5.576334331703297e-001
3.874630939427412e+000	2.230229412018420e+000	5.653179816336273e-001
3.892084231947355e+000	2.231726838215557e+000	5.729889652032563e-001
3.909537524467298e+000	2.233307421428242e+000	5.806448598443855e-001
3.926990816987241e+000	2.234971131291878e+000	5.882841623793305e-001
3.944444109507184e+000	2.236717949788581e+000	5.959053902897642e-001
3.961897402027128e+000	2.238547870307125e+000	6.035070815509582e-001
3.979350694547072e+000	2.240460896701379e+000	6.110877944970878e-001
3.996803987067013e+000	2.242457042347176e+000	6.186461077165859e-001
4.014257279586959e+000	2.244536329197630e+000	6.261806199765121e-001
4.031710572106902e+000	2.246698786836964e+000	6.336899501748565e-001
4.049163864626845e+000	2.248944451533035e+000	6.411727373196684e-001
4.066617157146788e+000	2.251273365288760e+000	6.486276405338626e-001
4.084070449666731e+000	2.253685574892764e+000	6.560533390845086e-001
4.101523742186674e+000	2.256181130969634e+000	6.634485324353736e-001
4.118977034706616e+000	2.258760087030218e+000	6.708119403214472e-001
4.136430327226561e+000	2.261422498522518e+000	6.781423028441382e-001
4.153883619746503e+000	2.264168421883789e+000	6.854383805857742e-001
4.171336912266447e+000	2.266997906899957e+000	6.926992669128732e-001
4.188790204786391e+000	2.269911032293096e+000	6.999234878867093e-001
4.206243497306335e+000	2.272907833867733e+000	7.071088212864736e-001
4.223696789826278e+000	2.275988344481878e+000	7.142557808438036e-001
4.241150082346222e+000	2.279152642302761e+000	7.213625712613952e-001
4.258603374866164e+000	2.282400758630116e+000	7.284280793373538e-001
4.276056667386107e+000	2.285732730540740e+000	7.354512135675009e-001
4.293509959906051e+000	2.289148588656636e+000	7.424309043602675e-001
4.310963252425994e+000	2.292648356246683e+000	7.493661042569952e-001
4.328416544945937e+000	2.296232048339207e+000	7.562557881559724e-001
4.345869837465880e+000	2.299899670846700e+000	7.630989535384913e-001
4.363323129985823e+000	2.303651219703970e+000	7.698946206952202e-001
4.380776422505767e+000	2.307486680021023e+000	7.766418329511693e-001

4.398229715025709e+000	2.311406025252017e+000	7.833396568875259e-001
4.415683007545653e+000	2.315409216381596e+000	7.899871825586471e-001
4.433136300065597e+000	2.319496201129982e+000	7.965835237024982e-001
4.450589592585541e+000	2.323666913178108e+000	8.031278179428474e-001
4.468042885105484e+000	2.327921271414183e+000	8.096192269815548e-001
4.485496177625427e+000	2.332259179202918e+000	8.160569367793082e-001
4.502949470145371e+000	2.336680523678760e+000	8.224401577232108e-001
4.520402762665314e+000	2.341185175064315e+000	8.287681247796531e-001
4.537856055185257e+000	2.345772986015207e+000	8.350400976309643e-001
4.555309347705200e+000	2.350443790992476e+000	8.412553607943793e-001
4.572762640225143e+000	2.355197405663644e+000	8.474132237219323e-001
4.590215932745087e+000	2.360033626333431e+000	8.535130208799406e-001
4.607669225265030e+000	2.364952229405091e+000	8.595541118068359e-001
4.625122517784972e+000	2.369952970873236e+000	8.655358811481566e-001
4.642575810304916e+000	2.375035585848903e+000	8.714577386676148e-001
4.660029102824859e+000	2.380199788117583e+000	8.773191192332366e-001
4.677482395344803e+000	2.385445269730771e+000	8.831194827776649e-001
4.694935687864747e+000	2.390771700631537e+000	8.888583142318156e-001
4.712388980384691e+000	2.396178728314490e+000	8.945351234311703e-001
4.729842272904633e+000	2.401665977520394e+000	9.001494449941101e-001
4.747295565424577e+000	2.407233049965599e+000	9.057008381717765e-001
4.764748857944520e+000	2.412879524106291e+000	9.111888866690677e-001
4.782202150464463e+000	2.418604954937525e+000	9.166131984364940e-001
4.799655442984406e+000	2.424408873826772e+000	9.219734054327008e-001
4.817108735504349e+000	2.430290788381710e+000	9.272691633575931e-001
4.834562028024293e+000	2.436250182351776e+000	9.325001513561080e-001
4.852015320544236e+000	2.442286515562947e+000	9.376660716927601e-001
4.869468613064178e+000	2.448399223885043e+000	9.427666493972259e-001
4.886921905584122e+000	2.454587719230781e+000	9.478016318812907e-001
4.904375198104066e+000	2.460851389585668e+000	9.527707885276193e-001
4.921828490624009e+000	2.467189599067732e+000	9.576739102508741e-001
4.939281783143953e+000	2.473601688015980e+000	9.625108090318044e-001
4.956735075663897e+000	2.480086973106368e+000	9.672813174250152e-001
4.974188368183840e+000	2.486644747494016e+000	9.719852880411972e-001
4.991641660703783e+000	2.493274280980242e+000	9.766225930046699e-001
5.009094953223727e+000	2.499974820203004e+000	9.811931233871608e-001
5.026548245743669e+000	2.506745588849188e+000	9.856967886187962e-001
5.044001538263612e+000	2.513585787887155e+000	9.901335158773332e-001
5.061454830783555e+000	2.520494595817898e+000	9.945032494567141e-001
5.078908123303498e+000	2.527471168943103e+000	9.988059501160453e-001
5.096361415823441e+000	2.534514641377443e+000	1.003041594410158e+000
5.113814708343384e+000	2.541624126105546e+000	1.007210174002906e+000
5.131268000863329e+000	2.548798714698503e+000	1.011311694964397e+000
5.148721293383272e+000	2.556037477619835e+000	1.015346177053338e+000
5.166174585903216e+000	2.563339464665207e+000	1.019313652985710e+000
5.183627878423160e+000	2.570703705294214e+000	1.023214167690942e+000
5.201081170943102e+000	2.578129208966355e+000	1.027047777556784e+000
5.218534463463045e+000	2.585614965479322e+000	1.030814549664045e+000
5.235987755982989e+000	2.593159945307768e+000	1.034514561012319e+000
5.253441048502932e+000	2.600763099940739e+000	1.038147897737842e+000
5.270894341022875e+000	2.608423362215965e+000	1.041714654324531e+000
5.288347633542818e+000	2.616139646167566e+000	1.045215790681571e+000
5.305800926062761e+000	2.623910849754849e+000	1.048648841549206e+000
5.323254218582705e+000	2.631735850350108e+000	1.052016494514878e+000

5.340707511102648e+000	2.639613509866509e+000	1.055318011553723e+000
5.358160803622591e+000	2.647542672646328e+000	1.058553516876072e+000
5.375614096142535e+000	2.655522166222299e+000	1.061723138232724e+000
5.393067388662479e+000	2.663550801582526e+000	1.064827006105097e+000
5.410520681182422e+000	2.671627373419110e+000	1.067865252895310e+000
5.427973973702366e+000	2.679750660359014e+000	1.070838012116788e+000
5.445427266222309e+000	2.687919425175767e+000	1.073745417585922e+000
5.462880558742252e+000	2.696132414980623e+000	1.076587602615242e+000
5.480333851262194e+000	2.704388361391883e+000	1.079364699208509e+000
5.497787143782138e+000	2.712685980681054e+000	1.082076837258034e+000
5.515240436302081e+000	2.721023973894661e+000	1.084724143744495e+000
5.532693728822025e+000	2.729401026950502e+000	1.087306741939443e+000
5.550147021341967e+000	2.737815810707196e+000	1.089824750610602e+000
5.567600313861911e+000	2.746266981005927e+000	1.092278283230044e+000
5.585053606381853e+000	2.754753178683305e+000	1.094667447185194e+000
5.602506898901797e+000	2.763273029554318e+000	1.096992342992610e+000
5.619960191421741e+000	2.771825144364361e+000	1.099253063514374e+000
5.637413483941685e+000	2.780408118709372e+000	1.101449693176889e+000
5.654866776461628e+000	2.789020532923133e+000	1.103582307191811e+000
5.672320068981572e+000	2.797660951930794e+000	1.105650970778755e+000
5.689773361501514e+000	2.806327925067728e+000	1.107655738389408e+000
5.707226654021458e+000	2.815019985862806e+000	1.109596652932550e+000
5.724679946541400e+000	2.823735651785231e+000	1.111473744999494e+000
5.742133239061344e+000	2.832473423954029e+000	1.113287032089346e+000
5.759586531581287e+000	2.841231786809358e+000	1.115036517833458e+000
5.777039824101231e+000	2.850009207744727e+000	1.116722191218379e+000
5.794493116621173e+000	2.858804136699276e+000	1.118344025806569e+000
5.811946409141117e+000	2.867615005709218e+000	1.119901978954069e+000
5.829399701661061e+000	2.876440228417528e+000	1.121395991024285e+000
5.846852994181003e+000	2.885278199540996e+000	1.122825984596993e+000
5.864306286700947e+000	2.894127294293680e+000	1.124191863671611e+000
5.881759579220890e+000	2.902985867765786e+000	1.125493512863755e+000
5.899212871740834e+000	2.911852254257019e+000	1.126730796594038e+000
5.916666164260778e+000	2.920724766563326e+000	1.127903558268032e+000
5.934119456780723e+000	2.929601695216018e+000	1.129011619446273e+000
5.951572749300662e+000	2.938481307672128e+000	1.130054779003129e+000
5.969026041820607e+000	2.947361847454862e+000	1.131032812273353e+000
5.986479334340551e+000	2.956241533242968e+000	1.131945470185048e+000
6.003932626860492e+000	2.965118557907737e+000	1.132792478377789e+000
6.021385919380437e+000	2.973991087496366e+000	1.133573536304569e+000
6.038839211900379e+000	2.982857260160297e+000	1.134288316316225e+000
6.056292504420322e+000	2.991715185027116e+000	1.134936462726968e+000
6.073745796940267e+000	3.000562941014554e+000	1.135517590859601e+000
6.091199089460209e+000	3.009398575585006e+000	1.136031286068985e+000
6.108652381980152e+000	3.018220103438976e+000	1.136477102742293e+000
6.126105674500098e+000	3.027025505145776e+000	1.136854563274564e+000
6.143558967020040e+000	3.035812725709707e+000	1.137163157018052e+000
6.161012259539982e+000	3.044579673069943e+000	1.137402339203853e+000
6.178465552059929e+000	3.053324216532203e+000	1.137571529834263e+000
6.195918844579871e+000	3.062044185130288e+000	1.137670112544348e+000
6.213372137099813e+000	3.070737371957424e+000	1.137697448482535e+000
6.230825429619756e+000	3.079401505049796e+000	1.137652806858248e+000
6.248278722139701e+000	3.088034292337022e+000	1.137535481034675e+000
6.265732014659643e+000	3.096633270599508e+000	1.137344432872030e+000

```

6.283185307179585e+000  3.105194388397595e+000  1.137079641981548e+000
6.300638599699528e+000  3.113718801034708e+000  1.136739456658416e+000
6.318091892219473e+000  3.122202165496720e+000  1.136323236548596e+000];

```

```

% Use Richardson Extrapolation to calculate
% angular velocities and angular accelerations

```

```

rpd = 2*pi/360 ; %radians per degree
dps = 5*360; % degrees per second
rps = 10*pi; % radians per second

```

```

omega(:,1)=rps .* ones(362,1);
omega(1,2:3)= dps *((4*(theta(2,2:3)-theta(360,2:3))/2)- ...
    ((theta(3,2:3)-theta(359,2:3))/4))/3; %rad/s

```

```

omega(2,2:3)= dps *((4*(theta(3,2:3)-theta( 1,2:3))/2) - ...
    ((theta(4,2:3)-theta(360,2:3))/4))/3; %rad/s

```

```

omega(361,2:3)=omega(1,2:3);
omega(362,2:3)=omega(2,2:3);

```

```

for x=3:360
    u=x-2;
    v=x-1;
    y=x+1;
    z=x+2;
    omega(x,2:3)= dps*((4*(theta(y,2:3)-theta(v,2:3))/2) - ...
        ((theta(z,2:3)-theta(u,2:3))/4))/3; %rad/s
end

```

```

alpha(1,:)= dps*((4*(omega(2,:)-omega(360,:))/2) - ...
    ((omega(3,:)-omega(359,:))/4))/3; %rad/s

```

```

alpha(2,:)= dps*((4*(omega(3,:)-omega(1,:))/2) - ...
    ((omega(4,:)-omega(360,:))/4))/3; %rad/s

```

```

alpha(361,:)=alpha(1,:);
alpha(362,:)=alpha(2,:);

```

```

for x=3:360
    u=x-2;
    v=x-1;
    y=x+1;
    z=x+2;
    alpha(x,:)= dps * ((4*(omega(y,:)-omega(v,:))/2) - ...
        ((omega(z,:)-omega(u,:))/4))/3; %rad/s
end

```

```

%Define link lengths

```

```

AO = 3.055;
BA = 6.141;
CA = 3.666;

```

```

% define matrices

```

```

Ri=zeros(362,3);
Rj=zeros(362,3);
Vi=zeros(362,3);
Vj=zeros(362,3);
Ai=zeros(362,3);
Aj=zeros(362,3);

```

```
% CALCULATE POSITIONS OF POINTS A,B,C (in inches)
```

```

Ri(:,1)= AO .* cos(theta(:,1));
Ri(:,2)= Ri(:,1) + BA .* cos(theta(:,2));
Ri(:,3)= Ri(:,1) + CA .* cos(theta(:,2) + pi/2);

```

```

Rj(:,1)= AO .* sin(theta(:,1));
Rj(:,2)= Rj(:,1) + BA .* sin(theta(:,2));
Rj(:,3)= Rj(:,1) + CA .* sin(theta(:,2) + pi/2);

```

```
% CALCULATE VELOCITIES OF POINTS A,B,C (in fps)
```

```

Vi(:,1)= -(AO/12) * omega(:,1) .* sin(theta(:,1));
Vi(:,2)= Vi(:,1) - ((BA/12) * omega(:,2) .* sin(theta(:,2))));
Vi(:,3)= Vi(:,1) - ((CA/12) * omega(:,2) .* sin(theta(:,2) + pi/2));

```

```

Vj(:,1)= (AO/12) * omega(:,1) .* cos(theta(:,1));
Vj(:,2)= Vj(:,1) + ((BA/12) * omega(:,2) .* cos(theta(:,2))));
Vj(:,3)= Vj(:,1) + ((CA/12) * omega(:,2) .* cos(theta(:,2) + pi/2));

```

```
% CALCULATE ACCELERATIONS OF POINTS A,B,C (in f/s^2)
```

```

Ai(:,1)= -(AO/12) * cos(theta(:,1)) .* ((omega(:,1)).^2);
Ai(:,2)= Ai(:,1) - (BA/12) * ((sin(theta(:,2)) .* alpha(:,2)) + ...
    (cos(theta(:,2)) .* (omega(:,2).^2)));
Ai(:,3)= Ai(:,2) - (CA/12) * ((sin(theta(:,2) + pi /2) .* alpha(:,2)) + ...
    (cos(theta(:,2) + pi /2) .* (omega(:,2).^2)));

```

```

Aj(:,1)= -(AO/12) * sin(theta(:,1)) .* ((omega(:,1)).^2);
Aj(:,2)= Aj(:,1) + (BA/12) * ((cos(theta(:,2)) .* alpha(:,2)) - ...
    (sin(theta(:,2)) .* (omega(:,2).^2)));
Aj(:,3)= Aj(:,2) + (CA/12) * ((cos(theta(:,2) + pi /2) .* alpha(:,2)) - ...
    (sin(theta(:,2) + pi /2) .* (omega(:,2).^2)));

```

```
% Calculate the forces at pin joint c due to reversed inertial forces of
```

```
% parts #4 and #5.
```

```
% Estimate weights of part #4 = 4 lbs., #5 = 15 lbs., #2=1.2 lbs., #3=0.6 lbs.
```

```
m2=0.4084/32.17; %slugs
```

```
m3=0.196/32.17; %slugs
```

```
m4=1.25/32.17; %slugs
```

```
m5=33/32.17; %slugs
```

```
J3p=(m3/12) * ((1/12)^2 +(8/12)^2) + m3 * (3.5/12)^2; %slug ft^2
```

```
J2a=(m2/18)*((4.5/12)^2 +(7/12)^2) +m2 * (2.1/12)^2; %slug ft^2
```

```
% Multiply masses by the accelerations to get inertial forces
```

```
% at point c (Note: these are forces from link 4 to link 2)
```

```
Fci= -m4 * Ai(:,3); %lbs
Fcj= -(m4+m5) * Aj(:,3); %lbs
```

```
% Calculate the tangential component of the inertial forces, due to the
% motion of link 3, acting on pin joint at point B.
```

```
% These forces denote forces from link 3 to link 2.
```

```
Fbt= -(J3p * alpha(:,3) / (6.956/12)); %lbs
Fbti= -(J3p * alpha(:,3) / (6.956/12)) .* cos(theta(:,3)+pi/2); %lbs
Fbtj= -(J3p * alpha(:,3) / (6.956/12)) .* sin(theta(:,3)+pi/2); %lbs
%clear dthetapdt alpha3
```

```
%Calculate moments generated about point A by all known forces (Fc,Fbt)
```

```
MaFcj= Fcj .* (Ri(:,3)-Ri(:,1))/12; % ft lbs
MaFci= Fci .* (Rj(:,1)-Rj(:,3))/12; % ft lbs
MaFbti=Fbti .* (Rj(:,1)-Rj(:,2))/12; % ft lbs
MaFbtj=Fbtj .* (Ri(:,2)-Ri(:,1))/12; % ft lbs
Knownmoments=MaFcj+MaFci+MaFbti+MaFbtj; % ft lbs
```

```
% Calculate the radial forces at point B using a sum of Moments about
% Point A and the Moment of inertia and angular accelerations of link 2
% about point A.
```

```
Fbrma=(J2a * alpha(:,2)-(Knownmoments))/(6.141/12); % lbs
beta= - theta(:,3) + (theta(:,2)+pi/2);
Fbr=(Fbrma ./ cos(beta)); %lbs
Fbri=(Fbrma ./ cos(beta)) .* cos(theta(:,3)); %lbs
Fbrj=(Fbrma ./ cos(beta)) .* sin(theta(:,3)); %lbs
```

```
% Check the radial force calculation
```

```
MaFbri=Fbri .* (Rj(:,1)-Rj(:,2))/12; % ft lbs
MaFbrj=Fbrj .* (Ri(:,2)-Ri(:,1))/12; % ft lbs
check=J2a * alpha(:,2)- Knownmoments - MaFbri - MaFbrj;
```

```
%Calculate Forces at point A transmitted from link 1 to link 2.
```

```
%use D'Alambert's principle to get Fax and Fay.
```

```
Fai=(m2*Ai(:,3))-Fci-Fbti-Fbri;% lbs
Faj=(m2*Aj(:,3))-Fcj-Fbtj-Fbrj;% lbs
```

```
%Calculate the magnitudes of force on pin joints.
```

```
Fc=(Fci.^2 + Fcj.^2).^0.5; %lbs
Fb=((Fbti.^2 + Fbtj.^2) + (Fbri.^2 + Fbrj.^2)).^0.5; %lbs
Fa=(Fai.^2 + Faj.^2).^0.5; %lbs
```

```
%Calculate radial and tangential loads from crank
```

```
Fat=Faj .* cos(theta(:,1)) + Fai .* cos(pi/2 + theta(:,1));
Far=-Faj .* sin(theta(:,1)) - Fai .* sin(pi/2 + theta(:,1));
%
```

```
%plot results
axis('square');
```

#### %POINT TRAJECTORIES

```
%plot(2.54*Ri,2.54*Rj)
%xlabel('X (cm)')
%ylabel('Y (cm)')
%grid
```

#### %POINT VELOCITIES

```
%axis([-6 4 -5 5])
%plot(.305*Vi,.305*Vj)
%xlabel('Vx (m/s)')
%ylabel('Vy (m/s)')
%grid
```

#### %POINT ACCELERATIONS

```
%axis([-250 200 -250 200])
%plot(.305*Ai,.305*Aj)
%xlabel('Ax (m/s^2)')
%ylabel('Ay (m/s^2)')
%grid
```

```
phase=1:360;
```

#### %FORCE TRANSMITTED AT C IN X-DIRECTION

```
%plot (phase,4.45*Fci(1:360))
%xlabel('crank phase (degrees)')
%ylabel('F42,i (N)')
%grid
```

#### %FORCE TRANSMITTED AT C IN Y-DIRECTION

```
%plot (phase,4.45 * Fcj(1:360))
%xlabel('crank phase (degrees)')
%ylabel('F42,j (N)')
%grid
```

#### % TOTAL FORCE TRANSMITTED AT C

```
%plot (phase,4.45*Fc(1:360))
%xlabel('crank phase (degrees)')
%ylabel('F42 (N)')
%grid
```

#### %FORCE TRANSMITTED AT B IN tangential DIRECTION

```
%plot (phase,4.45*Fbt(1:360))
%xlabel('crank phase (degrees)')
%ylabel('F32,t (N)')
%grid
```

#### % FORCE TRANSMITTED AT b IN RADIAL-DIRECTION

```
%plot (phase,4.45*Fbr(1:360))
%xlabel('crank phase (degrees)')
%ylabel('F32,r (N)')
%grid
```



```
% total FORCE TRANSMITTED AT b
%plot (phase,4.45*Fb(1:360))
%xlabel('crank phase (degrees)')
%ylabel('F32 (N)')
%grid
```

```
%FORCE TRANSMITTED AT a IN tangential DIRECTION
%plot (phase,4.45*Fat(1:360))
%xlabel('crank phase (degrees)')
%ylabel('F12,t (N)')
%grid
```

```
% FORCE TRANSMITTED AT a IN RADIAL-DIRECTION
%plot (phase,4.45*Far(1:360))
%xlabel('crank phase (degrees)')
%ylabel('F12,r (N)')
%grid
```

```
% total FORCE TRANSMITTED AT a
plot (phase,4.45*Fa(1:360))
xlabel('crank phase (degrees)')
ylabel('F12 (N)')
grid
```

## **BIBLIOGRAPHY**

**Barron, J., Dow Chemical, Inc. (Personal Communication).**

**Beer, F. and Johnston, E., "Vector Mechanics for Engineers - Dynamics", 5th ed., McGraw Hill, New York, 1988.**

**Ericson, M & Berglund, L., "Processing and Mechanical Properties of Oriented Glass Mat Reinforced Thermoplastics", 1991.**

**Frutiger, R. and Baskar, S., "Composite Floorpan", "Automotive Engineering", SAE International, Brimfield, OH, February, 1993.**

**Jander, M., 1991, "Industrial RTM -- New Developments in Molding and Preforming Technologies", Advanced Composite Materials; New Developments and Applications Conference Proceedings, Detroit, MI, Sept. 30 - Oct. 3, 1991.**

**Potter, M. and Foss, J., "Fluid Mechanics", Great Lakes Press, Inc., Okemos, MI, 1982.**

**Rothbart, H., "Cams - Design, Dynamics, and Accuracy", John Wiley & Sons, Inc., New York, 1956.**

**Shigley, J. and Mischke, C., "Mechanical Engineering Design", 5th ed., McGraw Hill, New York, 1989**

**Soni, A., "Mechanism Synthesis and Analysis", Robert E. Krieger Publishing Co., Malabar, FL, 1981.**

**Tesar, D. and Matthew, G., "The Dynamic Synthesis, Analysis, and Design of Modeled Cam Systems", Lexington Books, D.c. Heath and Co., Toronto, 1976.**

**Thompson, B., "Design Creativity", Infotrans, Inc., Okemos, MI, 1992.**

**Tuttle, S., "Mechanisms for Engineering Design", John Wiley and Sons, Inc., New York, 1967.**

**Wahl, A., "Mechanical Springs", McGraw Hill Book Company, Inc., New York, 1963**